

## INFORMATION TO USERS

This reproduction was made from a copy of a document sent to us for microfilming. While the most advanced technology has been used to photograph and reproduce this document, the quality of the reproduction is heavily dependent upon the quality of the material submitted.

The following explanation of techniques is provided to help clarify markings or notations which may appear on this reproduction.

1. The sign or "target" for pages apparently lacking from the document photographed is "Missing Page(s)". If it was possible to obtain the missing page(s) or section, they are spliced into the film along with adjacent pages. This may have necessitated cutting through an image and duplicating adjacent pages to assure complete continuity.
2. When an image on the film is obliterated with a round black mark, it is an indication of either blurred copy because of movement during exposure, duplicate copy, or copyrighted materials that should not have been filmed. For blurred pages, a good image of the page can be found in the adjacent frame. If copyrighted materials were deleted, a target note will appear listing the pages in the adjacent frame.
3. When a map, drawing or chart, etc., is part of the material being photographed, a definite method of "sectioning" the material has been followed. It is customary to begin filming at the upper left hand corner of a large sheet and to continue from left to right in equal sections with small overlaps. If necessary, sectioning is continued again—beginning below the first row and continuing on until complete.
4. For illustrations that cannot be satisfactorily reproduced by xerographic means, photographic prints can be purchased at additional cost and inserted into your xerographic copy. These prints are available upon request from the Dissertations Customer Services Department.
5. Some pages in any document may have indistinct print. In all cases the best available copy has been filmed.

**University  
Microfilms  
International**

300 N. Zeeb Road  
Ann Arbor, MI 48106



8314769

Hemmati, Mostafa

THE EXACT SOLUTION OF THE ELECTRON-FLUID DYNAMICAL  
EQUATIONS

*The University of Oklahoma*

PH.D. 1983

University  
Microfilms  
International 300 N. Zeeb Road, Ann Arbor, MI 48106



PLEASE NOTE:

In all cases this material has been filmed in the best possible way from the available copy. Problems encountered with this document have been identified here with a check mark .

1. Glossy photographs or pages \_\_\_\_\_
2. Colored illustrations, paper or print \_\_\_\_\_
3. Photographs with dark background \_\_\_\_\_
4. Illustrations are poor copy \_\_\_\_\_
5. Pages with black marks, not original copy \_\_\_\_\_
6. Print shows through as there is text on both sides of page \_\_\_\_\_
7. Indistinct, broken or small print on several pages
8. Print exceeds margin requirements \_\_\_\_\_
9. Tightly bound copy with print lost in spine \_\_\_\_\_
10. Computer printout pages with indistinct print \_\_\_\_\_
11. Page(s) \_\_\_\_\_ lacking when material received, and not available from school or author.
12. Page(s) \_\_\_\_\_ seem to be missing in numbering only as text follows.
13. Two pages numbered \_\_\_\_\_. Text follows.
14. Curling and wrinkled pages \_\_\_\_\_
15. Other \_\_\_\_\_

University  
Microfilms  
International



THE UNIVERSITY OF OKLAHOMA  
GRADUATE COLLEGE

THE EXACT SOLUTION OF THE ELECTRON-FLUID DYNAMICAL  
EQUATIONS

A DISSERTATION  
SUBMITTED TO THE GRADUATE FACULTY  
in partial fulfillment of the  
requirements for the degree of  
DOCTOR OF PHILOSOPHY

BY  
MOSTAFA HEMMATI  
Norman, Oklahoma  
1983

THE EXACT SOLUTION OF THE ELECTRON-FLUID DYNAMICAL  
EQUATIONS

APPROVED BY:

Richard B. Fowler

J. M. Hoffaker

Herbert Ryan

Paul Massatt

Thomas M. Miller

DISSERTATION COMMITTEE

## ACKNOWLEDGMENTS

It is a pleasure to acknowledge the interest and un-failing enthusiasm of Professor Richard G. Fowler throughout his direction of this study. The patience and love of my mother, Golzar, have been a source of strength throughout these years of graduate study. Acknowledgment is also due to all members of my committee for their interest and suggestions and to Jaquine Littell for her skill in typing this thesis. I would also like to express my appreciation to the University of Oklahoma for the large amount of computer time allotted me for my research.

## TABLE OF CONTENTS

	Page
LIST OF FIGURES . . . . .	v
LIST OF SYMBOLS . . . . .	viii
Chapter	
I. INTRODUCTION. . . . .	1
II. BACKGROUND. . . . .	4
III. THE BASIC EQUATIONS AND EARLY APPROACHES TO THEIR SOLUTION. . . . .	18
IV. CLASS I PROFORCE WAVES. . . . .	33
V. CLASS II PROFORCE WAVES . . . . .	56
VI. ANTIFORCE AND CLASS III WAVES . . . . .	67
VII. CONCLUSION. . . . .	82
BIBLIOGRAPHY. . . . .	88
APPENDIX. . . . .	91

## LIST OF FIGURES

Figure	Page
1. Electric field ( $\eta$ ) as a function of drift velocity ( $\psi$ ) . . . . .	35
2. Electric field ( $\eta$ ) as a function of drift velocity ( $\psi$ ) . . . . .	36
3. Temperature ( $\theta$ ), electron density ( $\nu$ ), and ionization rate ( $\mu$ ) as a function of position ( $\xi$ ). .	36
4. Electric field ( $\eta$ ) as a function of drift velocity ( $\psi$ ) . . . . .	40
5. Temperature ( $\theta$ ), electron density ( $\nu$ ), and ionization rate ( $\mu$ ) as a function of position ( $\xi$ )	40
6. Electric field ( $\eta$ ) as a function of drift velocity ( $\psi$ ) . . . . .	44
7. Temperature ( $\theta$ ), electron density ( $\nu$ ), and ionization rate ( $\mu$ ) as a function of position ( $\xi$ ). .	44
8. Electric field ( $\eta$ ) as a function of drift velocity ( $\psi$ ) for Ar at $\alpha=0.01$ , $\psi_1=0.31953$ , $\nu_1=0.025$ , $\kappa=1.18179$ . . . . .	50
9. Electric field ( $\eta$ ) and drift velocity ( $\psi$ ) as a function of position for Ar at $\alpha=0.01$ , $\psi_1=0.31953$ , $\nu_1=0.025$ , $\kappa=1,18179$ . . . . .	50

Figure	Page
10. Electron temperature ( $\theta$ ), electron density ( $\nu$ ), ionization rate ( $\mu$ ) as a function of position ( $\xi$ )	51
11. Electric field ( $\eta$ ) and drift velocity ( $\nu$ ) as a function of position ( $\xi$ ) for Ar at $\alpha=2$ , $\psi_1=0.0845$ , $\nu_1=7.7$ , $\kappa=0.6498$ . . . . .	51
12. Electron temperature ( $\theta$ ), electron density ( $\nu$ ), and ionization rate ( $\mu$ ) as a function of position ( $\xi$ ) for Ar at $\alpha=2$ , $\psi_1=0.0845$ , $\nu_1=7.7$ , $\kappa=0.6498$ . .	53
13. Electron density ( $\nu$ ) as a function of position ( $\xi$ ) for Ar, $N_2$ , He at $\alpha=2$ . . . . .	54
14. Ionization rate ( $\mu$ ) as a function of position ( $\xi$ ) for Ar, $N_2$ , He at $\alpha=2$ . . . . .	54
15. Electric field ( $\eta$ ) as a function of drift velocity ( $\psi$ ) for $\alpha=0.01$ . . . . .	64
16. Electric field ( $\eta$ ) and drift velocity ( $\psi$ ) as a function of position ( $\xi$ ) for $\alpha=0.01$ at $\psi_0=3 \times 10^{-5}$ , $\psi_1=0.287$ , $\kappa=1.5227$ , $\nu_1=0.00315$ . . . . .	66
17. Temperature ( $\theta$ ), electron density ( $\nu$ ), and ioniza- tion rate ( $\mu$ ) as a function of position ( $\xi$ ) for $\alpha=0.01$ at $\psi_0=3 \times 10^{-5}$ , $\kappa=1.5227$ , $\psi_1=0.287$ , $\nu_1=0.00315$ . . . . .	66
18. Electric field ( $\eta$ ) as a function of drift velocity ( $\psi$ ) for $\alpha=0.01$ and $\nu_1=2.6$ at $\psi_1=0.68$ , $\kappa=1.3$ , $\nu_1=0.83$ . . . . .	78

Figure	Page
19. Electric field ( $\eta$ ) and drift velocity ( $\psi$ ) as a function of position ( $\xi$ ) for $\alpha=0.01$ and $\nu=2.6$ at $\psi_1=0.68$ , $\kappa=1.3$ , $\nu_1=0.83$ . . . . .	78
20. Electron temperature ( $\theta$ ), electron density ( $\nu$ ), and ionization rate ( $\mu$ ) as a function of position ( $\xi$ ) for $\alpha=0.01$ and $\nu=2.6$ at $\psi_1=0.68$ , $\kappa=1.3$ , $\nu_1=0.83$ . . . . .	80
21. Electric field ( $\eta$ ) as a function of drift velocity ( $\psi$ ) for $\alpha=0.01$ and $\nu=0.0$ at $\psi_1=0.649$ , $\kappa=1.3$ , $\nu_1=0.886$ . . . . .	79
22. Electric field ( $\eta$ ) and drift velocity ( $\psi$ ) as a function of position ( $\xi$ ) for $\alpha=0.01$ and $\nu=0.0$ at $\psi_1=0.645$ , $\kappa=1.3$ , $\nu_1=0.886$ . . . . .	79
23. Temperature ( $\theta$ ), electron density ( $\nu$ ), ionization rate ( $\mu$ ) as a function of position ( $\xi$ ) for $\alpha=0.01$ and $\nu=0.0$ at $\psi_1=0.645$ , $\kappa=1.3$ , $\nu_1=0.886$ . . . . .	80
24. Wave constant vs. wave velocity . . . . .	85

## LIST OF SYMBOLS

$k$	Boltzmann's constant
$T$	Temperature
$m$	Electron mass
$\alpha$	Nondimensionalized ionization potential
$\beta$	Ionization frequency
$\phi_i$	Ionization potential
$E$	Electric field
$e$	Electron charge
$\Delta( )$	Transfer operator for indicated quantity inside the parentheses
$\xi$	Nondimensionalized length coordinate
$\theta$	Nondimensionalized electron temperature
$\nu$	Nondimensionalized electron density
$\psi$	Nondimensionalized electron velocity
$\eta$	Nondimensionalized electric field
$\mu$	Nondimensionalized ionization rate
$\kappa$	Constant determining relation of wave speed to applied field
$\epsilon_0$	MKS permittivity
$n$	Electron number density

$v$  Electron velocity  
 $V$  Heavy particle velocity  
 $V_0$  Wave velocity

## CHAPTER I

### INTRODUCTION

In the past few decades introduction of technology and better measuring devices into the study of luminous pulses have provided better data and consequently better understanding of this phenomenon. Throughout the past century, experimentalists have observed the propagation of luminosity fronts associated with the electric breakdown of a gas. J. J. Thomson was the first to observe that the luminosity did not start simultaneously throughout the length of the discharge tube, but seemed to start at the anode and travel the tube to the cathode at a finite and measurable speed. He recorded that the luminosity front might move at a speed as high as half the speed of light.

In the late 1920s Beams studied the propagation of the luminosity fronts in long discharge tubes. He concluded that the luminosity always moves from the electrode to which the potential is applied (high voltage electrode)

toward the electrode maintained at ground potential regardless of the polarity of the impressed surge. All the attempts to identify the breakdown waves with solutions to Maxwell's equations failed. In the spectrum of the emitted radiation no Doppler shift has been detected, which indicates that the excited atoms are not in motion and their mass motion is negligible. This and the fact that the luminous pulses travel with speed as high as half the speed of light supports the idea that the luminous pulses are caused by an electron fluid motion. Since the geometrical configurations of the discharge tubes used by the experimenters have been different and the data recorded by many experimenters have been meaningful only under their operating conditions (pressure, applied voltage, type of gas, etc.), the understanding and analysis of the data taken by experimenters have been very difficult. The phenomenon of breakdown waves has been less completely understood than the structure of the nucleus, even though the phenomenon has been studied by scientists for a long time.

Starting in the 1930s, the theories about the nature of the breakdown waves were presented, but it was in the 1960s that most of the advances took place. Fowler and Shelton, by some modification of Fowler and Paxton's formulas developed earlier, were able to present better equations for breakdown waves, and later they solved them with approximate methods. In our earlier work on computer

solution of the electron-fluid equations several terms in the energy equation which were neglected by Shelton were included. After extensive computer analysis we concluded that the heat conduction, the random electron heat loss, and the directed electron kinetic energy loss terms were important and could not be neglected. Also the results showed that there is no weak proforce wave, and all proforce waves are strong shock waves.

Also in the present work the advance of the breakdown waves into a preionized gas (with or without a current present) has been investigated. The results were highly dependent on the ion velocity and concentration in front of the wave, and not very much dependent on the current in front of the wave. The last part of this work is an investigation of the problem of the antiforce waves. In his work on antiforce waves Sanmann formulated the problem by sign changes of constants in the standard proforce formulation, but it will be shown that this cannot be done. The revised equations can be solved and the results indicate that there can be antiforce waves into either a neutral gas or a preionized gas. These waves are shock antiforce waves rather than the weak waves described by Sanmann. Solutions were also found for an antiforce wave with an artificial current discontinuity at the front, but none for proforce waves.

## CHAPTER II

### BACKGROUND

In 1795 Hauksbee<sup>1</sup> was the first one to notice the similarities between lightning and the luminous pulses which he produced in partial vacuum. But it was Wheatstone<sup>2</sup> who proposed a propagation mechanism with luminous fronts in low pressure discharge tubes subjected to high potential differences. Using rotating mirrors he was unable to detect luminous front motion at velocities less than  $10^5$  m/sec, because his equipment was not fast enough and did not have good time resolution. With improved equipment, a glass tube 5 mm in diameter, J. J. Thomson<sup>3</sup> found a velocity nearly half that of light for the velocity of the luminous pulse through a discharge in air at a pressure of 0.5 mm of mercury. Also he was the first to observe that the luminosity did not start simultaneously throughout the length of the tube but it started near the anode and traveled to the cathode at a finite speed, approaching that of light. He measured the velocity of luminosity by uniting the light from two locations along the discharge tube which were several meters apart using a reflecting mirror. Also he experimented with many different electrodes and concluded that the velocity of the

luminosity was independent of the shape, size and material of the electrodes. Because of the absence of an observable Doppler effect in the spectrum lines and the high value of the velocity measured by Thomson, he concluded that the propagation of the luminous pulse was not due to the motion of the emitting atoms and molecules, and their mass motion was negligible. Fowler<sup>4</sup> has concluded that Thomson's observations were not of a breakdown wave but of a return stroke traveling from the anode to the cathode through a preionized region.

Beams<sup>5</sup> called these waves "potential" waves; some have called them breakdown waves. From the examination of the process of formation and distribution of space charge in the tube he proposed a qualitative theory consistent with the observed total lack of heavy particle motion in the wave. He theorized that the electrons are the main element in the wave propagation, and in the neighborhood of the pulsed electrode, due to its shape and irregularities, the field is very high and intense ionization takes place. The large difference in the mobilities (mass difference) of positive ions, negative ions and of electrons was thought to cause the establishment of a space charge. The highest field intensity would be near the pulsed electrode (the electrode to which the potential is applied). This field accelerates the free electrons until they attain enough energy for collisional ionization of the gas near

the electrode. The ionized gas because of being a conductor can not hold internal electric field, thus the potential of the electrode will determine the potential of the ionized region. The highest field intensity was considered to be located at the interface between the ionized gas and the neutral gas. This intense field causes the continuation of this process and propagation of the interface into the neutral gas. This view is consistent with our work on proforce waves.

In recording the results of his experiment he noted that for 40 or 50 cm of the beginning of his discharge tube the velocity of the luminosity was about  $3.8 \times 10^4$  m/sec, but then the velocity of the luminosity increased to  $4 \times 10^7$  m/sec and remained constant for the rest of the tube. He also noted that for a given tube this velocity is determined chiefly by the pressure of the gas and the magnitude of the applied potential. In addition to this initial impulse found in all discharges, he also occasionally observed a second pulse later than the first which started at the ground potential electrode and moved in the opposite direction. This was the kind of propagation that was observed by Allibone and Schonland<sup>6</sup> for a million-volt spark between point and plane. In the lightning stroke the first luminous pulse or "leader" which moves downward in a series of steps with speed averaging  $1 \times 10^7$  m/sec is known as the "stepped" leader. Leaders for strokes over

the same channel after the first discharge has occurred are generally continuous processes, called "dart" leaders.

The average speed for return strokes is about  $1 \times 10^8$  m/sec.

Snoddy, Beams and Dietrich<sup>7</sup> investigated the similarity in the lightning stroke and the observations on the propagation of luminosity in long discharge tubes. They applied potential ranging from 74 to 171 kV into the discharge tube containing gas of pressure 0.017 to 0.24 mmHg. They found that the velocity, voltage attenuation, wave form and energy carried in the wave front of the initial impulse vary with both pressure and applied potential.

A year later Snoddy and his associates<sup>8</sup> reported the results of another experiment in which they used positive and negative impulsive potentials of approximately 125 kV. They noted that in low pressure range the speed of the wave increases with increasing pressure, but at relatively high pressures the speed of the wave decreases and the wave shape is very much distorted. Also they found that the speed of the wave at constant pressure in dry air is approximately a linear function of the applied voltage. The initial wave which starts at the high voltage end of the tube and travels to the ground end is immediately followed by a return stroke starting at the grounded electrode and traveling in opposite sense. Mitchell and Snoddy<sup>9</sup> applied potentials from 25 to 115 kV on the discharge tube containing dry air and hydrogen with pressure range of

0.006 to 8 mmHg. They plotted the ratio of field strength to pressure in the tip of the "potential" discharge ( $E/p$  volts/cm/mmHg) against speed and found that the speed generally increased  $\propto E/p$ , but they derived a theory for increased  $\propto \sqrt{E/p}$ .

Fowler, Paxton and Hughes<sup>10</sup> studied mass motion shocks in ionized gases. They observed that the time required for electrical energy of the capacitor in the discharge tube to be converted to thermal energy of the gas molecules was an order of magnitude larger than that needed for initiation of a shock. Also they observed that the velocity of the luminous front is approximately ( $v^2 \approx kT_e/M$ ), where the  $T_e$  is the electron temperature in the discharge region, with ( $T_e \propto E/p$ ) and they produced an expression for electron energy. Based on their results Fowler and his associates abandoned the idea of a shock driven by hot gas. They hypothesized that electron pressure was the primary source for moving the shock front.

In another work Fowler and Fried<sup>11</sup> argued that the thermal expansion of the hot electron gas accelerates the cold ions, resulting in a shock front or moving electrostatic double layer.

Fowler, Paxton and Hughes also observed that in the gas breakdown in their apparatus, as superfast Beams-type wave moved between the electrodes.

Loeb, Westberg and Huang<sup>12</sup> studied in a point-anode plane-cathode gap with a 2.36-mm hemispherically capped cylinder opposite a 3-cm distant thin out-gassed  $N_i$  plane in the pressure range from 300 mm to 50 mm. They recorded that when the argon is purified in the absence of adequate photoionization the streamer mechanism does not occur. They proposed the necessity of adequate photoionizable impurities in Ar for the development of the filamentary streamer spark transition. In a discharge tube with similar geometry, but separate work, later Loeb<sup>13</sup> hypothesized a qualitative model for breakdown of a gas. In his model, emitted photons from excited atoms excite and ionize new atoms in front of the wave. The newly excited atoms in turn emit photons which continue the process. In this model the wave is moving forward on photo-ionization. This is, however, only one of several possible explanations of their experimental results on gas purity.

The earlier observations by Fowler, Paxton, and Hughes led Paxton and Fowler to formulate a fluid model and theory of breakdown wave propagation. In their model they presumed that near the electrode where the potential gradient in the gas is greatest, ionization of a small quantity of gas occurs and that the electrons produced are given kinetic energy by the electric field. The resulting localized high-temperature electron gas is considered to expand rapidly, thus producing an electron shock wave which

propagates into the undisturbed gas, partially ionizing the overrun neutral gas molecules. The energy necessary for driving the shock wave was considered to be given directly to the electrons in the shock zone by the local electric field. Using a one-dimensional, steady state, three-fluid, hydrodynamical model and assuming that the electron pressure is much greater than the partial pressures of the other species, they were able to write down the equations of conservation of the flux of mass, momentum, and energy:

$$MN_0V_0 = MNV + M_iN_iV_i + mnv ,$$

$$MN_0V_0^2 = MNV^2 + M_iN_iV_i^2 + mnv^2 + nkT_e + \frac{\epsilon_0}{2} (E_0^2 - E^2) ,$$

$$MN_0V_0^3 = MNV^3 + M_iN_iV_i^3 + mnv^3 + 5nkvT_e ,$$

where  $M$ ,  $M_i$ , and  $m$  are the masses of neutral atom, positive ion, and electron respectively, and  $N$ ,  $N_i$ ,  $n$  are the neutral atom, positive ion, and electron densities respectively.  $V$ ,  $V_i$ ,  $v$  were considered as flow velocity of neutral atoms, ions, and electrons and  $T_e$  as electron temperature, and  $E$  as the electric field strength. Quantities in front of the shock zone are designated with a zero subscript, while quantities behind the shock zone have no subscript. They reasoned that, under the quasi-steady-state conditions the change in heavy particle velocities can be neglected and  $V_0=V=V_i$  would be a good approximation. Using a zero current condition ( $nv-N_iV_i=0$ ) and ( $V_0=V=V_i$ ) they were able to find

a relation between  $N_i$  and  $N$  ( $N_i = N_0 - N = fN_0$ ,  $f$  is the degree of ionization in the gas) and they were able to solve the above equations in terms of the remaining variables ( $V_0^2 = 26kT_e/3m$ ). Using the expression that they had derived earlier,<sup>10</sup>  $kT_e = (1/3)(M/3m)^{1/2}\lambda_{eff}eE$ , where  $\lambda_{eff}$  is the effective electron mean free path, they were able to find  $V_0$  and electron density ( $n = 4N_i = 4fN_0$ ). The results listed for hydrogen in a table showed reasonable agreement with experimental data. Their work was important in demonstrating that a one-dimensional, time independent solution of the fluid equations might be applicable to the processes occurring in breakdown tubes, but they overlooked the ionization energy in their energy equation.

Nelson<sup>15</sup> in a criticism of the Paxton-Fowler concept of zero electrical current rejected the treatment of breakdown wave front as an electron shock wave. However, he actually used an identical formulation for current, apparently misunderstanding the nature of the P-F condition. He proposed a photo-ionization model, arguing that the radiation from the hot gas is the driving mechanism and soft x-ray emission due to bombardment of the initiating electrode could also provide a contribution.

In 1962 Fowler and Hood<sup>16a</sup> observed a new wave phenomenon which seemed to possess some unusual properties. They observed a fast-moving precursor in their electrically driven shock tube. They suggested that heat conduction

through the electron gas from the driver might be the major factor responsible for the propagation of a shock-fronted electron precursor wave.

Josephson and Hales<sup>16b</sup> reported appearance of two interesting features in their image converter camera pictures. The first was the presence of luminosity on the expansion wires stretched across their discharge tube, which was in the form of light coming from the tube as early as 0.5 microsecond after gas breakdown. They also mentioned that their fourth wire which was farthest from the discharge showed up as brightly as the wire nearest the discharge, whereas the two wires in between were not visible. The second feature was that a given wire was brightest in the center of the tube, indicating that the source of the light which was coming from the wires was strongly concentrated near the axis of the tube. They reported a speed of  $30 \pm 3$  cm per microsecond for this early luminous front. Based on their observations, they ruled out the idea of photo-ionization, and electrons moving out ahead of the plasma by their higher Maxwellian velocities, to explain this luminous front. They believed that deuterons are accelerated to energies of the order of kilovolts in instabilities that occur in the discharge tube and are observed either by their own impingement on a target or through their ionization electrons. At this time the existence of the electron-fluid dynamic wave was uncertain

and it is probable that that was what they were observing.

Following Fowler and Hood, Haberstich<sup>16c</sup> in his Ph.D. dissertation proposed that his experimental results on the velocity and attenuation of Beams-like waves and on the electron density at the wave front were directly applicable to the study of precursive effects in electrically driven shock tubes. He observed a one-to-one correspondence between the velocity of the wave and the front potential of the proforce waves. Based on the results of his experiment and the results that he obtained by using a one-dimensional theory he confirmed Beam's qualitative explanation of breakdown waves. Mills, Naraghi and Fowler<sup>16d</sup> substantiated this view.

Based on experimental evidence Shelton and Fowler<sup>17</sup> saw the strong probability for luminous pulses being fluid-dynamical phenomena. They argued that a fluid phenomenon involving no mass motion must be due to electron-fluid action. So they thought that the name "electron fluid-dynamical wave" represents a better description of the basic nature of the phenomena. They found that, due to their large inertia, the positive ion's and neutral atom's momentum and energy changes were of comparable magnitude to those of electrons even if the heavy particles had small velocities and could not be neglected. Considering a collision of an electron with arbitrary velocity with an atom at rest (treated as a hard sphere) they used the principle of frame invariance to find analytic forms for

both the elastic and inelastic collision terms in the energy and momentum equations.

They were able to write down the equations for conservation of total momentum and energy, and consequently derived the conditions existent at the leading edge of the wave  $(k(T_e)_1/m) = v_1(V_0 - v_1)$ . Based on these conditions they found a lower limit  $(\frac{1}{2}mV_0^2 \geq e\phi_i)$  on wave speed  $V_0$ , and using the conditions far behind the wave front  $(v \rightarrow V_0, E \rightarrow 0)$ , they found  $n \rightarrow \epsilon_0 E_0^2 / 2e\phi_i$ , which meant the entire pre-wave energy density  $\frac{1}{2}\epsilon_0 E_0^2$  went into ionizing the atoms. In another work Fowler and Shelton<sup>18</sup> developed a general procedure for solving the equations governing the electron gas in breakdown wave. They thought that experimentally observed waves with  $V_0^2 < (2e\phi_i/m)$  must be the second possibility in the initial conditions mentioned in their earlier paper which has  $n=0$  at  $x=0$ , and admits of a discontinuity in  $dn/dx$ . Comparing the calculation of the wave velocity with the experimental data available at that time they found very good agreement. They were able to analyze only one class of electron-fluid waves, the shock-fronted proforce wave (force on the electrons due to electric field is in the direction of wave motion) in one-dimensional, time-independent situations.

Winn<sup>19</sup> called these luminous waves "ionizing waves". He investigated the propagation of such waves into the neutral and pre-ionized gases. Experimenting on  $N_2$  he reported

the velocity increase from  $1 \times 10^7$  m/sec at zero density to around  $7 \times 10^7$  m/sec at a density of  $3 \times 10^9$  /cm<sup>3</sup>. He also reported the velocity dependence upon the magnitude of the voltage pulse, pressure, and the diameter of the coaxial shielding surrounding the glow-discharge tube. He observed that the shape of the wave front depended on the electron density, but it was more strongly affected by the pressure. He reported three differences between positive waves (waves originating from, i.e. traveling away from, a positive electrode) and negative waves, the major difference was that the velocities of positive waves depended more strongly on the initial electron density. Revising a technique used by Haberstich, Blais and Fowler<sup>20</sup> studied wave speed, and electron temperature and density behind the wave front. The measurements were carried out in helium at applied electrode voltages from 6 to 42 kV of both polarities and over a pressure range of 0.3 to 30.0 torr. They obtained good overall agreement with the theory of Shelton.

Klingbeil, Tidman and Fernsler<sup>21</sup> discussed a solution technique for antiforce problem, but concluded that no solution for the antiforce case exists without photoionization. Sanmann and Fowler<sup>22</sup> showed that a steady profile theory on the antiforce waves (electron mobility motion is in the opposite direction of wave advance) could be obtained from the basic equations developed by Shelton. Of the six

equations used by Shelton and Fowler, they employed five: those which represent conservation of heavy particle and of charge, balancing of electrons and electron momentum, and Poisson's equation. They avoided using the energy equation, because at the point where electron velocity became equal to wave velocity the energy equation resulted in negative temperature which was not acceptable. They included ion momentum terms in their equations arguing that, for proforce waves, the field dropped to zero too quickly to contribute velocity, momentum, or energy to the ions, but for antforce waves, the heavy particles had time to act as an energy sink. They thought that it was the slight difference in velocity,  $V_i - V_e$ , between the ions and neutrals, which permitted a solution for antforce waves. Their predicted velocities for the antforce waves that were in good agreement with the data of Blais and Fowler.<sup>20</sup>

Scott and Fowler<sup>23</sup> used the Blais apparatus to make extensive studies of initial breakdown wave speed in nitrogen and argon as a function of local electric field at the wave front. Their results were in basic agreement with the electron fluid dynamic theory of the phenomenon. They suggested that the success of the Klingbeil et al.<sup>21</sup> theory at low energies was due more to the electron pressure component introduced through the energy equation and coupled with a correct ionization statement than to photo ionization, while its failure at very large velocities was due to their admitted neglect of the electron's

kinetic energy. They thought that it was possible, even probable, that the peculiar constant velocity antiferce waves observed at very low gas densities might be propagated by photoionization processes.

In the present work computer solution of the electron fluid-dynamical equations for both proforce and antiferce waves with or without a current has been investigated extensively, resulting in improvements in their formulation, and in the understanding of the conditions under which solutions are possible. Also we have investigated the propagation of these waves into a pre-ionized medium. The most significant new discovery is the importance of heat conduction, even up to the shock front of the wave.

### CHAPTER III

#### THE BASIC EQUATIONS AND EARLY APPROACHES FOR THEIR SOLUTION

The purpose of this work is to find out whether the fluid-dynamical equations do possess solutions describing fast-moving electron waves which are very similar to breakdown waves. The three-component fluid equations will be the basis for investigating the problem of ionizing waves in the breakdown tubes. Following Shelton we first derive the basic equations of conservation of mass, momentum, and energy for a multifluid system consisting of neutral atoms, positive ions, and electrons subjected to an electric field  $E$  (applied field plus space charge field) applied in the negative  $x$  direction. The force on the electrons due to the applied electric field would be in the direction of wave propagation (proforce wave). The ionizing wave is an infinite plane wave which, in the laboratory, is traveling in the positive  $x$  direction with speed  $V_0$ . The equation of conservation of mass<sup>24</sup> for any component of the fluid could be derived by equating the time rate of change of the number density of the particles within a volume element with the sum of the particles created or lost within that volume per unit time, and

fluxes of particles through the surface of that volume.

$$\frac{\partial n}{\partial t} dx dy dz = \beta n dx dy dz + n v dy dz - \left( n + \frac{\partial n}{\partial x} dx \right) \left( v + \frac{\partial v}{\partial x} dx \right) dy dz,$$

where  $\beta n dx dy dz$  is the number of particles created in  $dV$  per second,  $n v dy dz$  is the particle flux into  $dV$ , and  $\beta$  is the ionization frequency (number of ionizations per unit volume per second per electron).  $\beta$  is given by  $\langle \sigma_i v' N \rangle$  where  $\sigma_i$  is the ionization cross section and the bracket is an average over the electron velocity ( $v'$ ) distribution. A constant mass term has been factored out of the above equation. The equation reduces to

$$\frac{\partial n}{\partial t} + \frac{\partial (nv)}{\partial x} = \beta n . \quad (1)$$

The equation of conservation of momentum for electrons can be derived in a similar fashion.

$$\begin{aligned} \frac{\partial}{\partial t} (mnv) dx dy dz &= mnv^2 dy dz - m \left( n + \frac{\partial n}{\partial x} dx \right) \left( v + \frac{\partial v}{\partial x} dx \right)^2 dy dz \\ &- enE dx dy dz - \Delta_e (mv) dx dy dz + \Delta_i (mv) dx dy dz \\ &+ \left( p_e - \left( p_e + \frac{\partial p_e}{\partial x} dx \right) \right) dy dz , \end{aligned}$$

where the third, fourth, fifth, and sixth terms on the right hand side are volume force due to electric field, elastic momentum loss to heavy particles, inelastic momentum gain from heavy particles, net force on  $dV$  due to pressure gradient. The above equation simplifies to

$$\frac{\partial}{\partial t} (mnv) + \frac{\partial}{\partial x} (mnv^2 + p_e) = -enE - \Delta_e (mv) + \Delta_i (mv) . \quad (2)$$

Similarly, the equation of conservation of energy for electrons would be

$$\begin{aligned} \frac{\partial}{\partial t}(\frac{1}{2}mnv^2+w_e) dx dy dz &= \frac{1}{2}mnv^3 dy dz - \frac{1}{2}m(n + \frac{\partial n}{\partial x} dx)(v + \frac{\partial v}{\partial x} dx)^3 dy dz \\ &+ (w_e v - (v + \frac{\partial v}{\partial x} dx)(w_e + \frac{\partial w_e}{\partial x} dx)) dy dz \\ &- env E dx dy dz + (p_e v - (p_e + \frac{\partial p_e}{\partial x} dx)(v + \frac{\partial v}{\partial x} \\ &dx)) dy dz - \Delta_e(\frac{1}{2}mv^2) dx dy dz + \Delta_i(\frac{1}{2}mv^2) dx dy dz. \end{aligned}$$

The third term on the right-hand side is the internal energy flux into the volume element, the fifth term is the work done against the electron pressure as the particles flow through the volume element, and  $w_e$  is the internal energy density of electrons (energy/volume). The energy equation reduces to

$$\frac{\partial}{\partial t}(\frac{1}{2}mnv^2+w_e) + \frac{\partial}{\partial x}(\frac{1}{2}mnv^3+(p+w_e)v+q_e) = -envE - \Delta_e(\frac{1}{2}mv^2) + \Delta_i(\frac{1}{2}mv^2). \quad (3)$$

In the above equations  $q_e$  is the electron heat conduction term and  $p_e$  is the electron pressure.  $\Delta_e(mv)$  is the momentum transfer operator due to elastic collision from electron to heavy particles, and  $\Delta_i(\frac{1}{2}mv^2)$  is the energy transfer operator due to inelastic collision from heavy particles to electrons.  $e$  denotes the absolute charge of an electron.

The equations for conservation of mass, momentum, and energy for heavy particles (positive ions and neutral

atoms) can be derived by using the same arguments. Since the electrons are the main element in the wave propagation, the electron production, momentum, and energy equations would be our main concern. The ion and neutral atom momentum and energy equations would be combined.

$$\frac{\partial N_i}{\partial t} + \frac{\partial}{\partial x} N_i V_i = \beta n , \quad (4)$$

$$\frac{\partial N}{\partial t} + \frac{\partial}{\partial x} NV = -\beta n , \quad (5)$$

$$\frac{\partial}{\partial x} (M_i N_i V_i + MNV) + \frac{\partial}{\partial x} (M_i N_i V_i^2 + MNV^2 + P_i + P) = eN_i E + \Delta_e (mv) - \Delta_i (mv) \quad (6)$$

$$\begin{aligned} \frac{\partial}{\partial x} \left( \frac{1}{2} M_i N_i V_i^2 + \frac{1}{2} MNV^2 + W_i + W \right) + \frac{\partial}{\partial x} \left( \frac{1}{2} M_i N_i V_i^3 + \frac{1}{2} MNV^3 + V_i (P_i + W_i) + V(P+W) \right. \\ \left. + Q_i + Q \right) = eN_i V_i E + \Delta_e \left( \frac{1}{2} mv^2 \right) - \Delta_i \left( \frac{1}{2} mv^2 \right) , \quad (7) \end{aligned}$$

where  $M$ ,  $N$ ,  $V$ ,  $P$ ,  $W$ ,  $Q$  are neutral atom mass, density, velocity, pressure, internal energy, and heat conduction respectively. Fowler<sup>25</sup> has revised the Shelton<sup>24</sup> calculation of the transfer operators for energy and momentum in an unpublished paper and the results are:

$$\Delta_e \left( \frac{1}{2} mv^2 \right) = \left( \frac{2m}{M} \right) n \sigma_0 N \left\{ \frac{3}{2} kT_e + \left( \frac{m}{2} \right) (v-V)^2 \right\} + n \sigma_0 N m V (v-V) , \quad (8a)$$

$$\Delta_e (mv) = n m \sigma_0 N (v-V) , \quad (8b)$$

$$\Delta_i (mv) = \beta m n V , \quad (8c)$$

$$\Delta_i^e \left( \frac{1}{2} mv^2 \right) = \frac{1}{2} m n \beta V^2 - \beta n e \phi_i , \quad (8d)$$

$$\Delta_i^n \left( \frac{1}{2} mv^2 \right) = \frac{1}{2} \beta m n V^2 . \quad (8e)$$

In the equations above  $\Delta_i^e(\frac{1}{2}mv^2)$  is the energy transfer operator for inelastic collisions from heavy particles to electrons, and  $\Delta_i^n(\frac{1}{2}mv^2)$  is the energy transfer operator for inelastic collisions from heavy particles to the neutrals.  $\sigma_0 N$  has the dimensions of 1/sec and denotes a collision frequency, and  $e\phi_i$  is the energy required to ionize a neutral atom. Writing  $K_1 = \sigma_0 N$ ,  $\Delta_e(\frac{1}{2}mv^2)$  and  $\Delta_e(mv)$  become:

$$\Delta_e(\frac{1}{2}mv^2) = \left(\frac{2m}{M}\right)nK_1\left(\frac{3}{2}kT_e + \left(\frac{m}{2}\right)(v-V)^2\right) + K_1 mnV(v-V) \quad (9a)$$

$$\Delta_e(mv) = mnK_1(v-V) \quad (9b)$$

The terms of order  $2m/M$  are small in most portions of the wave and were neglected by Shelton and by Sanmann.

Ionization of a neutral atom creates a pair of ion and electron, and the electron will have the kinetic energy it possessed before the collision, which is  $\frac{1}{2}mV^2$ . For an electron gas with number density  $n$  and ionization frequency of  $\beta$ , there will be  $\frac{1}{2}\beta nmV^2$  kinetic energy added to the electron gas because of neutral atom ionization. On the other hand, any electron ionizing an atom takes an amount of energy  $e\phi_i$  from the electron gas.

Therefore creation of  $\beta n$  electrons will require a supply of energy of  $\beta ne\phi_i$  from the electron gas. We assume that the electrons, neutral atoms, and ions behave like perfect gas so their internal energy densities  $w_e$ ,  $W$ ,  $W_i$  would be  $\frac{3}{2}nkT_e$ ,  $\frac{3}{2}NkT$ , and  $\frac{3}{2}N_i kT_i$ , respectively.

An observer watching a steady-profile wave from a reference frame traveling with the wave, would see a fixed wave structure with no time variation. So in the wave frame (reference frame moving along with the wave), a steady-profile wave has no time dependence. The absence of an experimentally observed Doppler shift indicates that neither ions nor the neutrals have appreciable motion in the laboratory and, based on this the velocity of ions and neutrals can be assumed to be equal. We define the positive x-direction of our frame of reference to be the direction of propagation of the wave. It has been reported and agreed by all the experimenters that the electron fluid-dynamical waves move from the electrode to which the potential is applied (high voltage electrode) toward the electrode maintained at ground potential regardless of the polarity of the impressed pulse. The reason for such a behaviour is that near the electrode with higher voltage there would be a strong electric field created. This electric field forces the electrons away from the discharge electrode toward the grounded electrode. Therefore, the positive x-direction will be in the direction of discharge electrode toward the grounded electrode. Therefore, if the electron fluid-dynamical wave front has a laboratory velocity  $V$ , the heavy particles will have a velocity  $-V$  in the wave frame. Taking all the points mentioned above into consideration, the equations of production, momentum trans-

transfer, and energy transfer for electrons, ions and neutral atoms will be:

$$\frac{\partial(nv)}{\partial x} = \beta n , \quad (10)$$

$$\frac{\partial(N_i V_i)}{\partial x} = \beta n , \quad (11)$$

$$\frac{\partial(NV)}{\partial x} = -\beta n , \quad (12)$$

$$\frac{\partial}{\partial x} (mnv^2 + nkT_e) = -enE - K_1 mn(v - V) + \beta mnV , \quad (13)$$

$$\frac{\partial}{\partial x} (M_i N_i V^2 + MNV^2 + N_i kT_i + NkT) = eN_i E + K_1 mn(v - V) - \beta mnV , \quad (14)$$

$$\frac{\partial}{\partial x} (\frac{1}{2} mnv^3 + \frac{5}{2} nvkT_e + q_e) = -envE - K_1 mnV(v - V) + \frac{1}{2} \beta mnV^2 - \beta ne\phi_i , \quad (15)$$

$$\frac{\partial}{\partial x} (\frac{1}{2} M_i N_i V^3 + \frac{1}{2} MNV^3 + \frac{5}{2} N_i V kT_i + \frac{5}{2} NVkT + Q_i + Q) = eN_i VE + K_1 mnV(v - V) - \frac{1}{2} \beta mnv^2 . \quad (16)$$

Now we will investigate the nature of the current in the electron fluid-dynamical waves. For this purpose we use the complete one-dimensional production equations for electrons and ions. Subtracting equation (1) from equation (4) and multiplying the result by  $e$  gives:

$$\frac{\partial}{\partial t} (e(N_i - n)) + \frac{\partial}{\partial x} (e(N_i V - nv)) = 0 .$$

Using the Poisson equation ( $\vec{\nabla} \cdot \vec{E} = p/\epsilon_0 = e(N_i - n)/\epsilon_0$ ) in the above equation, it reduces to

$$\frac{\partial}{\partial x} (\epsilon_0 \frac{\partial E}{\partial t} + e(N_i V - nv)) = 0 ,$$

$\epsilon_0$  is the permittivity in the MKS system. Integrating the

above equation, it reduces to

$$\epsilon_0 \frac{\partial E}{\partial t} + e(N_i V - nv) = i_0(t) , \quad (17)$$

which indicates that the total current, convection plus displacement is independent of the position. For the moment we assume that there is no convection current in front of the wave because it is moving into an unionized gas. Also since the electric field at the wave front is constant and equal to  $E_0$ , then equation (17) in the wave frame of a steady-profile wave will reduce to

$$e(N_i V - nv) = 0 . \quad (18)$$

This is called the zero current condition. It is the total current,  $i_0(t)$  which is zero. Equation (18) is true in the wave frame of a steady-profile wave, providing that the electron fluid-dynamical wave is moving into a neutral gas, because it has been derived from the basic fluid equations. In a stationary frame with no current and no applied or self-generated magnetic fields, the only equation remaining from Maxwell's equation is Poisson's equation:

$$\frac{\partial E}{\partial x} = \frac{e}{\epsilon_0} (N_i - n) . \quad (19)$$

Since the ions and neutral atoms have almost the same mass and stay in equilibrium during the passage of electron fluid-dynamical waves, we can assume their temperature to be the same ( $T_i = T$ ). At first we neglect the heat conduction term in the electron energy equation. The Poisson equation

with its new form found by use of the zero current condition, and equations of production, momentum transfer, and energy transfer form a set of equations which depend only on variables describing electron behavior inside the electron fluid-dynamical wave, and wave velocity. To simplify the equations further, we substitute  $d(nv)/dx$  in the momentum and energy equations for  $\beta n$ , from the production equation.

$$\frac{d(nv)}{dx} = \beta n , \quad (20)$$

$$\frac{dE}{dx} = \frac{e}{\epsilon_0} n \left( \frac{v}{V} - 1 \right) , \quad (21)$$

$$\frac{d}{dx} \{ mnv(v-V) + nkT_e \} = -enE - K_1 mn(v-V) , \quad (22)$$

$$\frac{d}{dx} \{ mnv(v^2 - V^2) + 5nvkT_e + 2e\phi_i nv \} = -2envE - 2K_1 mnV(v-V) , \quad (23)$$

and the ion-neutral momentum and energy equations become:

$$\frac{d}{dx} (MNV^2 + M_i N_i V^2 + (N + N_i) kT) = eN_i E + K_1 mn(v-V) - \beta mnV \quad (24)$$

$$\frac{d}{dx} (MNV^3 + M_i N_i V^3 + 5(N + N_i) V kT) = 2eN_i VE + 2VK_1 mn(v-V) - \beta mnV^2 . \quad (25)$$

It is more convenient to work with the electron fluid-dynamical equations in a non-dimensional form. Therefore we introduce the following dimensionless variables:

$$v = \frac{2e\phi_i}{\epsilon_0 E_0^2} n , \text{ the reduced electron density.}$$

$$\mu = \frac{\beta}{K_1} .$$

$$\psi = \frac{v}{V} , \text{ the reduced electron velocity.}$$

$\theta = \frac{kT_e}{2e\phi_i}$  , the reduced electron temperature.

$\eta = \frac{E}{E_0}$  , the reduced electric field.

$j = v\psi$  , the reduced electron current.

$\xi = \frac{eE_0}{mV^2} x$  , the reduced position variable.

We also define the following parameters:

$$\alpha = \frac{2e\phi_i}{mV^2} ,$$

$$\kappa = \frac{mV}{eE_0} K_1 ,$$

$$\mu = \frac{\beta}{K_1} .$$

The definitions of  $\theta$  and  $\mu$  have been changed from those used by Shelton. Shelton used  $\theta = (kT_e/mV^2)$  as dimensionless electron temperature variable, where  $kT_e$  is the electron's thermal energy, and  $mV^2$  is the kinetic energy of the electron traveling at wave velocity. However, the ionization process requires an amount of energy  $e\phi_i$  for each electron ion pair creation. Therefore,  $(kT_e/2e\phi_i)$  will represent  $1/3$  ( $3/2 kT_e/e\phi_i = n_\infty$ ) the number of electrons which could be created with the initial electron's thermal energy. Using the dimensionless variables the system of equations become:

$$\frac{d(v\psi)}{d\xi} = \kappa\mu v , \quad (26)$$

$$\frac{d\eta}{d\xi} = \frac{v}{\alpha} (\psi - 1) , \quad (27)$$

$$\frac{d}{d\xi} \{ \nu\psi(\psi-1) + \alpha\nu\theta \} = -\nu\eta - \kappa\nu(\psi-1) , \quad (28)$$

$$\frac{d}{d\xi} \{ \nu\psi(\psi^2-1) + \alpha\nu\psi(5\theta+1) \} = -2\nu\psi\eta - 2\kappa\nu(\psi-1) . \quad (29)$$

Now let us examine the structure of electron fluid-dynamical waves, and electron motion under the applied field. The force due to the applied field tends to accelerate the electrons in the positive x-direction. The excess electrons near the wave front will create a space charge field opposing the applied field. The relative motion between electrons and ions will be opposed by resistive forces which are presented as  $\Delta$  operators in the conservation of momentum and energy equations. These opposing forces tend to equalize the electron and ion velocities, which will happen when the electric field (applied field plus charge field) falls to zero. The velocity of electrons decreases from its initial value ( $v_1$  at the wave front) toward  $V$  ( $V < 0$ ). From Poisson's equation (21), the electric field increases from its negative value  $E_0$  at the wave front to its final value zero as  $dE/dx$  goes to zero when electron velocity approaches the ion-neutral velocity in the quasi-neutral region. The wave front can not be marked by a sudden change in the electric field because a discontinuity in the electric field results from a surface charge, or from an infinite volume charge density at the wave front, so the electric field has to be equal to  $E_0$  at the wave front. As long as the electrons have sufficient thermal energy to

ionize neutral atoms, ionization in the quasi-neutral region will continue.

In solving the electron fluid-dynamical equations, Shelton<sup>24</sup> was able to derive the conditions existent at the leading edge of the wave. We have used these initial conditions in our early approaches for solving the equations. These conditions could be derived from the equations for conservation of total momentum and energy. One can find the equation of conservation of baryons by adding the equations (11) and (12), integrating, and taking into consideration that there are only neutral atoms with number density  $N_0$  and velocity  $V_0$  ahead of the wave. Also assuming  $V=V_i$  this equation becomes:

$$(N + N_i)V = N_0V_0 . \quad (30)$$

Using equation (30) and  $(M-m)$  for  $M_i$ , in equations (24) and (25) one can find a different form for equations of conservation of momentum and energy for heavy particles,

$$\frac{d}{dx} \{ MVN_0V_0 - N_i mV^2 + (N+N_i)kT \} = eN_i E + K_1 mn(v-V) - \beta nmV , \quad (31)$$

$$\frac{d}{dx} (MV^2N_0V_0 - N_i mV^3 + 5N_0V_0kT) = 2eN_i VE + 2VK_1 mn(v-V) - \beta nmV^2 . \quad (32)$$

Adding equations (13) and (31), using Poisson's equation, and integrating the resultant integrable expression results in the equation of the total conservation of momentum:

$$nmv^2 + nkT_e + MN_0V_0V - mN_iV^2 + (N+N_i)kT = \frac{\epsilon_0}{2}E^2 + C . \quad (33)$$

Adding equations (15) and (32) with the heat conduction term neglected, using the zero current condition and equation (10), and integrating the resultant integrable expression results in the equation of the total conservation of energy:

$$mnv^3 + MN_0V_0V^2 - mN_iV^3 + 5nkvT_e + 5N_0V_0kT + 2nve\phi_i = C' . \quad (34)$$

Equations (33) and (34) are the global (all particle) momentum and energy equations respectively, for a three component gas composed of electrons, ions, and neutral atoms. C and C' are constants of integration to be determined by conditions ahead of the wave ( $E=E_0$ ,  $V=V_0$ ,  $n=n_0=0$ ,  $N_i=N_{i0}=0$ ,  $N=N_0$ ). Using the values of C and C' calculated ahead of the wave and zero current condition in equations (33) and (34), one will find:

$$mnv^2 + nkT_e + MN_0V_0(V-V_0) - mnvV + N_0k(T-T_0) - \frac{\epsilon_0}{2}(E^2 - E_0^2) = 0 , \quad (35)$$

$$mnv^3 + MN_0V_0(V^2 - V_0^2) - mnvV^2 + 5nkvT_e + 5N_0V_0k(T-T_0) + 2nve\phi_i = 0 . \quad (36)$$

At the wave front, due to their large mass, the change in heavy particles temperature and velocity are negligible ( $V=V_0$ ,  $T=T_0$ ). At the wave front the electrons will have a temperature of  $(T_e)_1$  and velocity  $v_1$ , and the equations (35) and (36) take the form:

$$n_1(v_1(v_1 - V_0) + \frac{k(T_e)_1}{m}) = 0 . \quad (37)$$

$$n_1v_1(v_1^2 - V_0^2 + 5 \frac{k(T_e)_1}{m} + \frac{2e\phi_i}{m}) = 0 . \quad (38)$$

Shelton thought that the case  $n_1=0$  which results in continuous solution might describe antiproforce waves. The second way to satisfy equations (37) and (38) is to require  $n_1 \neq 0$ . This results in discontinuous or shock solutions which he showed describe proforce waves only. Solving equations (37) and (38) for  $(T_e)_1$  and  $v_1$  gives

$$v_1 = \frac{5V_0}{8} \pm \frac{\{9V_0^2 + 16(\frac{2e\phi_1}{m})\}^{\frac{1}{2}}}{8}, \quad (39)$$

$$\frac{k(T_e)_1}{m} = v_1(V_0 - v_1). \quad (40)$$

Since the zero current condition requires  $V_0$  and  $v$  to have the same sign and since  $(T_e)_1$  has to be positive, one can determine that  $|v_1| < |V_0|$ . Using these conditions on equation (39) led Shelton to taking the negative sign in it and conclude that  $\frac{1}{2}mV_0^2 \geq e\phi_1$ . This imposes a lower limit on wave speed. The initial conditions expressed in terms of the dimensionless variables take the form

$$n_1 = 1 ; v_1 \neq 0 ,$$

$$\alpha\theta_1 = \psi_1(1 - \psi_1) , \quad (41)$$

$$\psi_1 = \frac{5 - \sqrt{9 + 16\alpha}}{8} ,$$

at the leading edge of the wave, and

$$n_2 = 0 ; (n')_2 = 0 ; \psi_2 = 1$$

at the trailing edge of the wave.

A different form for the energy and momentum equations which can be derived will be employed in the rest of this work. Multiplying equation (28) by 2, subtracting the result from equation (29), and using Poisson's equation results in the new energy equation. Also using the Poisson equation with the momentum equation would provide the new form of the momentum equation.

$$\frac{d}{d\xi} \{j(\psi - 1) + \alpha v \theta + \alpha \kappa \eta\} = -v \eta , \quad (42)$$

$$\frac{d}{d\xi} \{j(\psi - 1)^2 + \alpha v \theta (5\psi - 2) + \alpha j + \alpha \eta^2\} = 0 . \quad (43)$$

CHAPTER IV  
CLASS I PROFORCE WAVES

Fowler<sup>26</sup> divided electron waves into three categories:

- Those waves which move into a medium of substantially zero electron concentration were called Class I waves.
- Those waves which move into a medium of significant electron concentration were called Class II waves.
- Those waves which did not fulfill the zero-current condition were called Class III waves.

Our initial attempt at direct solution of the electron fluid equations (26-29) for Class I proforce waves was to use  $\eta$  as our integrating variable. This was not possible integrating either forward or backwards across the sheath because  $v$  is not known. Next, we chose  $j = v\psi$  as our integrating variable and tried to integrate backwards believing that the electron fluid equations should apply over both the quasi-neutral region and the sheath. We chose our initial conditions as  $\psi_2 = 1$ ,  $n_2 = 0$ ,  $j_2 = 1$ ,  $\theta_2 = \theta_\infty$ . This also failed without any result. It became evident that selection of  $\xi$  as integrating variable was the only logical approach. By using the initial condition on  $\theta$ , we

found<sup>27</sup> the integrating form of the set of the electron-fluid equations as:

$$\begin{aligned}\frac{dj}{d\xi} &= \frac{\kappa\mu j}{\psi}, \\ \frac{d\eta}{d\xi} &= \frac{j}{\alpha} \left( \frac{1}{\psi} - 1 \right), \\ \frac{dI}{d\xi} &= \frac{j\eta}{\alpha\psi}, \\ \theta &= \frac{\psi}{\alpha} (1 - \psi) + \frac{\psi(\kappa(1 - \eta) - I)}{j},\end{aligned}\tag{44}$$

$$4\psi^2 - 5\psi \left\{ 1 + \frac{\alpha}{j} (\kappa(1 - \eta) - I) \right\} + 1 + \frac{2\alpha}{j} (\kappa(1 - \eta) - I) - \alpha \left( 1 + \frac{\eta^2 - 1}{j} \right) = 0.$$

Now we had to solve a doubly branched quadratic equation for  $\psi$  which admits to solutions only under restricted conditions. To obtain a solution one must select the values of  $v_1$  and  $\kappa$  to cause the branches to meet in a horizontal tangent, and then change branches. This requires many iterative integrations. However, when found, the solution still does not converge to  $\eta=0$  at  $\psi=1$ . For the nearest approach to a solution we were able to find  $\eta$  changed sign at  $\psi=0.94$  for  $\alpha=0.01$ ,  $v_1=0.036523$ ,  $\psi_1=0.2466$ , and  $\kappa=1.3$ . The  $\eta$  versus  $\psi$  curve was like path (2) in the  $(\psi, \eta)$  plane shown in Figure 1, although the most desirable result would be something like path A. Figure 2 gives electric field ( $\eta$ ) as a function of drift velocity  $\psi$ , and Figure 3 gives temperature ( $\theta$ ), electron density ( $v$ ), and ionization rate ( $\mu$ ) as a function of position ( $\xi$ ).

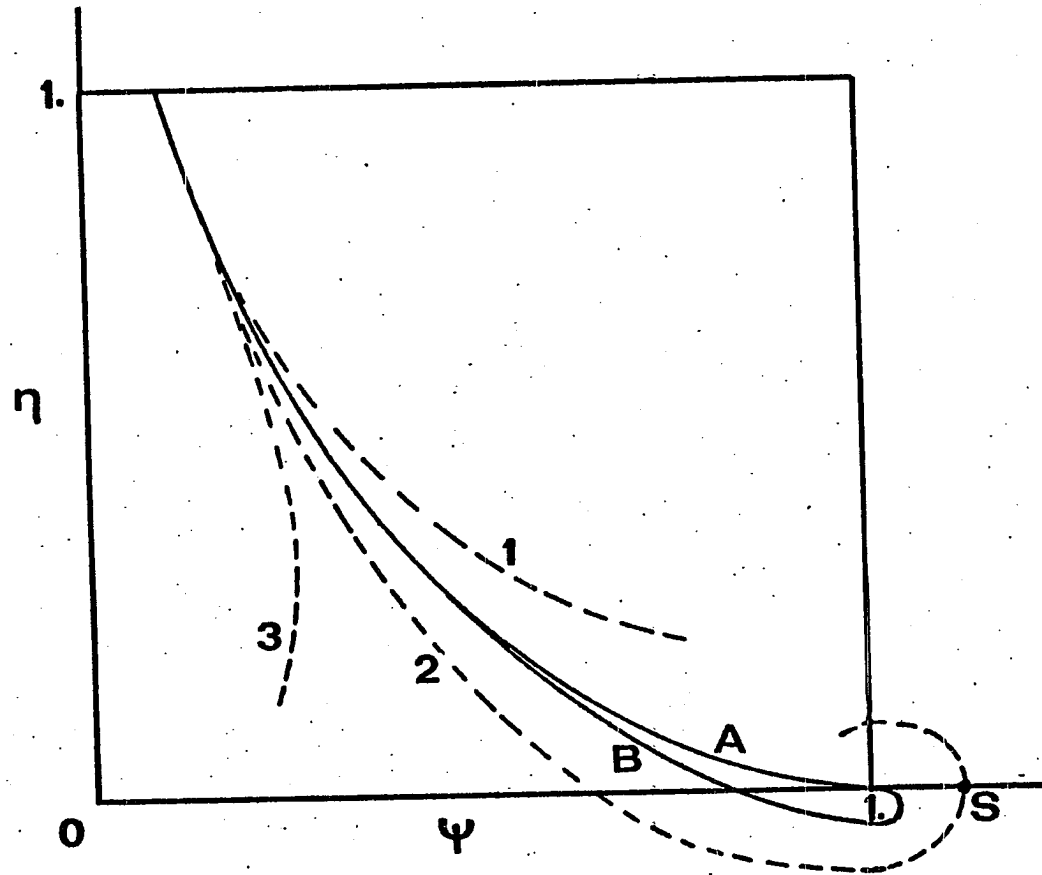


Figure 1. Electric field ( $\eta$ ) as a function of drift velocity ( $\psi$ ).

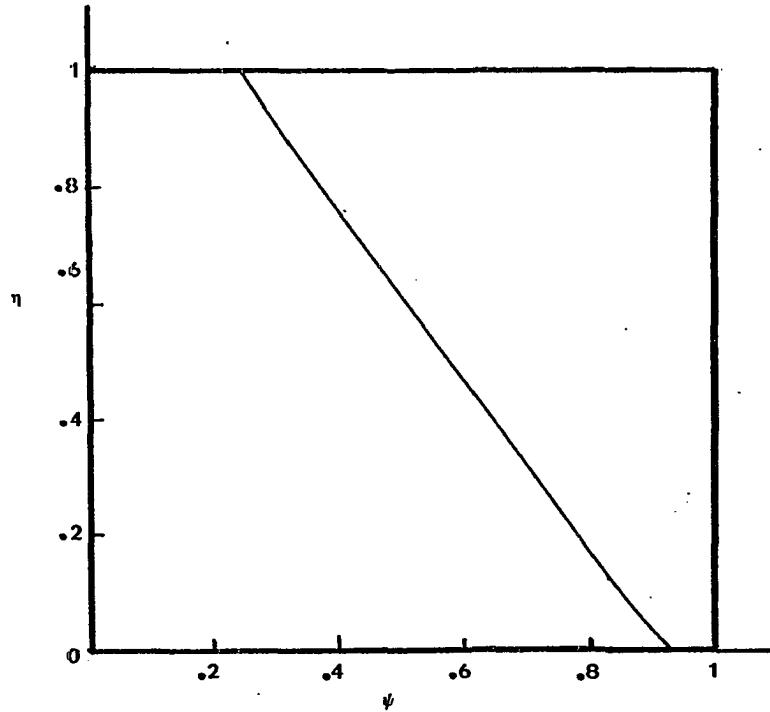


Figure 2. Electric field ( $\eta$ ) as a function of drift velocity ( $\psi$ ).

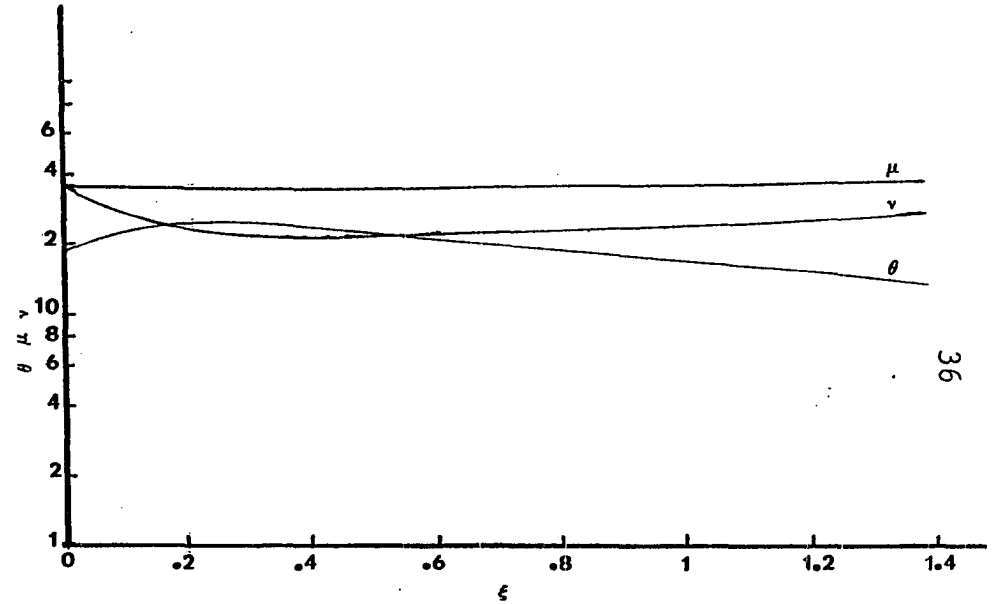


Figure 3. Temperature ( $\theta$ ), electron density ( $v$ ), and ionization rate ( $\mu$ ) as a function of position ( $\xi$ ). Scale factors: For  $v$  divide  $y$  by  $10^3$ , for  $\mu$  divide  $y$  by  $10^2$ .

Shelton assumed that  $\mu$  was constant, and later Fowler plotted  $\mu$  as a function of  $\theta$  which was reproduced by Sanmann.<sup>27</sup> This function changes from acceleration ionization at the wave front through directed velocity ionization in the intermediate stages to thermal ionization at the trailing edge of the wave. We replaced the assumption of ionization rate being only a function of temperature by a computation based on free trajectory theory by Fowler (see Appendix) which includes ionization from both random and directed electron motions according to the expression

$$\mu = \mu_0 \int_{1/\sqrt{2\theta}}^{\infty} \sigma_i z^2 \int_B^{\infty} \frac{e^{-(z-u)^2} - e^{-(z+u)^2}}{u} du e^{-2Cu} , \quad (45)$$

where  $B=(1-\psi)/\sqrt{2\alpha\theta}$  and  $C=\kappa\sqrt{2a\theta}/\eta$ .

The approximate solution obtained by Fowler and Shelton<sup>18</sup> was based on an assumed power law relation between  $\eta$  and  $\psi$  of the form:

$$\eta = \left( \frac{1 - \psi}{1 - \psi_1} \right)^a . \quad (46)$$

Integrating the energy equation (43) across the sheath provided them with an algebraic equation of the form

$$j(\psi-1)^2 + \alpha v(5\psi-2)\theta + \alpha j - \alpha(1-\eta^2) = 0 . \quad (47)$$

Using  $\eta$  as independent variable, and shock condition (41), closed form solution was possible. The energy equation (47) was redundant in the sheath because of the assumed  $\eta, \psi$

relation and was only used to avoid the temperature singularity at  $\psi=0.4$ . We maintained contact with this approximation type of solution by using the slope  $d\eta/d\psi$  of the exact solution at  $\psi=\psi_1$  to find an  $\underline{a}$  for Shelton's approximate solution. It was remarkable how little these solutions differed from the computed solution of equations (44) except at the end point. This again showed the general validity of the Shelton equations and led us now to investigate whether the neglected second order terms such as heat conduction and ion momentum might play a role in the fitting of the solution to the final states of  $\eta$  and  $\psi$  ( $\eta_2=0, \psi_2=1$ ).

The first correction term that we considered was addition to the energy equation of a heat conduction term which had been assumed to be small. Heat conduction is proportional to the gradient of temperature, and according to Fourier's law of heat conduction, the heat conduction  $q$  is

$$q = -K_T \frac{dT}{dx} ,$$

where  $T$  is the temperature, and  $K_T$  is the coefficient of thermal conduction. The heat conduction coefficient takes the standard form  $-(5/2)(k^2 n T / m K_1)(dT/dx)$ , and when multiplied by 2 inside the energy equation and in terms of dimensionless variables becomes:

$$- \frac{5\alpha^2 v \theta}{\kappa} \frac{d\theta}{d\xi} . \tag{48}$$

The heat conduction term must be added inside the bracket on the left side of the energy equation (43). Integrating

equation (43) across the sheath results in a differential equation for  $\theta$  which must be integrated. The momentum equation became a quadratic equation for  $\psi$  with the same branch transition problem as before. The new equation for calculation of  $\theta$  was

$$\frac{d\theta}{d\xi} = \frac{\kappa\psi}{5\alpha^2\theta} \{(\psi-1)^2 + (5\psi-2)\frac{\alpha\theta}{\psi} + \alpha - \alpha(1-\eta^2)/v\psi\} \quad (49)$$

Introduction of the heat conduction term alone in the energy equation with the regular initial conditions produced an even earlier sign change of  $\eta$  at about  $\psi=0.78$ . It was the largest value of  $\psi$  which could be achieved, with  $\kappa=0.7$ ,  $v_1=0.04657$ . Figure 4 gives  $\eta$  as a function of  $\psi$ , and Figure 5 gives  $\theta$ ,  $\mu$ ,  $v$  as a function of  $\xi$ .

The next correction to be considered was ion momentum which must be added to the energy equation. Sanmann and Fowler<sup>22</sup> showed that when approaching the energy equation by writing the global momentum and energy equations, each contains the heavy particle temperature change and the ion momentum change in the field as unknown. To obtain an energy equation, one has his choice of eliminating either heavy particle temperature change or ion momentum change and then evaluating the other. Shelton argued that the temperature change was negligible, but ion momentum change was significant, though small. Since both ion momentum change and heavy particle temperature change were difficult to evaluate, and interfered with the approximate

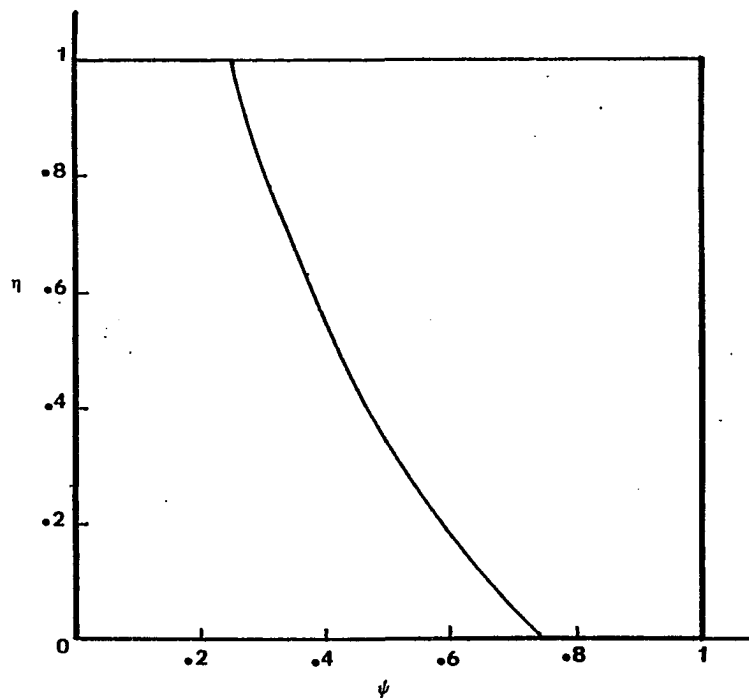


Figure 4. Electric field ( $\eta$ ) as a function of drift velocity ( $\psi$ ).

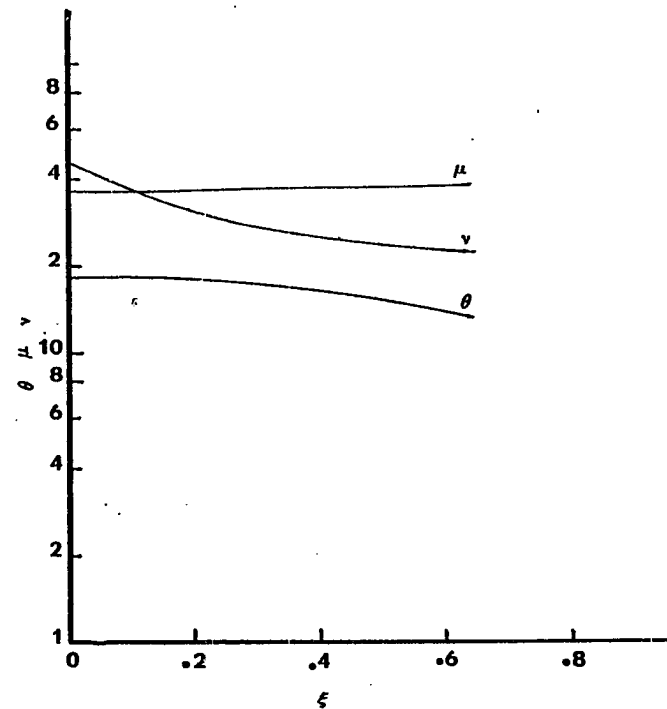


Figure 5. Temperature ( $\theta$ ), electron density ( $\nu$ ), and ionization rate ( $\mu$ ) as a function of position ( $\xi$ ). Scale factors: For  $\nu$  divide  $y$  by 10, for  $\mu$  divide  $y$  by  $10^2$ .

solution, he chose to ignore the temperature change term and eliminate the ion momentum change. Since then it has been possible to derive expressions representing these changes, but heavy particle temperature change has two parts: elastic loss from the ion excess velocity and elastic loss by electron collisions. This makes heavy particle temperature change a more complicated correction term than the ion momentum change, so Sanmann chose the course of eliminating temperature change, and which proved to be the best course of action for the approximate solutions.

In deriving equations (35) and (36), the ion velocity  $V_i$  was assumed to be equal to the neutral velocity  $V$ , for the purpose of finding the initial conditions. To obtain ion momentum change, one has to take almost the same course of action taken for deriving equations (35) and (36), and use the equation of conservation of baryons and the zero current conditions, and use  $V_i \approx V_0$  except at the places that their differences appear.<sup>27</sup> The new form of the global momentum and energy equations would be

$$mnvV_0(v-V_0) + MnvV_0(V_i - V_0) + N_0V_0k\Delta T + nkT_eV_0 + \frac{\epsilon_0}{2}(E_0^2 - E^2)V_0 = 0, \quad (50)$$

$$mnv(v^2 - V_i^2) + 2MnvV_0(V_i - V_0) + 5N_0V_0k\Delta T + 5nvkT_e + 2e\phi nv + 2q = 0. \quad (51)$$

Labeling  $(V_i - V_0)$  as  $\Delta V$ , multiplying equation (50) by 5 and subtracting it from equation (51), one finds

$$mnv(v - 4V_0)(v - V_0) - 3MnvV_0\Delta V + 5nkT_e(v - V_0) + 2e\phi nv - \frac{5V_0\epsilon_0}{2}(E_0^2 - E^2)$$

$$+ 2q = 0 . \quad (52)$$

To find  $\Delta V$  one has to use the equations of conservation of momentum, energy, and mass for positive ions

$$\frac{d}{dx}(M_i N_i V_i^2 + N_i kT_i) = eN_i E - K_i M_i N_i (V_i - V) + \beta M_i nV , \quad (53)$$

$$\frac{d}{dx}(M_i N_i V_i^3 + 5N_i V_i kT_i) = 2eN_i V_i E - 2K_i M_i N_i V_i (V_i - V) + \beta M_i nV^2 , \quad (54)$$

$$\frac{d}{dx}(N_i V_i) = \beta n . \quad (55)$$

Using equation (55) for  $\beta n$  in momentum and energy equations, one will find

$$\frac{d}{dx}(M_i N_i V_i (V_i - V) + N_i kT_i) = eN_i E - K_i M_i N_i (V_i - V) , \quad (56)$$

$$\frac{d}{dx}(M_i N_i V_i (V_i^2 - V^2) + 5N_i V_i kT_i) = 2eN_i V_i E - 2K_i M_i N_i V_i (V_i - V) . \quad (57)$$

Multiplying equation (56) by  $5V$ , using the zero current condition, setting  $V_i \approx V$  except at the places that their differences appear, and labeling  $V_i - V$  as  $\Delta V$ :

$$\frac{d}{dx}(5M_i nV\Delta V + 5nvkT_i) = 5envE - 5K_i M_i nV\Delta V , \quad (58)$$

$$\frac{d}{dx}(2M_i nV\Delta V + 5nvkT_i) = 2envE - 2K_i M_i nV\Delta V . \quad (59)$$

Subtracting equation (59) from equation (58):

$$\frac{d}{dx}(Mnv\Delta V) = envE - K_i Mnv \Delta V \quad (60)$$

Introducing dimensionless variables into the equation (60):

$$\frac{d}{d\xi} (\nu\psi\Psi) = \frac{\omega}{2} \nu\psi\eta - \kappa_i \nu\psi\Psi , \quad (61)$$

where  $\omega=(2m/M)$ ,  $\Psi=(\Delta V/V)$ , and  $\kappa_i=(mVK_i/eE_0)$ . Multiplying both sides of equation (61) by  $e^{\kappa_i \xi}$  and solving that differential equation for  $v\psi\Psi$ , one has

$$v\psi\Psi = \frac{\omega}{2} e^{-\kappa_i \xi} \int_0^\xi e^{\kappa_i \xi} v\psi\Psi d\xi . \quad (62)$$

Introducing the dimensionless variables in equation (52), and substituting for  $\Psi$  from equation (62), results in the new form of the energy equation with the ion momentum change included. The new equation is also a differential equation for  $\theta$  which must be integrated. Setting  $\Omega=\frac{K_i}{K_e}$ :

$$\frac{d\theta}{d\xi} = \frac{\kappa\psi}{5\alpha\theta} \left\{ (\psi-1)(\psi-4)/\alpha + 5\theta(1-\frac{1}{\psi}) + 1 - \frac{5}{2}(1-\eta^2)/j \right. \\ \left. - \frac{3e^{-\Omega\kappa\xi}}{\alpha j} \int_0^\xi v\eta\psi e^{\Omega\kappa\xi} d\xi \right\} . \quad (63)$$

Solution of the electron-fluid equations with equation (63) as its energy equation was also disappointing. Either  $\eta$  reversed before  $\psi=1$  (path 2, Figure 1) or  $\theta$  became negative (path 1, Figure 1).  $\eta$  became negative even earlier, and the least bad case was  $\kappa=0.54$ ,  $v_1=0.07$ . In the case of  $\eta$  sign reversal before  $\psi=1$ , when we let the integration continue on either  $\psi$  passed through a maximum and ultimately became negative (path 3), or  $\eta$  spiraled around the ( $\eta=0, \psi=1$ ) point without converging to that point. Figure 6 gives  $\eta$  as a function of  $\psi$ , and Figure 7 gives  $\mu, \theta, v$  as a function of position ( $\xi$ ) for the case  $\kappa=0.54$ ,  $v_1=0.07$ .

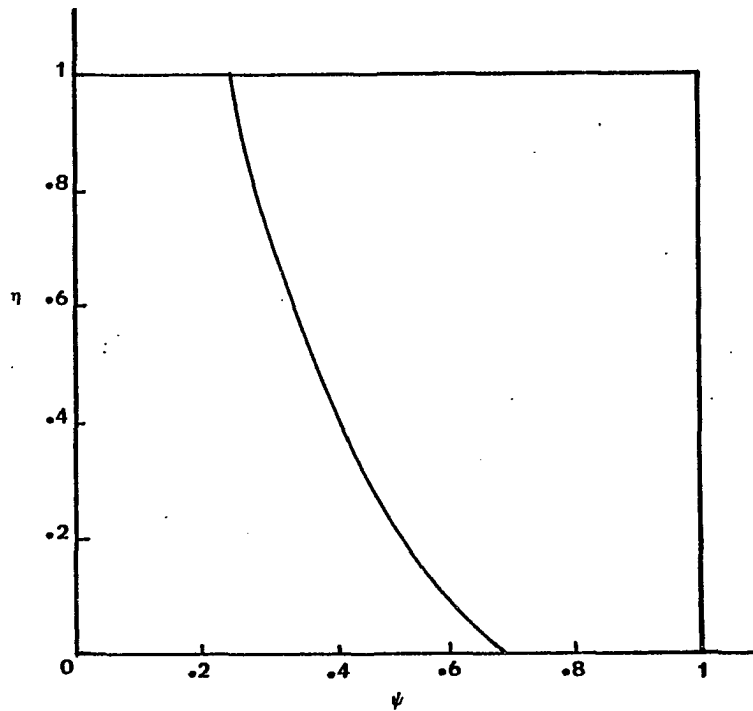


Figure 6. Electric field ( $\eta$ ) as a function of drift velocity ( $\psi$ ).

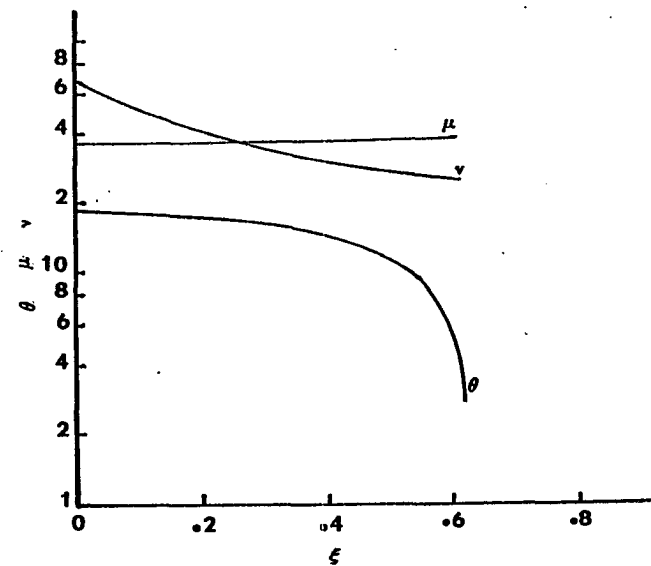


Figure 7. Temperature ( $\theta$ ), electron density ( $\nu$ ), and ionization rate ( $\mu$ ) as a function of position ( $\xi$ ). Scale factors: For  $\nu$  divide  $y$  by 10, for  $\mu$  divide  $y$  by  $10^2$ .

One  $\eta$  sign change which represents a charge sign reversal inside the wave might be tolerable, but the multiple sign change of  $\eta$  which takes place in the case of a spiral path around ( $\eta=0, \psi=1$ ) cannot be reasonable. A considerable investigation was then made of possible embedded shocks at ( $\eta=0, \psi>1$ ), but connection could never be made from the point S to the point ( $\psi=1, \eta=0$ ) for any solution by using the shock conditions. Also one might reach the point ( $\psi=1, \eta=0$ ) continuously by a single  $\eta$  sign change (path B), but we could not find a path such as B.

At this point it became clear that to achieve a solution which would meet the conditions on initial and final states of  $\eta$  and  $\psi$ , an additional degree of freedom was required. We decided to abandon the requirement that the derivative of the temperature must be zero at the wave front. In other words, to permit discontinuities at the wave front in the derivatives of the functions as well as the functions themselves. This was based on the argument that a strong discontinuity could override a weak discontinuity at the same point. In our earlier work we had abandoned this idea, thinking that a flow of heat ( $\theta'_1 \neq 0$ ) would then be crossing the wave front, but the heat conduction term is only one component of the energy balance, and the other variables also have derivative discontinuities. Also in many shock wave problems a temperature derivative discontinuity has been assumed. To find

the initial condition on  $\psi$ , with discontinuity on the temperature derivative allowed, we introduce the initial condition on  $\theta$

$$\alpha\theta_1 = \psi_1(1 - \psi_1) ,$$

and the values of other variables at the leading edge of the wave ( $\xi_1=0, \eta_1=1$ ) into the energy equation with the heat conduction term included:

$$\nu_1\psi_1(\psi_1-1)^2 + \nu_1\psi_1(1-\psi_1)(5\psi_1-2) + \alpha\nu_1\psi_1 + \alpha(\eta_1^2-1) - \frac{5\alpha\nu_1\psi_1(1-\psi_1)\theta_1'}{\kappa} = 0 ,$$

or

$$-4\psi_1^2 + 5\psi_1 - 1 + \frac{5\alpha\psi_1\theta_1'}{\kappa} + \alpha - \frac{5\alpha\theta_1'}{\kappa} = 0 .$$

Solving this quadratic equation for  $\psi_1$ , one finds the initial condition on  $\psi$ :

$$\psi_1 = \frac{5(1 + \frac{\alpha\theta_1'}{\kappa}) - \sqrt{(3 - 5\frac{\alpha\theta_1'}{\kappa})^2 + 16\alpha}}{8} . \quad (64)$$

Our first attempt to solve the electron-fluid equations with the new initial condition on  $\psi$  was the original method of integrating the impulse term of the momentum equation

$$I = \frac{1}{\alpha} \int_0^{\xi} \nu\eta \, d\xi ,$$

and solving the algebraic quadratic form of the momentum equation for  $\psi$ , either with or without the elimination of

$\theta$  from the energy equation. This again involved the horizontal tangent approach to the two branches of the quadratic equation, with a change of the branches, which was possible for certain combinations of  $\psi_1$ ,  $v_1$ , and  $\kappa$ . Finding these solutions was very time-consuming and also wasteful of computer time, but a few near solutions were found.

Next we shifted from the algebraic quadratic form of the momentum equation to the primitive differential form. By employing the production equation (26), one can write the momentum equation (28) as a differential equation for  $\psi$ . Electron production and momentum equations can be written as:

$$v \frac{d\psi}{d\xi} + \psi \frac{dv}{d\xi} = \kappa\mu v \quad (65)$$

$$(\psi-1) \frac{d(v\psi)}{d\xi} + v\psi \frac{d\psi}{d\xi} + \alpha\theta \frac{dv}{d\xi} + \alpha v \frac{d\theta}{d\xi} = -v\eta - \kappa v\psi + \kappa v \quad (66)$$

Substituting for  $(d(v\psi)/d\xi)$  from production equation, and for  $dv/d\xi$  from equation (65), one can solve equation (66) for  $d\psi/d\xi$ :

$$\frac{d\psi}{d\xi} = \frac{\kappa\psi(1-\psi)(1+\mu) - \kappa\mu\alpha\theta - \eta\psi - \alpha\psi \frac{d\theta}{d\xi}}{\psi^2 - \alpha\theta} \quad (67)$$

The singular behavior of the equation set which lies between  $0 < \psi < 1$  and has appeared in different forms in different combinations of equation sets before, is manifest here at  $\psi^2 = \alpha\theta$ . Since  $d\psi/d\xi$  can not be infinite without a shock, and no shock is possible between  $\psi_1$  and 1, then the numerator

in equation (67) must also be zero at the same point where the denominator became zero. This allows us to choose the initial value of  $\psi_1$  by trial and error for a given  $\kappa$ . The value of the numerator must be compared with that of the denominator each time and this can not be done without integration of the set up to the point of singularity. This course of action is somewhat more direct than use of the quadratic equation for  $\psi$ . With increasing  $\alpha$ , even as high as  $\approx 0.1$ , the singularity becomes so sharp that it can lie within a single step of integration. This makes the detection of the singularity difficult, especially for very high values of  $\alpha$ .

Since  $\theta'$  is dependent on  $v$ , the results, especially the action of  $\eta$  and  $\psi$  at the trailing edge of the sheath, were very much dependent on the initial value of  $v(=v_1)$ . Appropriate choice of  $v_1$  brought us very close to meeting the tangent conditions at  $\eta=0, \psi=1$  for the first time.

Because of the small rates of the heat loss by electrons in elastic collisions we like others had neglected terms like  $3m/M(nK_1kT_e)$  in our previous work. At this stage we chose an alternative formulation of the energy equation with the heat loss terms by the electrons to the heavy particles in elastic collisions included. The electrons heat loss term in their directed motion is  $(m/M)nK_1m(v-V)^2$ , which in terms of dimensionless variables would become  $\omega\kappa v/2 (\psi-1)^2$  and must also be subtracted from the right hand side of the energy equation.

In these terms  $\omega$  is  $2m/M$ . Adding the new correction terms to the energy equation one has

$$\frac{d}{d\xi} \left\{ \nu\psi(\psi-1)^2 + \alpha\nu\theta(5\psi-2) + \alpha\nu\psi + \alpha\eta^2 - \frac{5\alpha^2\nu\theta}{\kappa} \frac{d\theta}{d\xi} \right\} = -\omega\kappa\nu \{ 3\alpha\theta + (\psi-1)^2 \}. \quad (68)$$

We designated the right side of equation (68) as  $dW/d\xi$ ,

$$\frac{dW}{d\xi} = -\omega\kappa\nu \{ 3\alpha\theta + (\psi-1)^2 \}. \quad (69)$$

Bringing  $dW/d\xi$  to the left side of the energy equation, and integrating it across the sheath, one will find a differential equation for  $\theta$  which must be integrated.

$$\frac{d\theta}{d\xi} = \frac{\kappa}{5\alpha^2\nu\theta} \left\{ \nu\psi(\psi-1)^2 + \alpha\nu\theta(5\psi-2) + \alpha\nu\psi + \alpha(\eta^2-1) - W \right\}. \quad (70)$$

Using the shock conditions on  $\theta$  and  $\psi$ , with the temperature derivative discontinuity allowed and the initial condition on  $\eta$  ( $\eta_1=1$ ), one can easily find the initial condition on  $W$  which is  $W_1=\alpha$ .

Introduction of equation (68) as energy equation in the set of the electron-fluid equations, acceptance of the electron temperature derivative discontinuity ( $\theta'$ ) at the leading edge of the wave, the use of the momentum equation in the form of equation (67), and appropriate choice of  $\nu_1$ ,  $\psi_1, \kappa$  led to a completely satisfactory solution which met the tangent conditions at the trailing edge of the wave ( $\eta=0, \psi=1$ ) within the accuracy of the integration step. The results for the case of  $\alpha=0.01$ ,  $\kappa=1.18179$ ,  $\nu_1=0.025$ , and  $\psi_1=0.31953$  in argon are given in Figures 8-10. As

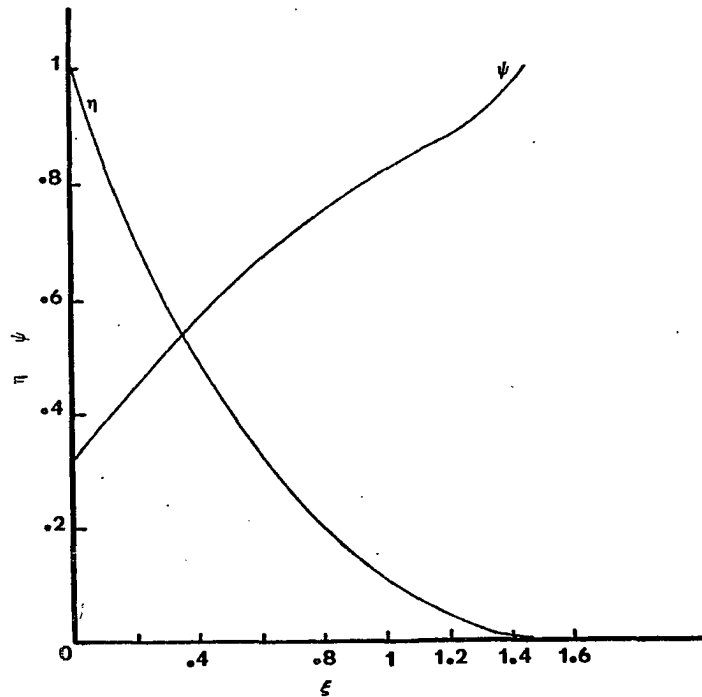


Figure 8. Electric field ( $\eta$ ) and drift velocity ( $\psi$ ) as a function of position for Ar at  $\alpha=0.01$ ,  $\psi_1=0.31953$ ,  $v_1=0.025$ ,  $\kappa=1.18179$ .

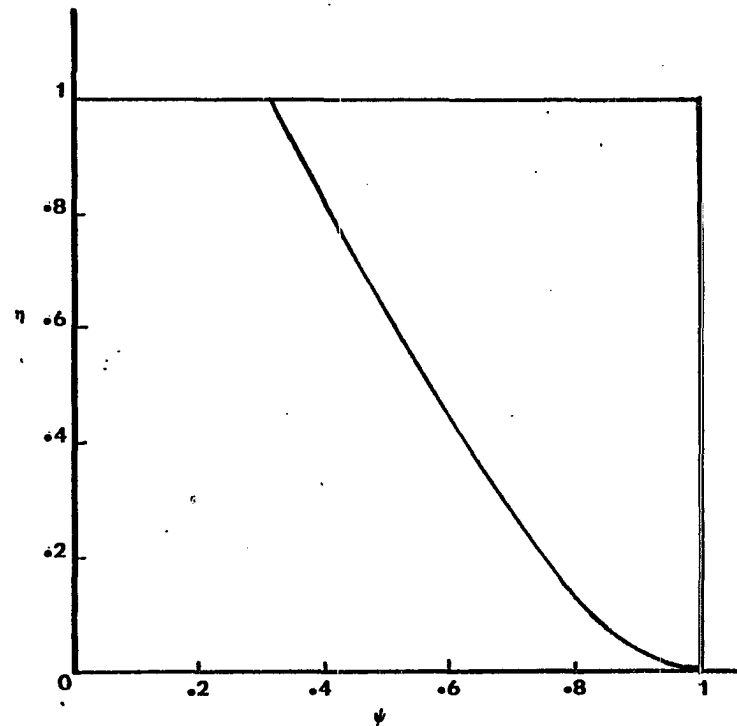


Figure 9. Electric field ( $\eta$ ) as a function of drift velocity ( $\psi$ ) for Ar at  $\alpha=0.01$ ,  $\psi_1=0.31953$ ,  $v_1=0.025$ ,  $\kappa=1.18179$ .

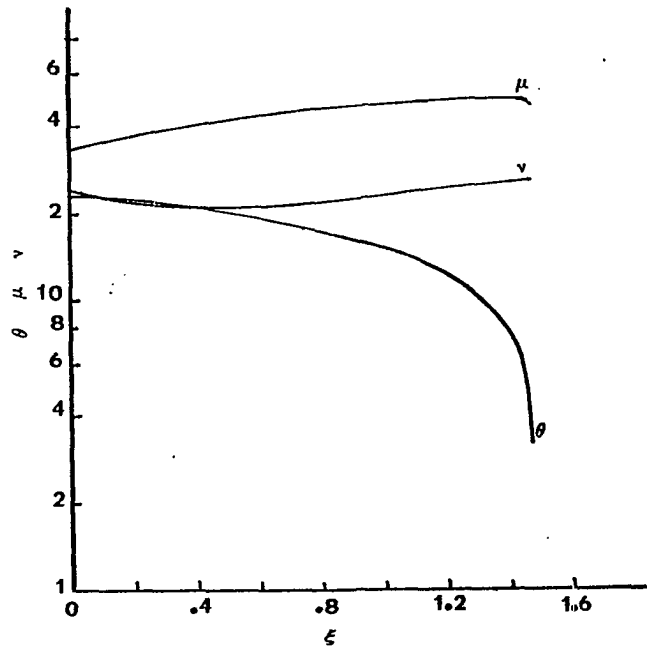


Figure 10. Electron temperature ( $\theta$ ), electron density ( $\nu$ ), ionization rate ( $\mu$ ) as a function of position ( $\xi$ ). Scale factors: For  $\nu$  divide  $y$  by  $10^3$ , for  $\mu$  divide  $y$  by  $10^2$ .

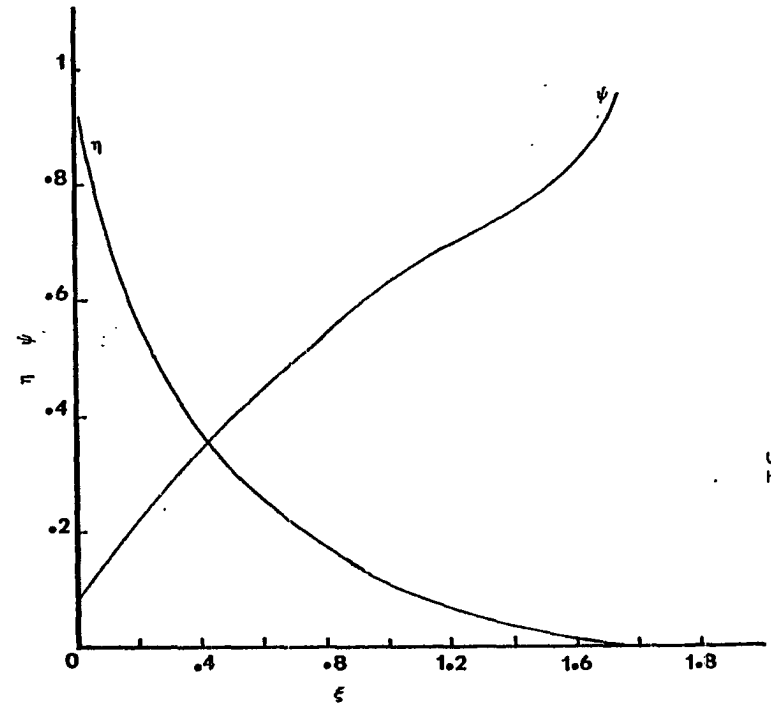


Figure 11. Electric field ( $\eta$ ) and drift velocity ( $\psi$ ) as a function of position ( $\xi$ ) for Ar at  $\alpha=2$ ,  $\psi_1=0.0845$ ,  $\nu_1=7.7$ ,  $\kappa=0.6498$ .

mentioned before, when  $\alpha$  becomes larger the singularity becomes very sharp, therefore very difficult to detect. We investigated the solutions for  $\alpha=0.01, 0.1, 1., 2., 4.$  and we were able to find solutions in all cases except for  $\alpha=4.$  In the case of  $\alpha=4$  the solution could not be made to converge to  $\eta=0$  at  $\psi=1$ , but  $\theta$  became negative at  $\psi=0.97$  for  $\kappa=0.54087$ ,  $\psi_1=0.015$ , and  $v_1=49.2$ . This indicates the existence of a cutoff close to  $\alpha^4$ . (expected from experiment!). Figure 11 gives electric field ( $\eta$ ) and drift velocity ( $\psi$ ) as a function of position ( $\xi$ ), and Figure 12 gives temperature ( $\theta$ ), ionization rate ( $\mu$ ), and electron density ( $v$ ) as a function of position ( $\xi$ ) for the case of  $\alpha=2., \kappa=0.6498$ ,  $v_1=7.7$ ,  $\psi_1=0.0845$  in argon.

We also investigated the solutions for two more gases, nitrogen and helium for above range of  $\alpha$ . The behavior of electric field as a function of drift velocity, electric field and drift velocity as a function of position, temperature and electron density as a function of position were very similar in all three gases. The only difference was that, for helium and argon the ionization rate approaches zero at the end of the sheath, and that of nitrogen remains non-zero but small. For comparison the electron density ( $v$ ) as a function of position ( $\xi$ ), and the ionization rate ( $\mu$ ) as a function of position ( $\xi$ ) are given in Figures 13 and 14 for the case of  $\alpha=2$  in argon, helium, and nitrogen.

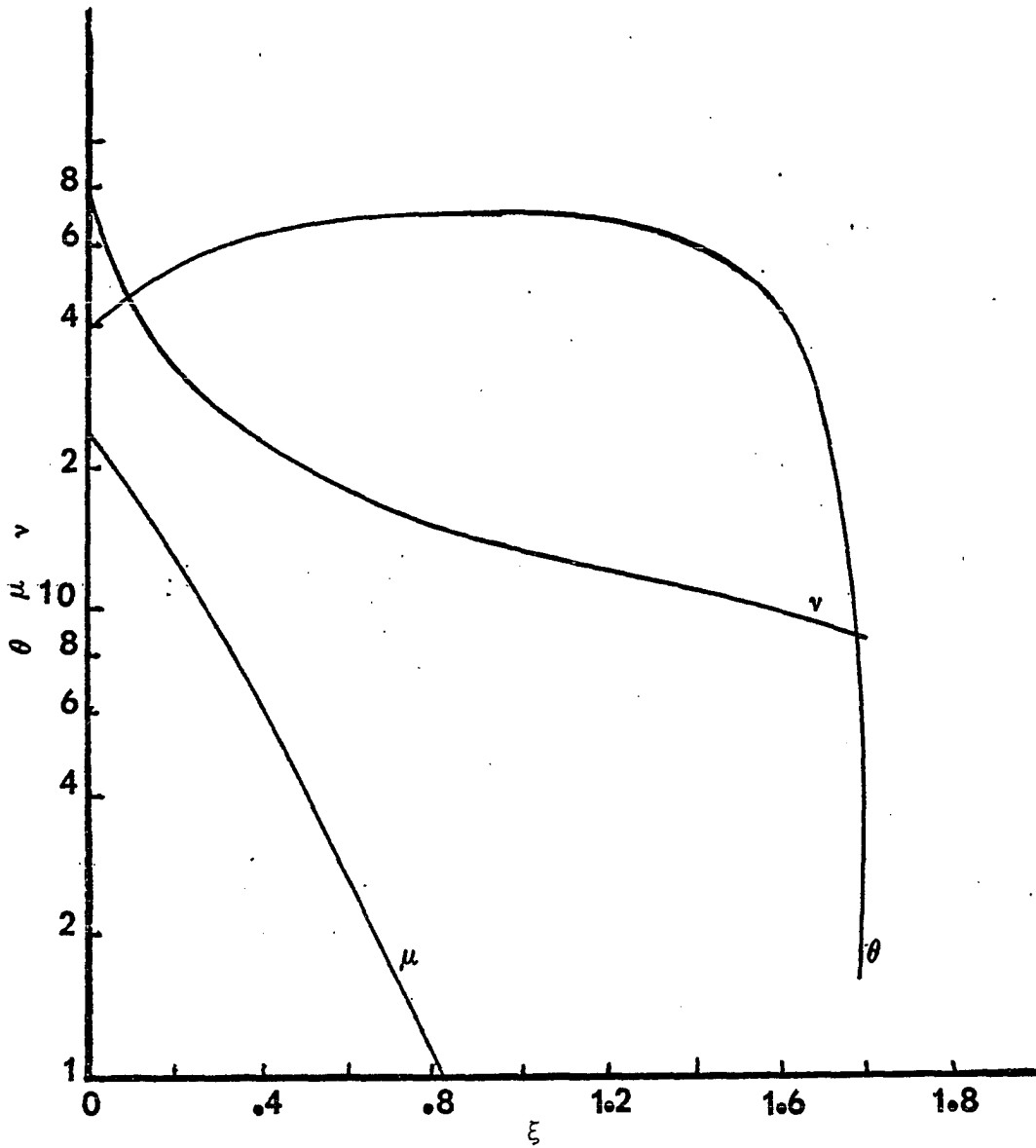


Figure 12. Electron temperature ( $\theta$ ), electron density ( $\nu$ ), and ionization rate ( $\mu$ ) as a function of position ( $\xi$ ) for Ar at  $\alpha=2$ ,  $\psi_1=0.0845$ ,  $\nu_1=7.7$ ,  $\kappa=0.6498$ .  
 Scale factors: For  $\theta$  divide  $y$  by  $10^3$ , for  $\nu$  divide  $y$  by 10, for  $\mu$  divide  $y$  by  $10^2$ .

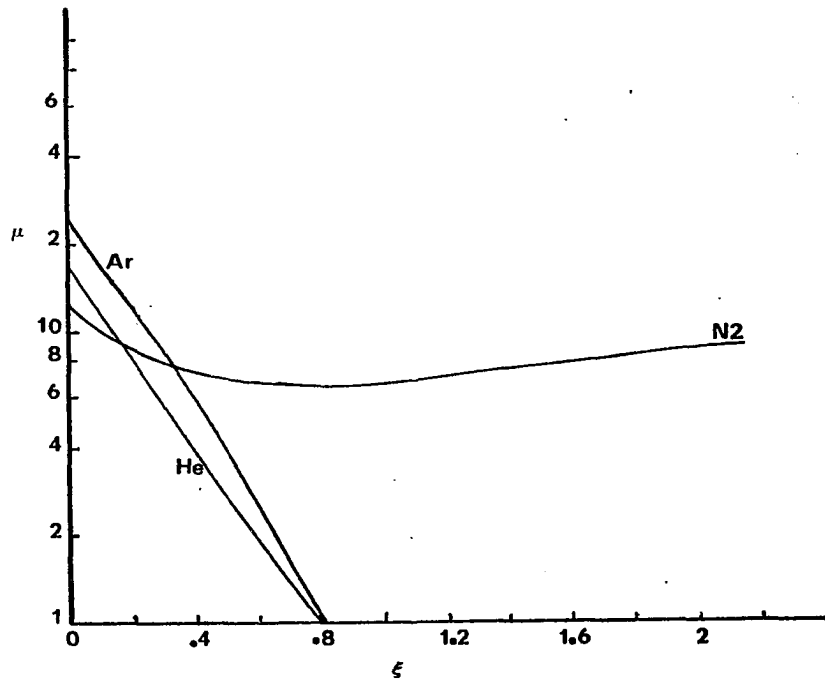


Figure 13. Ionization rate ( $\mu$ ) as a function of position ( $\xi$ ) for Ar, N<sub>2</sub>, He at  $\alpha=2$ .

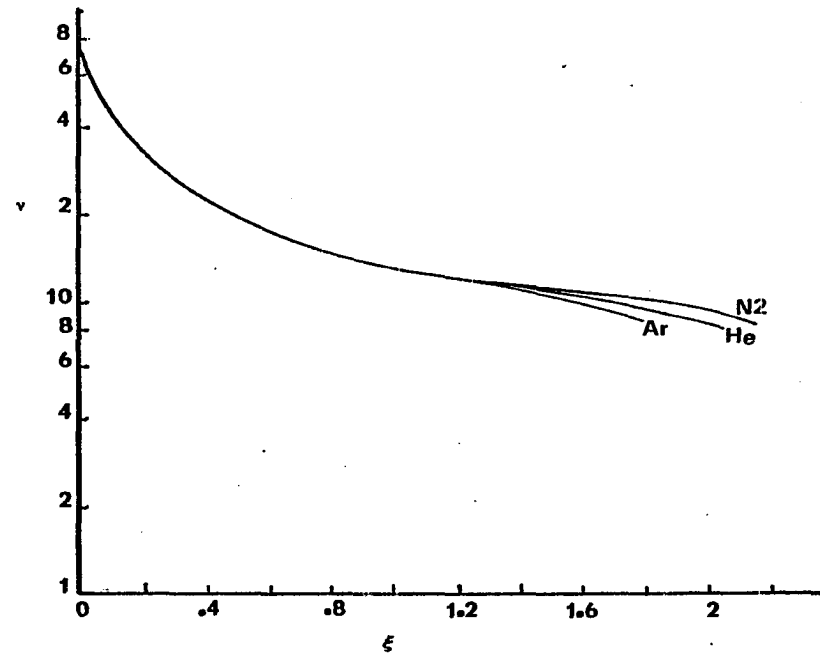


Figure 14. Electron density ( $\nu$ ) as a function of position ( $\xi$ ) for Ar, N<sub>2</sub>, He at  $\alpha=2$ . Scale factors: For  $\nu$  divide  $y$  by 10.

For the case of  $\alpha=0.01$  in nitrogen we gradually decreased the size of the integration step from  $\Delta\xi=0.01$ , to 0.005, 0.0025, 0.0008. The effect on the solutions is interesting but not significant. In nitrogen for  $\alpha=0.01$  and integration step of 0.01 the solution was found to be  $\kappa=1.2778$ ,  $\nu_1=0.025$ ,  $\psi_1=0.33455$ , where for integration step of 0.0008 it occurred for  $\kappa=1.1805$ ,  $\nu_1=0.025$ ,  $\psi_1=0.31903$ . The integration step is therefore important for a perfect result, but a step which does not invoke inordinate amounts of machine time possesses enough accuracy for proof of the existence of solutions.

CHAPTER V  
CLASS II PROFORCE WAVES

Up to this point we have studied the propagation of the ionizing waves in to a medium of substantially zero electron ion concentration (zero current in front of the wave). In this chapter we will consider the propagation of the proforce waves into a medium of significant ion concentration, which are called Class II proforce waves.

The ionized medium in the atmospheric case is usually a mixture of positive nitrogen ions and negative oxygen ions, where the electrons are loosely bound to the oxygen atoms. Application of a weak electric field to the positive and negative ions tend to accelerate the positive and negative ions in two different directions. The movement of these charges creates a small current in front of the wave. It will be shown that the waves propagating into an ionized medium will possess different structure than they had while moving into a nonionized medium, and the structure of the wave depends very much on the concentration of ions in front of the wave. The negative and positive ions have equal number density, and we will represent them as  $N_i^- = N_0^-$ ,

$N_1^+ = N_0^+$  respectively. The applied electric field will be represented as  $E_\infty$ , denoting the field far away from the wave front. Because of having almost equal mass, the positive and negative ions will acquire equal speeds in opposite directions. If in the lab frame the positive and negative ions were moving with a speed of magnitude  $v_0$ , then the electrons attached to the negative ions will be moving with the same speed, and also they will have equal number density as ions. Denoting the number density of electrons as  $n_0$ , one has

$$N_0^+ = N_0^- = n_0 \quad . \quad (73)$$

Assuming that in the lab frame the wave front is moving from left to the right (positive x direction) with a speed of  $V_0$ , then in one dimension and in the wave frame the neutral atoms will be swept into the wave front with a velocity  $-V_0$ , and depending on the direction of the  $E_\infty$  the positive and negative ions will possess a speed of either  $-(V_0+v_0)$ ,  $-(V_0-v_0)$  or the other way around. When an ionized medium is overrun by a proforce wave, the ions will no longer be under the influence of the remote field ( $E_\infty$ ), and for a very short time (the time that it takes for a thin front part of the sheath to traverse the ions) they will be influenced by the electric field existent at the wave front ( $E_0$ ). The front electric field will rip the loosely bound electrons off of the negative ions,

leaving them as neutrals. The ions entering the wave will make a few collisions with neutral atoms and acquire the same speed as neutral atoms. Also the electric field inside the sheath drops to zero very fast, in which short time the ions do not acquire speed in excess of neutral atoms. In proforce waves, the electrons because of their small mass will be driven toward the wave front, with a velocity smaller than  $V_0$  ( $|v| < |V_0|$ ). Therefore, in the wave frame the electrons will have a negative speed.

We began our attempts at direct solution by only considering the effect of the current in front of the wave in the Poisson's equation and neglecting its effect on the shock conditions. This failed to give any useful results, even if we used the same set of electron-fluid equations which in the case of proforce wave traveling into a non-ionized medium led us to a completely satisfactory solution meeting the boundary conditions at the trailing edge of the wave. The integrals produced negative values of  $\theta$  (path 1, Figure 1) before  $\psi$  reached unity, which is not acceptable. In this case the boundary conditions at the end of the wave would be different. While the electrons, ions, and neutral atoms come to an equilibrium ( $\psi \rightarrow 1$ ), and the first derivative of the electric field approaches zero ( $d\eta/d\xi \rightarrow 0$ ), this is not necessarily true of the electric field itself. According to Kirchhoff's law the current entering the wave front would be leaving the wave at the

end. The field  $E_{\infty}$  drives a current far ahead of the wave, so there must be a remaining field at the end of the wave to derive a current there also.

The next attempt was to consider the effect of the current ahead of the wave in the boundary conditions in front of the wave. Assuming that the electric field ahead of the wave points in the negative x direction, the oxygen atoms and the electrons attached to them will move to the right and the positive ions will move in the direction of the field with speeds of  $-(V_0 - v_0)$  and  $-(V_0 + v_0)$  respectively relative to the wave front. The absence of an experimentally observed Doppler shift indicates that neither the ions nor the neutrals have appreciable motion in the laboratory and, based on this, the velocity of ions and neutrals can be assumed to be equal to  $V_0$  inside the wave.

By using equation (73), the equation for conservation of current in the wave front becomes

$$env - eN_i V_0 = en_0(V_0 - v_0) - en_0(v_0 + V_0), \quad (74)$$

where  $n$  and  $N_i$  are the electron and ion concentrations inside the sheath respectively. Solving equation (74) for  $N_i$ , one has

$$N_i = \frac{nv}{V_0} + \frac{2n_0 v_0}{V_0}. \quad (75)$$

Substituting for  $N_i$  from equation (75) in the Poisson's equation of the form of equation (19), one has

$$\frac{dE}{dx} = \frac{en}{\epsilon_0} \left( \frac{v}{V_0} - 1 \right) + \frac{2en_0 v_0}{\epsilon_0 V_0}. \quad (76)$$

Introducing the dimensionless variables into the Poisson's equation it becomes:

$$\frac{d\eta}{d\xi} = \frac{v}{\alpha} (\psi - 1) + 2 \frac{j_0}{\alpha}, \quad (77)$$

where  $j_0$  is the current ahead of the wave.

The global (all particle) momentum equation can be written in the following way:

$$nmv^2 + N_i M_i V^2 + MNV^2 + nkT + (N + N_i)kT = \frac{\epsilon_0}{2} E_0^2 + C, \quad (78)$$

where  $C$  is a constant to be determined by condition ahead of the wave.

$$\begin{aligned} nmv^2 + N_i M_i V_0^2 - mN_i V_0^2 + MNV_0^2 + nkT_e - n_0 k(T_e)_0 + (N + N_i)kT - (N_0 + N_{i_0})kT_0 \\ - n_0 m(V_0 - v_0)^2 - N_{i_0} (M - m)(V_0 + v_0)^2 - MN_0 V_0^2 = 0 \end{aligned} \quad (79)$$

where  $(T_e)_0$ , and  $T_0$  are electron and neutral temperature respectively ahead of the wave, and the electric field right at the wave front is no longer  $E_\infty$ , but it becomes  $E_0$ . The source of the temperature difference,  $T - T_0$ , must be collisions of electrons with the neutrals since the electron-ion collisions are so infrequent as to be negligible. Sanmann<sup>28</sup> calculated the energy transfer rate for electron-neutral collisions, and concluded that  $T - T_0$  increases with position  $x$  through the wave and is of the order of  $4K(nT_e/N_0V_0)(m/M)x$ . Calculating  $N_0V_0/nT_e$ , he found that even for the extreme case of helium, if the wave velocity is greater than  $10^5$  m/sec, this term is as small as  $10^{-7}$ .

Also at the wave front  $N=N_0$ , and  $N_i=N_{i_0}=n_0$ , because the ionization does not take place at the wave front but inside the sheath. Considering the above arguments the terms  $(N+N_i)kT$  and  $(N_0+N_{i_0})kT_0$  in equation (79) cancel each other. The electrons ahead of the wave are attached to the oxygen atoms, therefore the electron temperature  $(T_e)_0$  which is in the order of the room temperature would be negligible compared to the electron temperature inside the sheath. Compared to the wave velocity  $V_0$ , the neutral-ion velocity  $v_0$  ahead of the wave is very small, therefore the terms having  $v_0^2$  could be neglected. Taking all the above into consideration, and employing the equation of conservation of particles:

$$N_0 + n_0 = N + N_i \quad (80)$$

in equation (79), it simplifies to:

$$nmv^2 - mN_i V_0^2 + nkT_e + 4n_0 m n_0 V_0 - 2n_0 v_0 V_0 M = 0 .$$

Employing equation (75) in this expression, one has

$$nkT_e = -nmv^2 + nmvV_0 - 6n_0 m v_0 V_0 + 2n_0 v_0 V_0 M . \quad (81)$$

Denoting the values of the variables at the wave front by a subscript 1, substituting for  $n_1$  at the wave front from equation (75), and dividing both sides by  $mV_0^2$  equation (81) reduces to:

$$\frac{k}{mV_0^2} (T_e)_1 = \frac{v_1}{V_0^2} (V_0 - v_1) + \frac{2v_0 v_1}{(V_0 + 2v_0)V_0} \left(\frac{M}{m} - 3\right) . \quad (82)$$

Introducing dimensionless variables in this expression, one finally obtains the boundary condition on the electron temperature:

$$\theta_1 = \frac{\psi_1}{\alpha} (1 - \psi_1) + \frac{2\psi_1\psi_0}{\alpha(1 + 2\psi_0)} \left(\frac{M}{m} - 3\right), \quad (83)$$

where  $\psi_0 = v_0/V_0$  is the ion velocity in front of the wave.

To find the initial condition on  $\psi$ , we took the same course of action as we had previously in the case of pro-force waves propagating into the nonionized medium. At the wave front crosswise, and directed motion of the electrons are zero, which makes the heat loss term  $3\alpha\theta\omega\kappa\nu$ ,  $\omega\kappa\nu(\psi-1)^2$  by electrons zero. The energy equation gives the shock condition on  $\psi_1$  as:

$$\nu_1(\psi_1(\psi_1-1)^2 + \alpha\theta_1(5\psi_1-2) + \alpha\psi_1 - \frac{5\alpha^2\theta_1\theta_1'}{\kappa}) = 0.$$

Since  $\nu_1 \neq 0$ , then substituting for  $\theta_1$  from equation (84), and factoring out  $\psi_1$  results in a quadratic equation on  $\psi_1$  which could be solved for it. Also the initial condition on  $W$  as in previous case becomes  $\alpha$ . Using the above initial conditions with appropriate values of  $\psi_0$ ,  $\psi_1$ ,  $\nu_1$ ,  $\kappa$ , and the electron-fluid equation set in the form of:

$$\begin{aligned} \frac{d(\nu\psi)}{d\xi} &= \kappa\nu, \\ \frac{d\eta}{d\xi} &= \frac{\nu}{\alpha} (\psi-1) + \frac{2j_0}{\alpha}, \\ \frac{d\psi}{d\xi} &= \frac{\kappa(1-\psi)(1+\mu) - \alpha\psi\theta' - \kappa\mu\alpha\theta - \eta\psi}{\psi^2 - \alpha\theta}, \end{aligned} \quad (84)$$

$$\frac{d}{d\xi} \left\{ v\psi(\psi-1)^2 + \alpha v\theta(5\psi-2) + \alpha v\psi + \alpha\eta^2 - \frac{5\alpha^2 v\theta}{\kappa} \frac{d\theta}{d\xi} \right\}$$

$$= -\omega\kappa v(3\alpha\theta + (\psi-1)^2),$$

led to a completely satisfactory solution which met the boundary conditions at the trailing edge of the wave ( $d\eta/d\xi = 0$ ,  $\psi=1$ ).

The results were extremely sensitive to  $\psi_0$  and  $v_0$ .  $v_0$  is the measure of charge in front of the wave; the more electrons we have out in front of the wave, the higher the temperature is in the shock front. Equation (83) shows that because of the large value of  $M/m$ , a small change in  $\psi_0$  will result in a large change in the electron temperature in the shock front. The results were not very much dependent on  $j_0$ , but one has to take its relation with  $\psi_0$  and  $v_0$  ( $j_0 = v_0\psi_0$ ) into consideration. For  $\psi_0 = 10^{-6}$  the results were quite similar to the case of proforce wave moving into a nonionized medium, with the boundary conditions of ( $\eta=0, \psi=1$ ) at the trailing edge of the wave. We investigated the solutions for higher values of  $\psi_0$ , and were able to find solutions for  $\psi_0$  as high as  $5 \times 10^{-5}$ , although for  $\psi_0 = 5 \times 10^{-5}$ , the reduction in the electric field across the sheath was very small, and the value of the electric field at the end of the sheath was very high. Figure 15 gives the electric field ( $\eta$ ) as a function of drift velocity ( $\psi$ ) for  $\psi_0 = 10^{-6}$ ,  $10^{-5}$ ,  $3 \times 10^{-5}$ ,  $4 \times 10^{-5}$ ,  $5 \times 10^{-5}$ . For high values of  $\psi_0$ , the solutions occur at

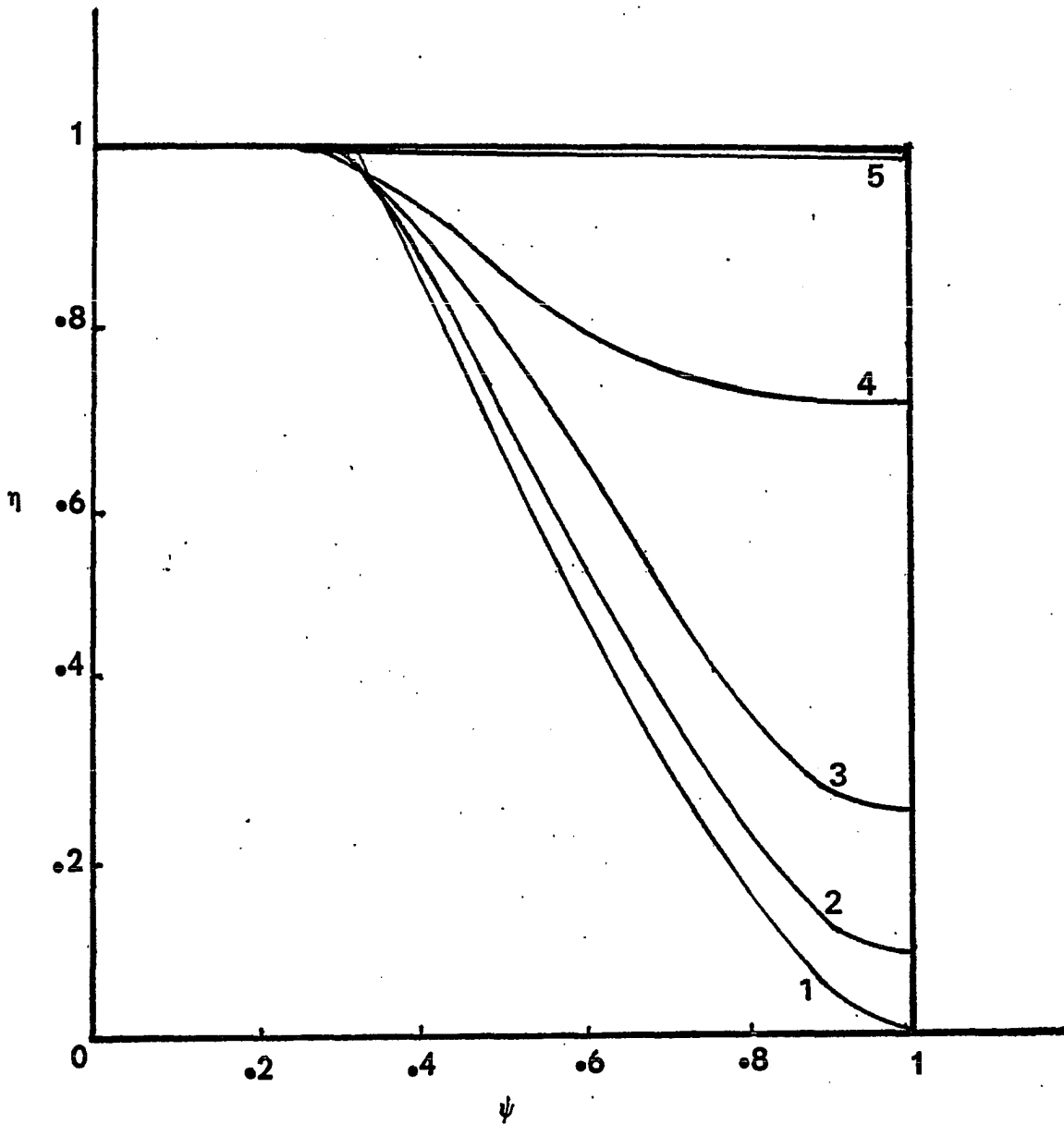


Figure 15. Electric field ( $\eta$ ) as a function of drift velocity ( $\psi$ ) for  $\alpha=0.01$ . Curves (1),  $\kappa=1.2088$ ,  $\psi_1=0.32499$ ,  $\psi_0=10^{-6}$ ; (2),  $\kappa=1.21537$ ,  $\psi_1=0.31835$ ,  $\psi_0=10^{-5}$ ; (3),  $\kappa=1.5227$ ,  $\psi_1=0.287$ ,  $\psi_0=3 \times 10^{-5}$ ; (4),  $\kappa=1.5986$ ,  $\psi_1=0.263$ ,  $\psi_0=4 \times 10^{-5}$ ; (5),  $\kappa=1.81216$ ,  $\psi_1=0.245$ ,  $\psi_0=5 \times 10^{-5}$ .

larger  $\kappa$ . For instance in nitrogen for  $\alpha=0.01$ ,  $\kappa$  was equal to 1.2088 for  $\psi_0=10^{-6}$ ,  $\psi_1=0.32499$ ,  $v_1=0.022$ ,  $j_0 \approx 2 \times 10^{-9}$ , and it was 1.5227 for  $\psi_0=3 \times 10^{-5}$ ,  $\psi_1=0.287$ ,  $v_1=0.00315$ ,  $j_0 \approx 10^{-10}$ . Figure 16 gives the electric field ( $\eta$ ) and the drift velocity ( $\psi$ ) as a function of position ( $\xi$ ), and in Figure 17 the electron temperature ( $\theta$ ), ionization rate ( $\mu$ ), and the electron density ( $\nu$ ) are given as a function of position ( $\xi$ ).

Comparing Figure 16 with Figure 9, one can see that the sheath is longer in the case of the proforce waves traveling into an ionized medium, than when propagating into a nonionized medium. Also in the former case the temperature is very high at the leading edge of the wave, which is as expected.

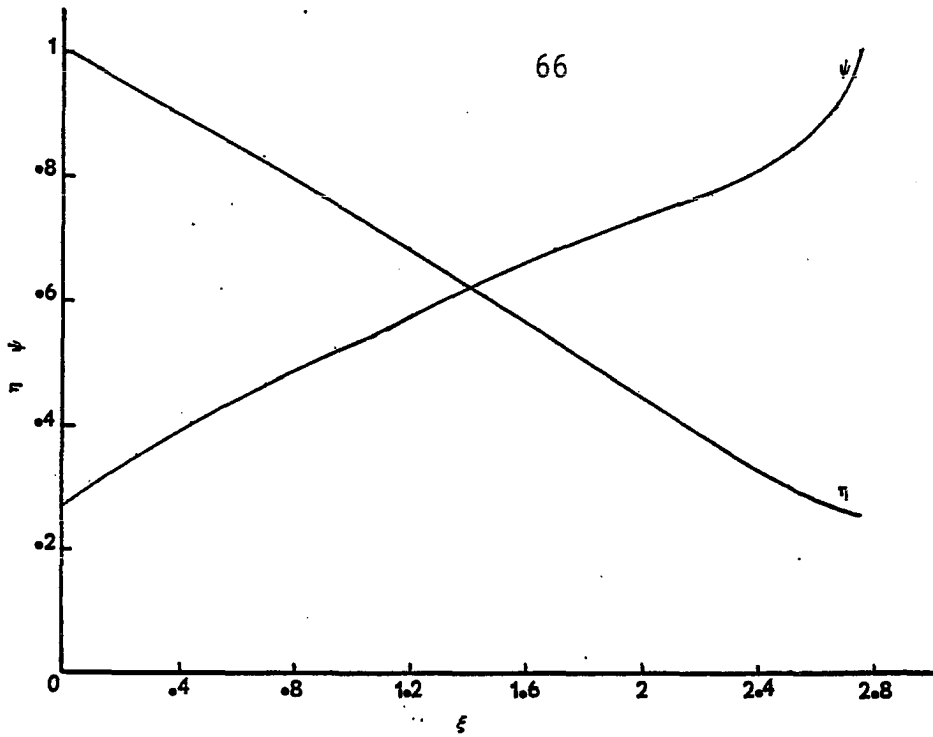


Figure 16. Electric field ( $\eta$ ) and drift velocity ( $\psi$ ) as a function of position ( $\xi$ ) for  $\alpha=0.01$  at  $\psi_0=3\times 10^{-5}$ ,  $\psi_1=0.287$ ,  $\kappa=1.5227$ ,  $v_1=0.00315$ .

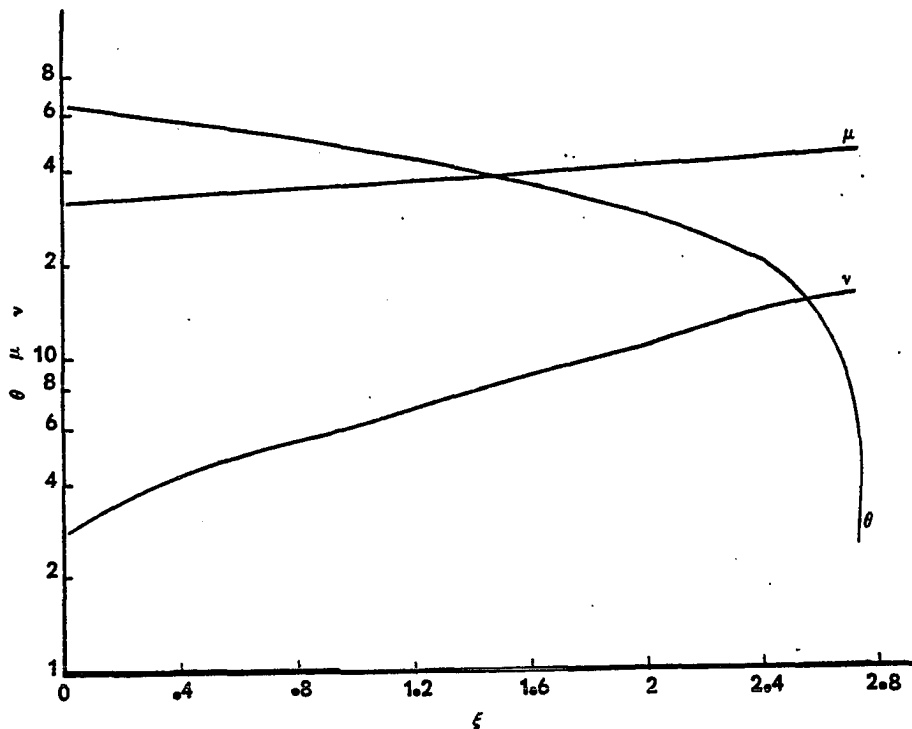


Figure 17. Temperature ( $\theta$ ), electron density ( $\nu$ ), and ionization rate ( $\mu$ ) as a function of position ( $\xi$ ) for  $\alpha=0.01$  at  $\psi_0=3\times 10^{-5}$ ,  $\kappa=1.5227$ ,  $\psi_1=0.287$ ,  $v_1=0.00315$ . Scale factors: For  $\nu$  divide  $y$  by  $10^3$ , for  $\mu$  divide  $y$  by  $10^2$ .

CHAPTER VI  
ANTIFORCE AND CLASS III WAVES

The fluid dynamical model is that of a plane wave which in the laboratory is propagating in the positive  $x$  direction with speed of  $V_0$ . Remembering that the heavy particles are assumed to be at rest in the laboratory, then in a frame where the wavefront is stationary at  $x=0$  the wave extends from  $x=0$  to  $x=-\infty$ , and the plane  $x=0$  divides the gas in front of the wave from the three component gas composed of the electrons, ions, and neutrals behind the wave. The propagation of the wave in the laboratory is governed by the motions of the electrons; the heavy particle motions are very small. In the antiferce waves, the direction of the electric field is such as to cause the average drift velocity of the electrons to be away from the wave front. The electron fluid pressure is assumed to be large enough to provide the driving force to cause the wave to move down the tube with the observed velocities. This implies that the electron temperature must be large enough to sustain its motion despite the net electron drift away from the wavefront.

In analyzing the proforce waves, Shelton<sup>24</sup> found a solution with a strong discontinuity, but concluded that the equations were incompatible at the leading edge with such a solution in the antiforce case, and that one must choose the weak discontinuity condition  $n_1=0, (dn/dx)_1 \neq 0$  at the leading edge of the wave.

Sanmann<sup>28</sup> began a search for a solution having a weak discontinuity at the leading edge of the wave. Expanding the continuity equation, setting  $n=0$  at  $x=0$ , and assuming  $(\partial n/\partial x)_1 \neq 0$  he found a condition on electron velocity at the leading edge of the wave ( $v_1=0$ ). Introducing this condition in the Poisson's equation, he found the initial conditions for the field as  $E=E_0, (\partial E/\partial x)_1=0$ . In the case of antiforce waves, nondimensional variables such as  $\kappa (\kappa=mVK_1/eE_0)$  because  $V<0, E_0>0, K>0$ , will be intrinsically negative. In solving the antiforce wave case Sanmann changed the sign of the constants in the standard proforce equation set, and omitting the energy equation he used it as a set of electron-fluid dynamical equations for antiforce waves. We will show that to change formally from the standard proforce formulation by simple sign changes of constants is not possible.

Assuming the current flowing inside the wave to be  $i_1$ , whether we are in the laboratory or wave frame, the current in the quasi-neutral region is  $i_1$ , because it is a conduction current in a locally neutral gas. In the wave frame, the composition of the current at the front differs from

that at the quasi-neutral region, and also as seen from the laboratory, but the value remains the same because of Kirchhoff's law. In the wave frame, the current at the front is largely negative convection, but in the laboratory it is convection plus displacement, the convection being increased by the larger value of electron velocity, but cancelled out by displacement. In either case, the value remains unchanged at  $i_1$ .

Although our fluid dynamical model is one dimensional, the electrical model is three dimensional with rotational symmetry being a cylindrical rod with charged end. Assuming that the ionizing wave is propagating into a medium of glow-discharge ion concentration, the current in front of the wave ( $i_0$ ) might be on the order of  $10 \text{ A/m}^2$ . In other words, the field of an infinite plane wave could not be felt away from the front, that is to say, our one dimensional model does not apply to the field itself. There are two reasons for such a small current in an ionized medium ahead of the wave: (1) heavy positive and negative ions at glow discharge concentration can only carry  $\sim 10^5 \text{ A/m}^2$  in a field as big as  $E_0 \sim 5 \times 10^5 \text{ V/m/Torr}$ ; (2) negative ions would be stripped in such a strong field. We must therefore invoke something like the inverse square law to reduce the field rapidly away from the front. The electric field  $E$  at a distance  $\underline{r}$  ahead of a wave with front radius  $\underline{a}$  and front electric field  $E_0$  can be calculated from:

$$E = E_0 \frac{a^2}{r^2}, \quad (85)$$

then with  $a \sim 1 \text{ cm}$ ,  $i_0$  ( $i = e^2 n E / m K$ ) would be less than  $10 \text{ A/m}^2$  at a distance of 1 meter. Thus the inverse square law may account for much of the apparent sharpness of the discontinuity.

In the wave frame  $e N_i V_i$  carries a substantial portion of the current, but in the lab frame it is a near zero portion. Thus behind the wave front one has

$$e N_i V_i - n v = i_1. \quad (85a)$$

Based on the absence of an experimentally observed Doppler shift, which indicates that neither the ions nor the neutrals have appreciable motion in the laboratory, we can assume the velocity of ions and neutrals to be equal ( $V_i = V$ ). Substituting  $V$  for  $V_i$  in equation (85a) and solving it for  $N_i$

$$N_i = \frac{i_1}{eV} + n \frac{v}{V}. \quad (85b)$$

Substituting the above expression in the Poisson's equation of the form (19):

$$\frac{dE}{dx} = \frac{e}{\epsilon_0} \left( \frac{i_1}{eV} + n \frac{v}{V} - n \right). \quad (86)$$

One can write the other three electron-fluid equations in the form:

$$\frac{d}{d\xi} (nv) = \beta n, \quad (87)$$

$$\frac{d}{dx} \{mnv(v-V) + nkT_e\} = -enE - K_1mn(v-V) , \quad (88)$$

$$\frac{d}{dx} \{mnv(v-V)^2 + nkT_e(5v-2V) + 2e\phi_i nv - 5 \frac{k^2 nT_e}{mK_1} \frac{dT_e}{dx}\} = -2enE(v-V) . \quad (89)$$

We must be very careful about introducing dimensionless variables into the antiforce case. Let  $n=av$ ,  $v=V\psi$ ,  $T_e=b\theta$ ,  $E=\eta E_0$ ,  $x=-c\xi$ , where  $a, b, c > 0$ , and  $v, \psi, \theta, \eta, \xi > 0$ . Assuming  $x$  to be positive forward, then in this case  $\xi$  would be positive backward. Introducing the above dimensionless variables in equations (86-88), one has:

$$\frac{d\eta}{d\xi} = - \frac{ace}{\epsilon_0 E_0} \left( \frac{i}{eaV} + v(\psi-1) \right) , \quad (90)$$

$$\frac{d}{d\xi} (v\psi) = - \frac{c\beta v}{V} , \quad (91)$$

$$\frac{d}{d\xi} \left\{ v\psi(\psi-1) + v\theta \frac{2e\phi_i}{mV^2} \frac{bk}{2e\phi_i} \right\} = \frac{ceE_0}{mV^2} v\eta + c \frac{K_1}{V} v(\psi-1) . \quad (92)$$

If we wish our equations to be invariant from the proforce case in algebraic form, then for antiforce waves,

$$\frac{ceE_0}{mV^2} = -1 , \quad \frac{cK_1}{V} = -\kappa , \quad \frac{kb}{2e\phi_i} = 1 .$$

The above expressions result in

$$c = - \frac{mV^2}{eE_0} , \quad \kappa = \frac{mVK_1}{eE_0} , \quad b = \frac{2e\phi_i}{k} .$$

Since for antiforce waves  $E_0 > 0$ , and  $V < 0$ , then  $c$  and  $\kappa$  both would be negative. But this contradicts our definition of  $c$ , which was defined positive! It is consistent only for proforce waves where  $E_0 < 0$ . Therefore, we must let  $c$  be

equal to  $mV^2/eE_0$ , and  $\kappa = -mK_1V/eE_0$ , so that now both  $c$  and  $\kappa$  will be positive. Substituting the values of  $c$  and  $\kappa$  in equations (91) and (92) gives

$$\frac{d(v\psi)}{d\xi} = \kappa\mu v, \quad (93)$$

$$\frac{d}{d\xi}\{v\psi(\psi-1) + \alpha v\theta\} = v\eta - \kappa v(\psi-1), \quad (94)$$

where  $\mu = \beta/K_1 > 0$  and  $\alpha = 2e\phi_i/mV^2$ . Substituting  $mV^2/eE_0$  for  $c$  in Poisson's equation (90):

$$\frac{d\eta}{d\xi} = \frac{-aemV^2}{e\varepsilon_0E_0^2 2e\phi_i} 2e\phi_i \left( \frac{i_1}{aeV} + v(\psi-1) \right).$$

Substituting  $\kappa$  for  $-mK_1V/eE_0$ , setting  $a2e\phi_i/\varepsilon_0E_0^2 = 1$  in the above expression:

$$\frac{d\eta}{d\xi} = -\frac{v}{\alpha}(\psi-1) + \kappa \frac{i_1}{\varepsilon_0E_0K_1}.$$

If we represent  $i_1/\varepsilon_0E_0K_1$  by  $\nu$ , the above equation becomes:

$$\frac{d\eta}{d\xi} = -\frac{v}{\alpha}(\psi-1) + \kappa\nu. \quad (95)$$

From  $a2e\phi_i/\varepsilon_0E_0^2 = 1$ , one can solve for  $a$ :

$$a = \frac{\frac{1}{2}\varepsilon_0E_0^2}{e\phi_i},$$

where  $a$  is the ratio of the electromagnetic energy density to the energy required to ionize one atom, or in other words it is the number of the atoms which could be ionized with the discharge potential. Using the values found for  $a, b, c, \kappa$  in energy equation (89):

$$\frac{d}{d\xi} \{ v\psi(\psi-1)^2 + \alpha v\theta(5\psi-2) + \alpha v\psi - \frac{5\alpha^2 v\theta}{\kappa} \frac{d\theta}{d\xi} \} = 2v\eta(\psi-1). \quad (96)$$

Now let us look at the sign problem in  $\xi$  again. Suppose we decide to have  $n=av$ ,  $v=V\psi$ ,  $T_e=b\theta$ ,  $E=\eta E_0$ ,  $x=c\xi$  with  $a, b, c > 0$  and  $v, \psi, \theta, \eta > 0$ . Therefore  $\xi$  has to be negative because  $x$  is negative: i.e., we are going to integrate the equations backwards. In the latest form of the nondimensional variables the electron-fluid equations for antiproforce waves become:

$$\frac{d}{d\xi} (v\psi) = -\kappa\mu v, \quad (97)$$

$$\frac{d\eta}{d\xi} = \frac{v}{\alpha} (\psi-1) - \kappa_1, \quad (98)$$

$$\frac{d}{d\xi} \{ v\psi(\psi-1) + \alpha v\theta \} = -v\eta + \kappa v(\psi-1), \quad (99)$$

$$\frac{d}{d\xi} \{ v\psi(\psi-1)^2 + \alpha v\theta(5\psi-2) + \alpha v\psi - \frac{5\alpha^2 v\theta}{\kappa} \frac{d\theta}{d\xi} \} = -2v\eta(\psi-1), \quad (100)$$

where we have substituted  $\kappa = -(mVK_1/eE_0)$ ,  $c = mV^2/eE_0$ ,  $kb/2e\phi_i = 1$ ,  $a(2e\phi_i/\epsilon_0 E_0^2) = 1$ ,  $\alpha = (2e\phi_i/mV^2)$ , in the above expressions. In equations (97-100) all quantities but  $\xi$  are intrinsically positive, including  $\kappa$ .

The electron-fluid equations for the case of proforce waves, with  $\xi$  positive backward are:

$$\frac{d}{d\xi} (v\psi) = \kappa\mu v, \quad (101)$$

$$\frac{d\eta}{d\xi} = \frac{v}{\alpha} (\psi-1), \quad (102)$$

$$\frac{d}{d\xi} \{ v\psi(\psi-1) + \alpha v\theta \} = -v\eta - \kappa v(\psi-1), \quad (103)$$

$$\frac{d}{d\xi} \{v\psi(\psi-1)^2 + \alpha\theta(5\psi-2) + \alpha v\psi - \frac{5\alpha^2 v\theta}{\kappa} \frac{d\theta}{d\xi}\} = -2v\eta(\psi-1) . \quad (104)$$

To change formula from the standard proforce formulation we assume primes on all above quantities, and set  $\kappa = -\kappa'$ ,  $\xi = -\xi'$ . As one can see this action does not produce either set (97-100) or set (93-96) of the electron-fluid equations in the antforce case. Therefore, we are doubtful about some aspects of Sanmann's work.

If we include the electrons' heat loss term in their directed motion  $(m/M)nK_1m(v-V)^2$ , and electrons' heat loss term in their random motion  $(3m/M)nK_1kT_e$ , in the energy equation, the set of electron-fluid equations in the anti-force case with  $\xi$  positive backward will become:

$$\frac{d(v\psi)}{d\xi} = \kappa\mu v , \quad (105)$$

$$\frac{d\eta}{d\xi} = -\frac{v}{\alpha}(\psi-1) + \kappa_1 , \quad (106)$$

$$\frac{d}{d\xi} \{v\psi(\psi-1) + \alpha v\theta\} = v\eta - \kappa v(\psi-1) , \quad (107)$$

$$\begin{aligned} \frac{d}{d\xi} \{v\psi(\psi-1)^2 + \alpha v\theta(5\psi-2) + \alpha v\psi - \frac{5\alpha^2 v\theta}{\kappa} \frac{d\theta}{d\xi}\} \\ = 2v\eta(\psi-1) - \omega\kappa v(3\alpha\theta + (\psi-1)^2) . \end{aligned} \quad (108)$$

In solving the antforce case problem we will use the set of equations (105-108), where all quantities including  $\kappa$  are intrinsically positive. Writing the momentum equation (107) as a differential equation for  $\psi$ , substituting for  $dv/d\xi$  and  $d(v\psi)/d\xi$  from production equation (105), and

solving the resultant expression for  $d\psi/d\xi$  one will find:

$$\frac{d\psi}{d\xi} = \frac{\kappa\psi(1-\psi)(1+\mu) - \alpha\psi\theta' - \alpha\kappa\mu\theta + \eta\psi}{\psi^2 - \alpha\theta} . \quad (109)$$

Employing the Poisson's equation (106) in the energy equation (108) it becomes:

$$\frac{d}{d\xi} \left\{ \nu\psi(\psi-1)^2 + \alpha\nu\theta(5\psi-2) + \alpha\nu\psi + \alpha\eta^2 - \frac{5\alpha^2\nu\theta}{\kappa} \frac{d\theta}{d\xi} \right\} = 2\alpha\eta\kappa_i - \omega\kappa\nu(3\alpha\theta + (\psi-1)^2) . \quad (110)$$

Setting

$$\frac{dW}{d\xi} = 2\alpha\eta\kappa_i - \omega\kappa\nu\{3\alpha\theta + (\psi-1)^2\} , \quad (111)$$

one can solve the energy equation (110) for  $d\theta/d\xi$ :

$$\frac{d\theta}{d\xi} = \frac{\kappa}{5\alpha^2\nu\theta} \{ \nu\psi(\psi-1)^2 + \alpha\nu\theta(5\psi-2) + \alpha\nu\psi + \alpha(\eta^2-1) - W \} . \quad (112)$$

For antiferce waves, the shock condition on electron temperature will be different. To find the electron temperature at the shock front, we use the global momentum equation, which in the wave front becomes:

$$mnv^2 + nkT_e + MNV^2 + M_i N_i V_i^2 + NkT + N_i kT_i + \frac{\epsilon_0}{2}(E_0^2 - E^2) = MN_0 V_0^2 + N_0 kT_0 , \quad (113)$$

where ahead of the wave  $n$  and  $N_i$  are equal to zero,  $V$  equals  $V_0$ ,  $E$  equals  $E_0$ , and  $N$  equals  $N_0$ . Now exactly at the front, as in Chapter V we assume  $V=V_i=V_0$ ,  $T=T_i=T_0$ , and  $E=E_0$ , which reduces equation (113) to:

$$mn_1 v_i^2 + n_1 k(T_e)_1 + (MN + M_i N_i - MN_0) V^2 = 0 .$$

Using the equation of conservation of particles (30) and (M-m) for  $M_i$  in this expression:

$$mn_1v_1^2 + nkT_e - mN_iV^2 = 0 .$$

Substituting for  $N_i$  from equation (85b) at the wave front, one has

$$n_1v_1(v_1-V) + n_1 \frac{k}{m} (T_e)_1 - \frac{i_1V}{e} = 0 . \quad (114)$$

Introducing the nondimensional variables in equation (114) and substituting  $\iota$  for  $i_1/\epsilon_0 E_0 K_1$  it becomes:

$$\theta_1 = \psi_1(1-\psi_1)/\alpha - \kappa_1/v_1 . \quad (115)$$

To find the initial condition on  $W$ , one has to take the same course of action as we had previously in the case of proforce waves, and  $W_1=\alpha$  at the wave front.

Determining  $K_1$  from experimental curves<sup>29</sup> gives  $K_1/p = 3 \times 10^8$  for helium and  $K_1/p = 4.8 \times 10^7$  for nitrogen at 273°K. At a temperature of  $10^5$  K<sub>1</sub> will be  $2.4 \times 10^9$  and  $9 \times 10^9$  for helium and nitrogen respectively. Applied fields are usually of the order of  $10^5$  V/m; the current inside the antiforce waves is of the order of  $10^8$  A; and  $\epsilon_0$  is  $8.85 \times 10^{-12}$  farad/m. Considering that  $E_0, K_1, \beta$  in our formulas are scaled with  $p$  (the electron pressure) and using the values of  $i_1, \epsilon_0, E_0, K_1$  one can estimate the value of  $\iota$  which is of the order of one.

Using the equations (105), (106), (109), (111), and (112), acceptance of an electron temperature derivative discontinuity at the front, and the use of equation (115) for a shock condition on electron temperature led us to a completely satisfactory solution in both cases with and without current inside the wave which met the boundary conditions at the trailing edge of the wave.

The results were not very much dependent on the current inside the wave. We investigated the solutions both with and without current inside the wave. For the case of antiferce wave moving in nitrogen for  $\alpha=0.01$  we were able to find a solution at  $\kappa=1.3$ ,  $v_1=0.83$ ,  $\psi_1=0.68$ ,  $\iota=2.6$ . Figure 18 gives the electric field ( $\eta$ ) as a function of velocity ( $\psi$ ). Also for this case the electron temperature ( $\theta$ ), electron density ( $v$ ), ionization rate ( $\mu$ ) are drawn as a function of position ( $\xi$ ) in Figure 20.

For the case of zero current we were able to find a solution for antiferce waves propagating in nitrogen. The solution for  $\alpha=0.01$  were found at  $\kappa=1.3$ ,  $\psi_1=0.645$ ,  $v_1=0.886$  and  $\iota=0.0$ . Figure 21 gives the electric field ( $\eta$ ) as a function of electron drift velocity ( $\psi$ ), and Figure 22 gives electric field and velocity as a function of position ( $\xi$ ). In Figure 23 electron temperature ( $\theta$ ), electron density ( $v$ ), ionization rate ( $\mu$ ) are drawn as a function of position.

Comparing Figure 22 (antiferce case) with Figure 9 (proforce case) one can see a thickness of almost three

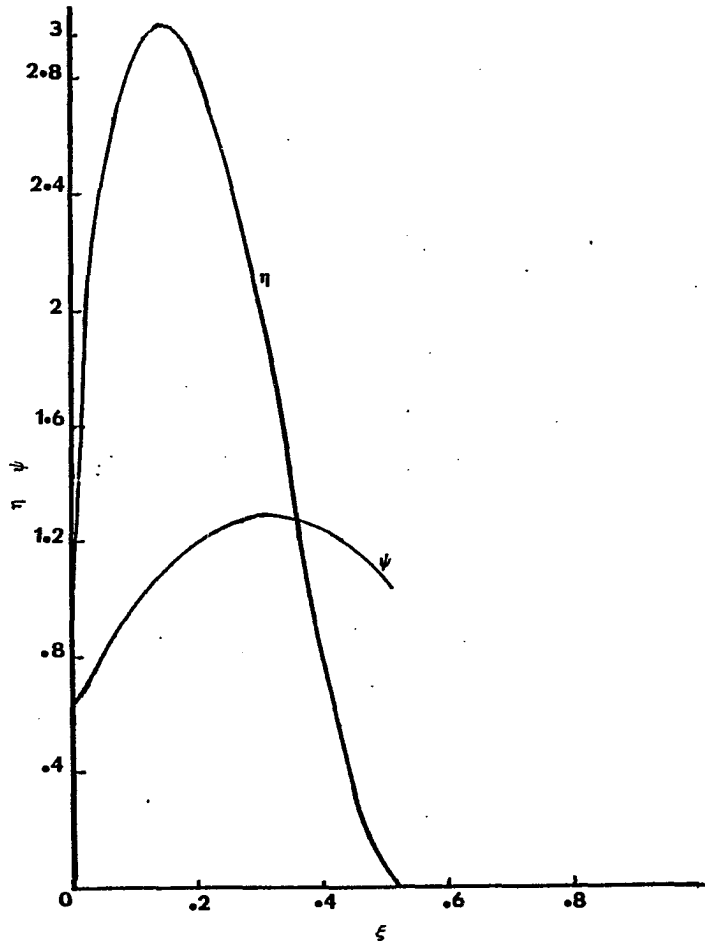


Figure 18. Electric field ( $\eta$ ) and drift velocity ( $\psi$ ) as a function of position ( $\xi$ ) for  $\alpha=0.01$  and  $\nu=2.6$  at  $\psi_1=0.68$ ,  $\kappa=1.3$ ,  $v_1=0.83$ .

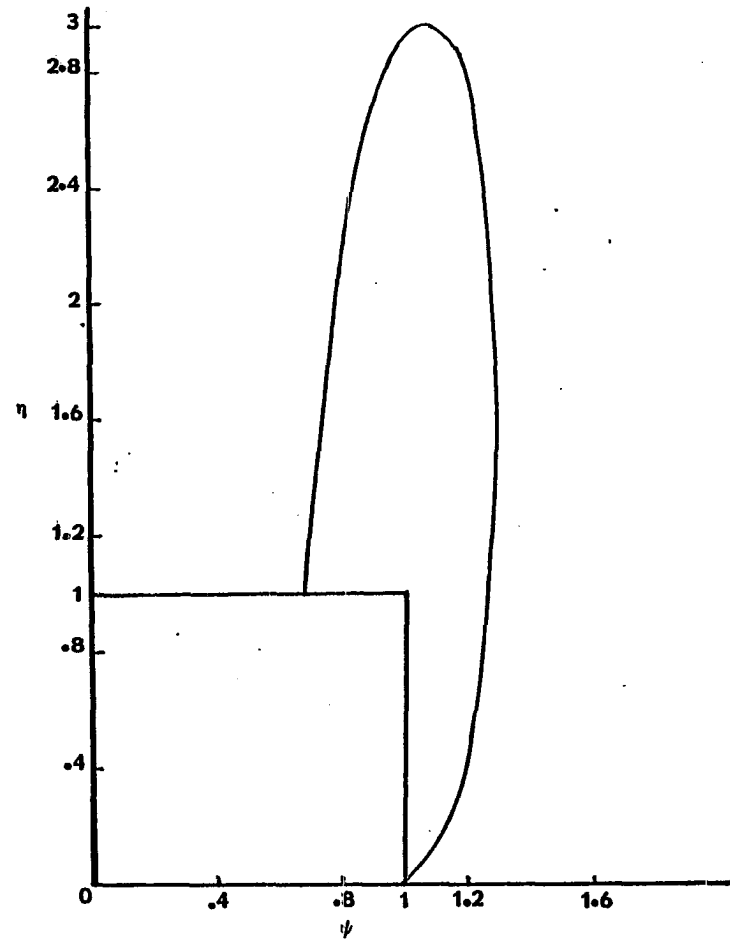


Figure 19. Electric field ( $\eta$ ) as a function of drift velocity ( $\psi$ ) for  $\alpha=0.01$  and  $\nu=2.6$  at  $\psi_1=0.68$ ,  $\kappa=1.3$ ,  $v_1=0.83$ .

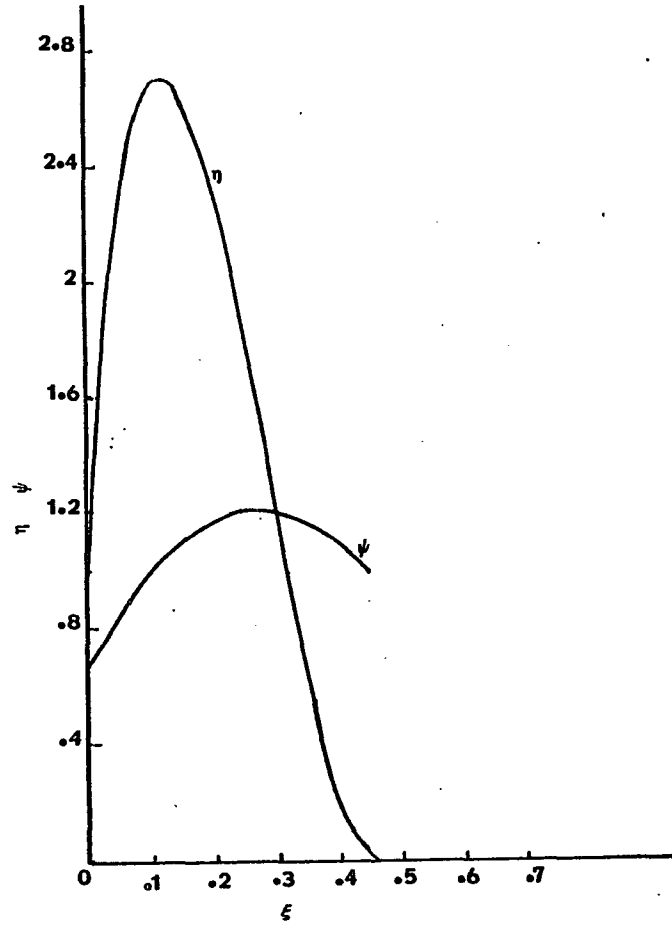


Figure 22. Electric field ( $\eta$ ) and drift velocity ( $\psi$ ) as a function of position ( $\xi$ ) for  $\alpha=0.01$  and  $\nu=0.0$  at  $\psi_1=0.645$ ,  $\kappa=1.3$ ,  $\nu_1=0.886$ .

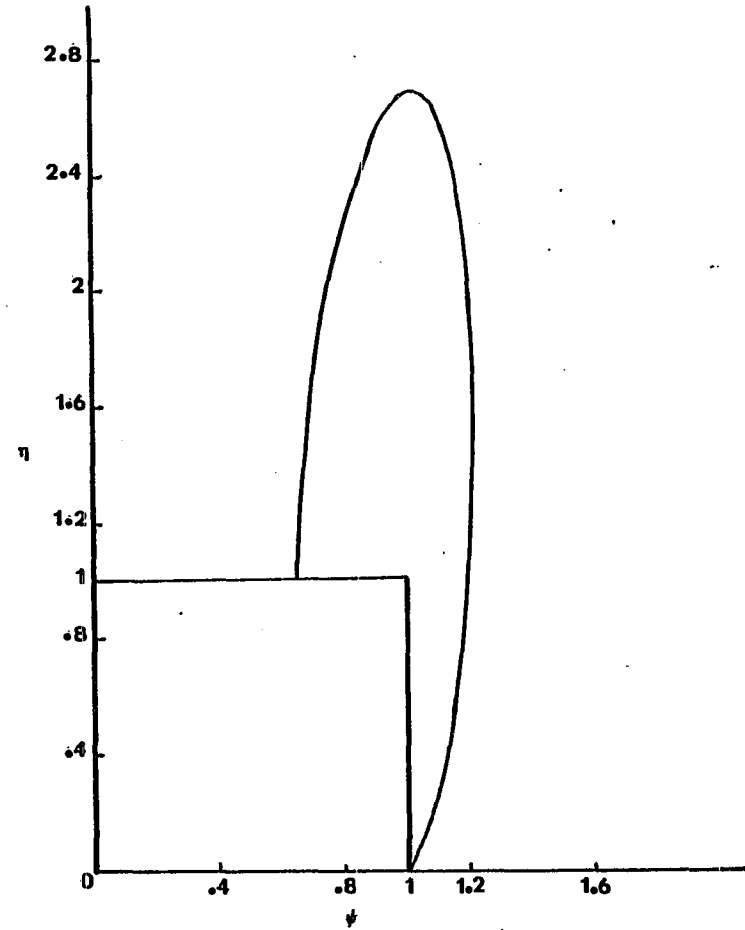


Figure 21. Electric field ( $\eta$ ) as a function of drift velocity ( $\psi$ ) for  $\alpha=0.01$  and  $\nu=0.0$  at  $\psi_1=0.649$ ,  $\kappa=1.3$ ,  $\nu_1=0.886$ .

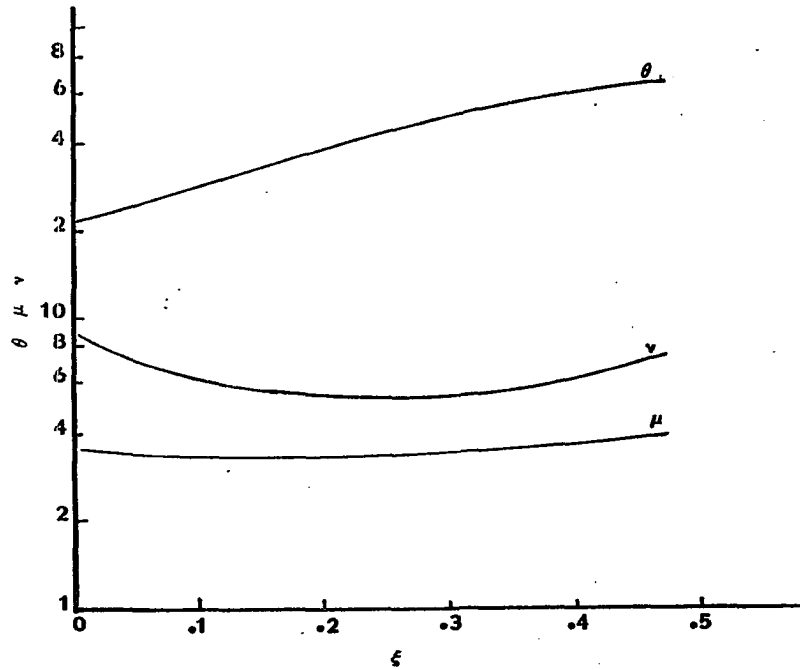


Figure 23. Temperature ( $\theta$ ), electron density ( $\nu$ ), ionization rate ( $\mu$ ) as a function of position ( $\xi$ ) for  $\alpha=0.01$  and  $\iota=0.0$  at  $\psi_1=0.645$ ,  $\kappa=1.3$ ,  $\nu_1=0.886$ .

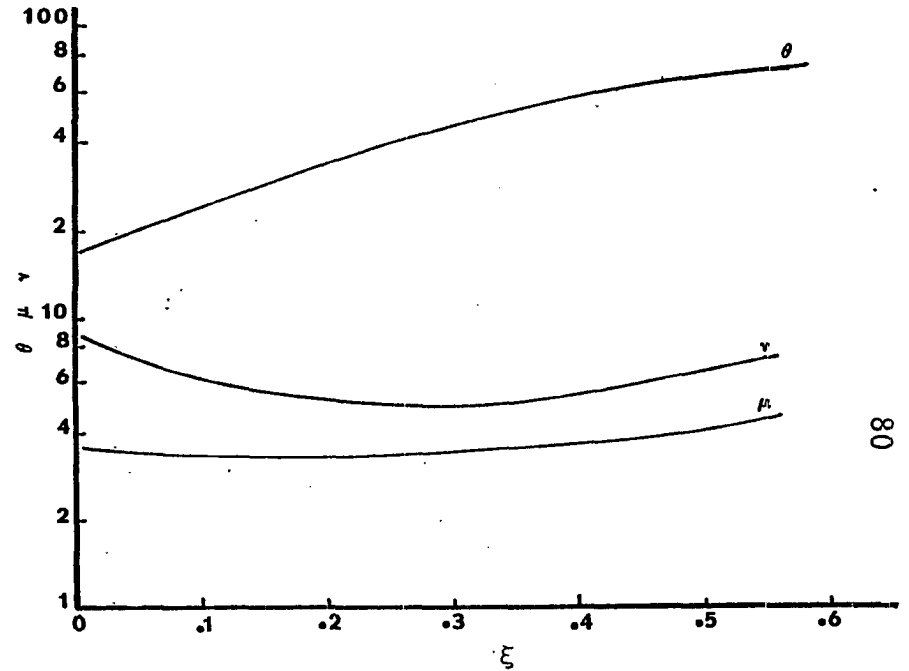


Figure 20. Electron temperature ( $\theta$ ), electron density ( $\nu$ ), and ionization rate ( $\mu$ ) as a function of position ( $\xi$ ) for  $\alpha=0.01$  and  $\iota=2.6$  at  $\psi_1=0.68$ ,  $\kappa=1.3$ ,  $\nu_1=0.83$ .

times larger for the sheath in the proforce case, where Sanmann<sup>28</sup> had reported a thicker sheath for antforce waves than for proforce waves.

## CHAPTER VII

### CONCLUSION

It has been shown that the assumption of ionizing waves being steady in profile is a good assumption, and the set of equations chosen from among the twelve possibilities are adequate to obtain a solution for ionizing waves. A one-dimensional theory for describing real two dimensional waves, heavy ion energy and momentum, and energy losses by the electrons of order  $m/M$  have a third order effect on the final results. The ionization rate and collision frequency in the region where electric field is present remains substantially constant. The assumption of heat conduction term being negligible has been abandoned, and it has been proven that it is essential for any solution of the electron-fluid equations. The concept of continuity in the initial derivatives of the functions must also be abandoned, particularly in the case of the temperature derivative. There is also a discontinuity in the derivatives (weak discontinuity) at the trailing edge of the wave sheath, between the sheath and the quasi-neutral region.

In the case of proforce waves propagating into an un-ionized medium, it has been shown that in the sheath prior

to the quasi-neutral region, the electric field and its derivative both fall to zero. In the case of the electron-fluid-dynamical waves moving into an ionized medium, only the derivative of the field approaches zero, and a residual field is responsible for deriving the current.

Electrons are the main element in deriving the electron fluid-dynamical waves. In the case of proforce waves the electron pressure and field force are both active agencies, but in the case of antiforce waves the electron pressure becomes the main driving force of the wave. In both cases pro and antiforce waves, the electrons and heavy particles come to rest relative to one another at the end of the sheath.

Shelton believed that essentially all the energy of the electric field ( $\frac{1}{2}\epsilon_0 E_0^2$ ) goes to ionizing the neutral atoms, but our computer solution of the electron-fluid equations which meet the boundary conditions ( $\eta=0, \psi=1$ ) within the accuracy of the integration step at the end of the wave, show otherwise. Energy is also lost in elastic processes, and does not show up in ionization, so that  $v$  does not reach unity.

From his shock conditions on electron temperature and velocity, Shelton concluded a minimum velocity condition ( $V_0 \geq \sqrt{2e\phi_i/m}$ ) exists on the strong discontinuity solutions, i.e., to  $0 < \alpha < 1$ , which had limited him to proforce waves.

The assumption of the temperature derivative discontinuity at the wave front allowed a lower range of electron drift velocities which have been observed experimentally. Since the zero current condition requires  $V$  and  $v_1$  to be of the same sign, from equation (64) one can have

$$5\left(1 + \frac{\alpha\theta_1'}{\kappa}\right) - \sqrt{\left(3 - 5 \frac{\alpha\theta_1'}{\kappa}\right)^2 + 16\alpha} > 0 ,$$

or

$$0 < \alpha < \left(1 - 5 \frac{\theta_1'}{\kappa}\right)^{-1} .$$

With positive values of  $\theta_1'$ ,  $\alpha$  admit values larger than one and we were able to find solutions for values of  $\alpha$  as large as 4.

Figure 24 shows the computer solution for the wave constant  $\kappa$  which relates wave velocity to electric field for an almost arbitrary gas placed against a background of data taken by Blais and Fowler, and Scott and Fowler in three gases, helium, argon and nitrogen. The data seems to scatter considerably about the theoretical curve, but taking the difficulties in the measurements (especially at the high velocity end of the range where the scatter is worst) into consideration, the agreement is very good. By using  $\kappa = mKV/eE$  as the ordinate the major dependence of the data has been taken out. This has been done for simplicity of comparison, but it loses most of the flavor of excellence of the agreement with the experimental data. The uncompressed version where velocity is plotted simply against

# WAVE CONSTANT

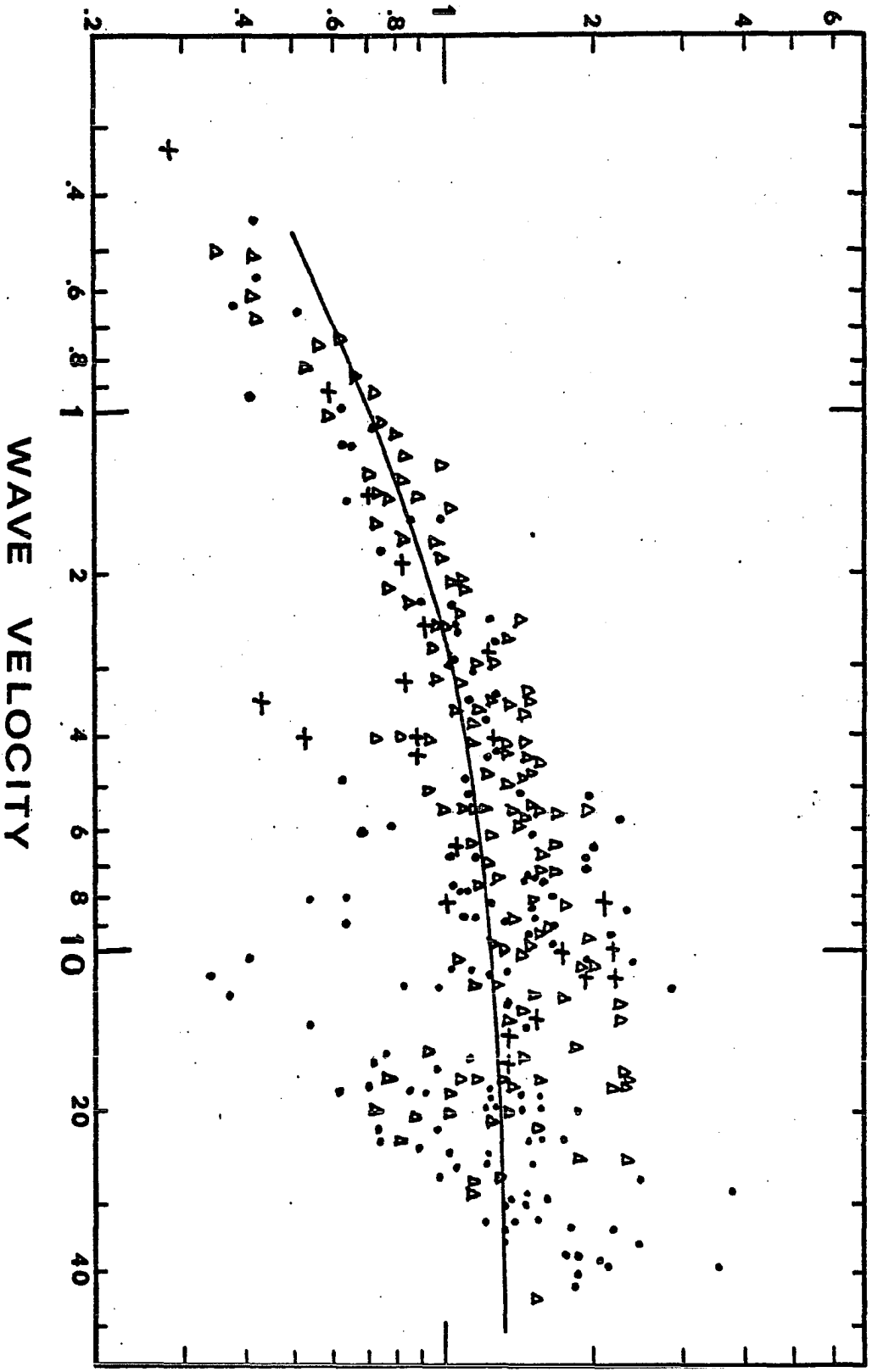


Figure 24.

electric field can be seen in the original work of Scott, although it is not as striking as it could have been because at that time the computer solution was not available.

It has been shown that the waves moving into an ionized medium have different structure than they possessed while moving into a non-ionized medium. The structure of these waves depend very much on the ion speed and concentration in front of the wave.

In the case of the anti-force waves we have shown that to change formally from the standard proforce formulation by sign changes of constants cannot be done. The new form of the electron-fluid equations with acceptance of an electron temperature derivative discontinuity in front of the wave led to a completely satisfactory solution which met the boundary conditions within the accuracy of the integration step. These waves are shock antiforce waves rather than the weak waves described by Sanmann.

Although the probable application of the theory of the electron fluid to lightning has been obvious ever since it was proposed by Paxton and Fowler, the deficiencies of the only solution of the complete equation set available deprived the Oklahoma group of the confidence with which they might otherwise have espoused this theory. Now, with the successful completion of the numerical solution we believe that the promise shown by the graph presented by Fowler and Scott, in which it was posited that the lightning phenomena

as well as other fast electron breakdowns are all consistent members of this electron acoustic wave family, has been borne out as to be expected, and that further efforts to use this theory is developing better models of the lightning column will be profitable. As applied to lightning it should take its most simplified form

$$V = \kappa \frac{eE}{mK} ,$$

where  $\kappa$  is given by the theoretical curve in Figure 24, and the electric field at the wave front is known.

## BIBLIOGRAPHY

1. F. Hauksbee, Phil. Trans. 24, 2129 (1705)
2. C. Wheatstone, Phil. Trans. 124, 583 (1834)
3. J. J. Thompson, Recent Researches 115 (1893)
4. R. G. Fowler, Adv. Elec. Electron Phys. 35, 1 (1974)
5. J. W. Seams, Phys. Rev. 36, 997 (1930)
6. T. E. Allibone and B.F.J.Schonland, Nature 134, 736 (1934)
7. L. B. Snoddy, J. W. Beams and J. R. Dietrich, Phys. Rev. 50, 739 (1937)
8. L. B. Snoddy, J. R. Dietrich and J. W. Beams, Phys. Rev. 52, 739 (1937)
9. F. H. Mitchell and L. B. Snoddy, Phys. Rev. 72, 1202 (1947)
10. R. G. Fowler, G. W. Paxton and H. G. Hughes, Phys. Fluids 4, 234 (1960)
11. R. G. Fowler and B. D. Fried, Phys. Fluids 4, 767 (1960)
12. L. B. Loeb, R. G. Westberg and H. C. Huang, Phys. Rev. 123, 43 (1961)
13. L. B. Loeb, Science 148, 1417 (1965)
14. G. W. Paxton and R. G. Fowler, Phys. Rev. 128, 993 (1962)

15. R. A. Nelson, Phys. Fluids 8, 23 (1964)
- 16a. R. G. Fowler and J. D. Hood, Phys. Rev. 128, 991 (1962)
- 16b. V. Josephson and R. W. Hales, Space Technology Laboratories, Inc., STL/TR/60-0000-13913 (1960)
- 16c. A. Haberstich, Ph.D. Dissertation, University of Maryland (1964)
- 16d. J. I. Mills, M. Naraghi and R. G. Fowler, Phys. Fluids \_\_, (1973)
17. G. A. Shelton, Jr. and R. G. Fowler, Phys. Fluids 11, 740 (1968)
18. R. G. Fowler and G. A. Shelton, Jr., Phys. Fluids 17, 334 (1974)
19. W. P. Winn, J. Appl. Phys. 38, 783 (1966)
20. R. N. Blais and R. G. Fowler, Phys. Fluids 16, 2149 (1973)
21. Klingbeil, D. A. Tidman and R. F. Fernsler, Phys. Fluids 15, 1969 (1972)
22. E. E. Sanmann and R. G. Fowler, Phys. Fluids 18, 1433 (1975)
23. R. P. Scott and R. G. Fowler, Phys. Fluids 20, 27 (1977)
24. G. A. Shelton, Ph.D. Dissertation, University of Oklahoma (1967)
25. R. G. Fowler, unpublished book manuscript
26. R. G. Fowler, Academic Press 41 (1976)
27. M. Hemmati, M.S. Thesis, University of Oklahoma (1980)

28. E. E. Sanmann, Ph.D. Dissertation, University of Oklahoma (1974)
29. E. W. McDaniel, Collision Phenomena in Ionized Gases (New York: Wiley, 1964)

APPENDIX

A Trajectory Theory of Ionization

in

Strong Electric Fields

Used by permission of

Richard G. Fowler

Department of Physics

University of Oklahoma 73019

### **Abstract**

A method is presented for averaging the ionization cross section over the electron energy distribution with due allowance for the curvature of the trajectory which becomes an important factor in strong electric fields whether or not the distribution is Maxwellian. The ionization rate is then found to depend on the electron acceleration, mean velocity, and temperature as independent parameters. This theory has proved to be essential to an exact solution of the equations for electron wave breakdown, and can be successfully applied to the data on swarms in strong fields.

## Introduction

Treatments of the discrepancy between the results of experiment in strong electric fields and the ionization rates obtained by averaging over a Maxwell distribution of electrons generally assign the entire correction to the distribution function (1,2), and highly sophisticated electron distributions have been devised both empirically and theoretically on this premise (3). In this approach the electron's path between collisions is implicitly assumed to be rectilinear. In fact, in strong electric and magnetic fields it is highly curved, and even returns on itself in many cases. Recognition of this fact has permitted a rigorous derivation of the Bohm diffusion coefficient (4), and an analysis of the mobility of electrons in strong fields (5). The success of these analyses has prompted this extension to the calculation of the ionization rate in a strong field. In particular our own motivation has been to have an analytical expression which could be introduced in the electron fluid equations for electron breakdown waves to replace the assumption necessary to the approximate solutions obtained by Shelton (6) that this rate was constant throughout the wave.

## General trajectory theory of an inelastic process

Let the electron begin its trajectory as in Fig. 1 with a speed  $v_0$ , at a polar angle  $\theta_0$ . Let its speed be  $v_f$  and its angle be  $\theta_f$  prior to the terminal collision.

If we consider trajectories of the same kind which end in a volume  $dAdz$ , then they will all have begun in a volume of the same size and shape, since each corner of the two volumes is connectable by parallel rigid displacements of the basic trajectory.

From kinematics,

$$v_0 \sin \theta_0 = v_f \sin \theta_f \quad (1)$$

$$v_0 \cos \theta_0 + \frac{eE}{m} t = v_f \cos \theta_f \quad (2)$$

Drift velocity is an essential factor in the electron distribution in an electric field. As a result of it, the longitudinal component of velocity  $v_0 \cos \theta_0$  includes a contribution which is absent from the transverse component. Let this be  $V$ . Then the appropriate expressions for the trajectory equations in terms of a distribution of initial velocities  $u, \theta$  (which is assumed to be isotropic in a drift-free frame of reference) are

$$u \sin \theta = v_0 \sin \theta_0 = v_f \sin \theta_f \quad (3)$$

$$u \cos \theta + V + \frac{eE}{m} t = v_f \cos \theta_f \quad (4)$$

We now desire to compute the number of inelastic collisions per unit volume and time. We choose the volume  $dA(v_f \cos \theta) dt$  at the end of the trajectory, and a similar volume at the head, and determine the number of times that targets in the former are exposed to projectiles that are in the latter, over the interval during which the one volume passes through the other. It follows that

number of inelastic collisions per unit volume and time =	number of projectiles participating in the collisions	x	fractional target area presented to projectile	
	effective time of exposure of targets	x	collision volume	(5)

Separately these concepts break down to

number projectiles participating =	number of projectiles of appropriate velocity in volume identical to collision volume, but at head of trajectory	x	probability that these projectiles joined the distribution in the initial volume and not further back	x	probability that they survive without collision for their full trajectory
					(6)

$$\text{fractional target area} = \frac{\text{number of targets per unit volume at end of trajectory} \times \text{area presented by each target for inelastic process} \times \text{collision volume}}{\text{face area of collision volume projected onto velocity flux plane}} \quad (7)$$

The effective time of exposure is the thickness of the collision volume divided by the velocity component in that direction if the computations of projectiles participating and of fractional target area are made as above by sweeping them up onto the face of the collision volume. This is simply the time  $dt$ . The alternative is to consider the time from initial melding of the projectile volume with target volume to their final separation. This will be twice as long, but in this interval and in this same collision volume an equal number of extra collisions will occur from the uncounted projectiles that lie ahead and behind the projectile volume.

Analytically these expressions evaluate to give

$$\frac{dn}{dt} = \frac{[dn(\vec{v}_0)] (\sigma N d\xi_0) (e^{-\int_0^{\xi} \sigma N d\xi}) (dAv_f dt \cos\theta_f) \frac{(N) (\sigma_i) (dAv_f dt \cos\theta_f)}{(dA \cos\theta_f)}}{(dt) \cdot (dAv_f dt \cos\theta_f)} \quad (8)$$

To obtain the ionization rate the integration must proceed over all three styles of trajectories that the final velocity permits those electrons which pass through the collision volume to possess. The total elastic cross section and the inelastic cross section are  $\sigma$  and  $\sigma_i$  respectively. The element  $d\xi_0$  is the trajectory length along which the trajectory entering collision occurred. At the head of the trajectory  $d\xi_0 = v_0 dt$ . The element  $d\xi$  lies at the terminus of the trajectory so that  $d\xi = v dt$ .

In terms of a general distribution fraction,  $dn(\vec{v}_0)$  becomes  $n f(\vec{v}_0) d\vec{v}_0$ , and since  $dn/dt = \beta n$ , we can express the rate of ionization  $\beta$  as

$$\beta = N^2 \int \sigma(v_0) f(v_0) d\vec{v}_0 \sigma_i(v_f) v_f e^{-\int_0^{\xi} \sigma N d\xi} du_0 \quad (9)$$

This is the basic formula sought. We now turn to evaluating it for use in strong fields.

### Ionization in a strong field with independent drift velocity

To this point one may use the distribution function of his choice, although purists in the evaluation of distribution functions would need to involve the expression above in the evaluation itself. To progress analytically, we assume as in the two previously cited trajectory method papers that the distribution of electrons in the drift frame is isotropic, and can be described by the speed  $u$  and polar angle  $\theta$ . Moreover, to obtain a practical expression for  $\beta$ , we will make use of the empirical fact that in the case of even moderate electron energies, the elastic cross sections behave as  $v^{-1}$ , and will introduce  $\sigma(v) = \sigma_0/v$ . For helium,  $\sigma_0 = 6.81 \times 10^{-8}$  cm<sup>3</sup>/sec.

We make a change from  $\xi$  to  $t$  momentarily, with  $d\xi_0 = v_0 dt$  and  $d\xi = v dt$ , so

$$\beta = NK \int_0^\infty f(v_0) d\vec{v}_0 \sigma_i(v_f) v_f e^{-Kt} dt \quad (10)$$

Here  $K = \sigma_0 N = 2.41 \times 10^9$  sec<sup>-1</sup> for helium. The limits of this integral are fictitious, as a result of the discontinuity in  $\sigma_i$ .

$$\sigma_i(v_f) = \begin{cases} 0 \\ \sigma_i(v_f) \end{cases} \text{ as } \begin{cases} v_f < v_i \\ v_f > v_i \end{cases} . \quad (11)$$

In velocity space we have axial symmetry, so azimuthal integration is immediately possible. We could now introduce the isotropic variable set  $(u, \theta, t)$ , but another choice is superior because its limits are not interconnected. It is the cylindrical system  $u_r, u_x, v_f$ . We first substitute  $(u_r, u_x)$  for  $(u, \theta)$ .

$$\beta = 2\pi NK \left(\frac{m}{2\pi kT}\right)^{3/2} \int_0^\infty \int_{-\infty}^\infty \int_{v_i}^\infty u_r du_r e^{-\frac{mu_r^2}{2kT}} du_x e^{-\frac{mu_x^2}{2kT}} \sigma_i(v_f) v_f e^{-Kt} dt \quad (12)$$

The limits, although no longer interconnected, are only nominally those given, and must be discussed below. For the change of variables from  $t$  to  $v_f$  we have

$$v_f^2 = u_x^2 + (u_x + at + V)^2 \quad (13)$$

where  $V$  is the electron fluid velocity, and  $a = \frac{eE}{m}$ . The  $t$  to  $v_f$  transformation is the equation of a cone in the  $u_x, u_x, v_f$  space. Then the ranges of  $v_f$  and  $u_x$  are

$$v_i < v_f < \infty \quad (14)$$

$$0 < u_x < v_f \quad (15)$$

For  $u_x$  there are two additive ranges or branches on which encounters are possible at the terminus: those trajectories on which the projectiles, colliding finally on a left to right course, may have originated on either the left or right hand sides of the control surface accordingly as the free parabolic trajectory is followed back to its starting point; and secondly, those trajectories which originate on the right, and the collision is made at the crossing from right to left. In the  $v_0, \theta_0, \xi$  system the first are both parts of the range of  $\theta_f > \pi/2$  and the second are for  $\theta_f < \pi/2$ . Then for the first range,  $-\infty < u_x < (v_f^2 - u_x^2)^{1/2} + u + V)/a$ . And for the second range,  $-\infty < u_x < -(v_f^2 - u_x^2)^{1/2} - V$  and  $t = -((v_f^2 - u_x^2)^{1/2} + u + V)/a$ . The integral thus proceeds from the inside of the cone on path A, as in Fig. 2, to  $-\infty$  for the first trajectories, and from the outside to  $-\infty$  for the latter, as on path B.

Now it is expedient to shift to  $v_f^2 - u^2 = w^2$  in place of  $u$ . Then  $w^2 = (u_x + at + V)^2$  so that  $v_f dv_f = w dt$ ;  $-u du = w dw$ . The new ranges of integration are

$$0 < w < v_f \quad (16)$$

$$-\infty < u_x < w - V \text{ matching with } t = \frac{w - u_x - V}{a} \quad (17)$$

and

$$-\infty < u_x < -w - V \text{ matching with } t = \frac{-w - u_x - V}{a} \quad (18)$$

Introducing the variables and limits into the expression for  $\beta$ ,

$$\beta = 2\pi N \left(\frac{m}{2\pi kT}\right)^{3/2} \frac{K}{a} \int_{-\infty}^{-\omega-V} du_x e^{-mu_x^2/2kT} \int_0^{v_f} dwe^{-m(v_f^2 - \omega^2)/kT} \dots$$

$$\dots \int_{v_i}^{\infty} (\sigma_i v_f^2) e^{K(\omega+u_x+V)/kT} dv_f + \int_{v_i}^{\infty} \int_0^{v_f} \int_{-\infty}^{\omega-V} du_x e^{-mu_x^2/2kT} dwe^{m(v_f^2 - \omega^2)/2kT} \dots$$

$$\dots (\sigma_i v_f^2) e^{K(-\omega+u_x+V)/kT} dv_f . \quad (19)$$

where we have further chosen to set the distribution Maxwellian. Rearranging integrations,

$$\beta = 2\pi N \left(\frac{m}{2\pi kT}\right)^{3/2} \frac{K}{a} e^{(K/a)V} \int_{v_i}^{\infty} dv_f e^{-mv_f^2/2kT} \sigma_i v_f^2 \dots$$

$$\dots \int_0^{v_f} \int_{-\infty}^{\omega-V} dwe^{(mu^2/2kT)+K\omega/a} du_x e^{-(mu_x^2/2kT)+(K u_x/a)} + \dots$$

$$\dots \int_0^{v_f} \int_{-\infty}^{\omega-V} dwe^{(m\omega^2/2kT)-(K\omega/a)} du_x e^{-(mu_x^2/2kT)+(K u_x/a)} . \quad (20)$$

Now, by letting  $\omega=-\omega$  in the second integral the whole can be thrown into the form

$$\beta = 2\pi N \left(\frac{m}{2\pi kT}\right)^{3/2} \frac{K}{a} e^{KV/a} \int_{v_i}^{\infty} dv_f e^{-mv_f^2/2kT} \sigma_i v_f^2 \int_{-v_f}^{v_f} dwe^{(m\omega^2/2kT)+(K\omega/a)} \dots$$

$$\dots \int_{-\infty}^{-\omega-V} du_x e^{-(mu_x^2/2kT)+(K u_x/a)} , \quad (21)$$

Introducing dimensionless variables,

$$\frac{mv_x^2}{2kT} = x^2, \quad \frac{mv_y^2}{2kT} = y^2, \quad \frac{mv_z^2}{2kT} = z^2. \quad (22)$$

and dimensionless constants

$$\sqrt{\frac{mv_i^2}{2kT}} = A, \quad \sqrt{\frac{m}{2kT}} V = B, \quad \sqrt{\frac{2kT}{m}} \frac{K}{a} = 2C, \quad \text{and} \quad (23)$$

$$\beta_0 = 4 \sqrt{\frac{2e\phi_i}{\pi m}} \frac{NC}{A} e^{2BC} \quad (24)$$

then

$$\beta = \beta_0 \int_A^\infty dz e^{-z^2} z^2 \sigma_i \int_{-z}^z dy e^{y^2+2Cy} \int_{-\infty}^{-(y+B)} dx e^{-x^2+2Cx} \quad (25)$$

Exact integration over  $y$  is possible by letting  $x = s-y-B$ . Then

$$\beta = \frac{\beta_0}{2} \int_A^\infty dz (z^2 \sigma_i) \int_{-\infty}^0 ds \frac{[e^{-(z-s+B)^2} - e^{-(z-s+B)^2}] e^{2C(s-B)}}{s-B} \quad (26)$$

Let  $s-B = u$ . Then

$$\beta = \frac{\beta_0}{2} \int_A^\infty dz (z^2 \sigma_i) \int_{-\infty}^{-B} du \frac{e^{-(z-u)^2} - e^{-(z+u)^2}}{u} e^{2Cu} \quad (27)$$

There appears to be a pole at  $u=0$ , but it is only a pseudopole because the numerator of the integrand also vanishes. When  $B > 0$ , the integration avoids  $u=0$  anyway. When  $B < 0$ , let  $u = -u$ . Then

$$\frac{\beta}{\beta_0} = 1/2 \int_A^\infty (z^2 \sigma_i) dz \int_B^\infty \frac{e^{-(z-u)^2} - e^{-(z+u)^2}}{u} du e^{-2Cu} \quad (28)$$

When  $B < 0$ , the integration passes through the pseudopole and must be watched carefully. When  $B < 0$ , let  $B = -|B|$ ,  $u = -u$ ,

$$\frac{\beta}{\beta_0} = 1/2 \int_A^\infty dz (z^2 \sigma_i) \int_{-|B|}^\infty \frac{e^{-(z-u)^2} - e^{-(z+u)^2}}{u} du e^{-2Cu} \quad (29)$$

Because of the factor  $\exp(-2Cu)$  both integrals are convergent.

To understand the integration of this expression we explore the location of the maxima of the integrand.

$$F = (z^2 \sigma_i) \left[ \frac{e^{-(z-u)^2} - e^{-(z+u)^2}}{u} \right] e^{-2Cu} \quad (30)$$

$F$  is the difference of two terms of which we need examine only the first term, remembering that  $\sigma_i = 0$  for  $z < A$ .

It will be shown below that

$$\frac{z}{A} \sigma_i \left( \frac{z}{2} - 1 \right)^{1+\epsilon} \quad (31)$$

where  $\epsilon < 1$  is an excellent approximation to the ionization cross section for these purposes, yielding

$$\frac{\partial F}{\partial z} = (1 + \epsilon) z + (z - A)^2 (u - z) = 0. \quad (32)$$

From this the equation for the maxima at constant  $u$  is

$$u = z - \frac{(1 + \epsilon)z}{z - A} \quad (33)$$

This expression describes a ridge with a declining crest, asymptotic to  $z = A$  for  $u \rightarrow \infty$  and to the line  $z = u$  as  $z \rightarrow \infty$ . The crest drops as  $\exp(-2Cu)$ . For constant  $z$  the maxima are along the curve

$$z = u + C + \frac{1}{2u} \quad (34)$$

These results, and the domain of integration are depicted in Fig. 3.

Evaluation of the function is best made directly from the double integral in the  $z, u$  form, and a Fortran IV program has been written to carry it out. Samples of the result for helium are given in Figures 4 to 6. The only peculiarity of the program is an algorithm to begin the integration of each vertical strip close to the ridge, and to stop just beyond it to avoid immense numbers of zero increments.

#### **Empirical cross section functions**

Tate and Smith (7) and Rapp and Englander-Golden(8) have measured ionization cross sections for a wide variety of gases. Considering how old the former measurements are, they are in remarkable agreement with the latter recent ones, and lend confidence to the uses to which they have been put over the years. The discrepancies can be reduced even further by use of the empirical functions presented in the previous section, which tend to show quite conclusively that they differ by scale factors that can no doubt be traced to inaccurate pressure measurements in the Tate and Smith data, and by small threshold offsets which are present in both works, but are considerably larger for the former. Wannier (9) has shown that it is theoretically to be expected that near the threshold ionization yield varies as about the 1.127 power of the excess energy. Beyond this however one finds that if  $X$  is the ratio of electron energy to the ionization energy,  $W/W_i$ , and  $X-1$  is used as abscissa, and the product of  $X$  and the collision probability as measured by the authors is used as ordinate on a log-log plot, an extraordinary fit is achieved from

only slightly above threshold to four or five times the ionization potential. That is to say again,  $P_i$  can be fitted by

$$P_i = A (W/W_i - 1)^n W_i/W \quad (35)$$

In fact if accuracy commensurate with the Tate-Smith cross sections is adequate, with a slight sacrifice of the fit at the lower energies, all the data on a log-log plot can be fitted with a single straight line within the experimental error. With the RE-G data, however, a second range of linearity is usually noticeable between about three and six times threshold, and above six times threshold, the Born approximation theoretical logarithmic form

$$P_i = C \ln (b W/W_i) (W_i/W) \quad (36)$$

agrees elegantly with the RE-G data, and is some improvement for the Tate-Smith data over the fit to a single power of  $(X-1)$ . This power law approximation was applied by the author some years ago (10), and a similar but somewhat more complex single fitting function has recently been reported independently by Green, Jackman and Garvey (11). Jackman, Garvey and Green (12) have also made new measurements of the various cross sections but the numerical values were not published and are not available for comparison. The constants for the piecewise continuous power fit are given in Table 1. They give a fit to the Rapp and Englander-Golden data which is generally better than  $\pm 1\%$ , and have proved very useful to us in ionizing wave studies. A sample of the quality of the data fit is given in Table 2. The RG-E data have been converted from cross sections to ionization probabilities by multiplying by 3.112.

The ionization potentials indicated by the best fit to the power law are slightly offset from the generally accepted spectroscopic values by amounts of the order of .1 volt, but are variable with the nature of the gas in a manner which suggests differences in contact potential. Only the complex molecules NO, CO<sub>2</sub>, and N<sub>2</sub>O, whose ionization potentials do not seem to be well known, show large

discrepancies, some of which are no doubt attributable to their large electronegativeness. This interpretation is strengthened by the few cases of Tate-Smith data which are extensive enough at low energies to permit an estimate. Since their apparatus would have employed different materials, different contact potentials would be anticipated. These results are summarized in Table 3. Small pressure discrepancies also exist between the two data sets, on an average about 5%, but more seriously, for many of the Tate-Smith curves, especially in gases like argon which are partially condensible at liquid air temperature, the pressure seems likely to have varied by as much as 10% over the duration of the experiment. Another probable factor accounting for the disagreement of order 20% at large energies is a systematic change of collector efficiency as the beam field penetrated the collector in the Tate-Smith apparatus.

#### **Application to ionizing waves**

The ionizing waves present in electrical breakdown of a gas form a particularly interesting situation in which to apply the trajectory calculation of ionization rate because the three parameters which govern the rate, namely temperature (random velocity), drift velocity (directed velocity), and electric field (acceleration) are independent of each other because of the electron shock which leads the wave, and are related only through the differential equations of balance for the electron fluid. Shelton (6) derived these equations some years ago, but was only able to solve them under the assumption that the ionization rate was constant through the vitally important sheath region of the wave. Nevertheless, this severe assumption led to predictions of wave velocity dependence on driving field which were in excellent agreement with observations. When the system of equations was first attacked with numerical integration, the natural thought was to use the usual average of the ionization cross section over a thermal distribution of electron velocities, with the resulting Arrhenius type function. It was immediately apparent that the low electron

temperature at the immediate leading edge of the ionizing wave could never produce ionization fast enough to bring the wave into being in the lower range of wave velocities. When, however, the trajectory theory was incorporated into the solution code, a complete solution of the equations was obtained which fitted better with experiment than any previous effort, and automatically gave an ionization rate that was nearly constant through the sheath (14). A sample of this calculation is given in Fig. 7, and values of the electron mobility form-factor defined as

$$\kappa = (mV/eE)K \quad (37)$$

by Shelton as characteristic of the wave process are given in Table 4.  $K$  is the momentum transfer collision frequency.

The relation between the wave quantities and the constants of the ionization integral can be found by the following reasoning. Shifting from the laboratory frame to the wave frame, moving at speed  $W$ , the electron fluid velocity becomes

$$v' = V - W \quad (38)$$

The ionization integral parameter  $B$  is determined by  $V$  and is therefore

$$B = (v' + W(m/2kT))^{1/2} \quad (39)$$

The parameters  $A$  and  $C$  are defined as before.

#### Application of trajectory ionization to swarms

The swarm ionization process lies at the other extreme from the wave process, and yet they are intimately related because the former goes over into the latter if the field is strong enough and the course is long enough. In the swarm process there is a steady or at worst a slowly changing state prevailing, in which the three parameters governing ionization are interrelated. Temperature and drift velocity (whenever the field is strong enough for it to be important) are directly determined by the electric field, and these relations can be both calculated and measured. The drift velocity  $V$  in the laboratory frame is now related directly to the ionization integral parameter  $B$  by the expression

$$B = (m/2kT)^{1/2}V \quad (40)$$

The parameters A and C are unchanged in definition, but are now interrelated by their common dependences on  $E/p$ . Both of these quantities are plotted in Fig. 8. The theory of noble gases is especially simple and accurate, but the example chosen here for detailed study, nitrogen, is notoriously difficult at low energies because of the unsatisfactory knowledge of the rotation and vibration cross sections. The vibration cross-sections of Engelhardt et al. (23) and the excitation cross-sections of Stanton and St. John (24) were included, but the former was unimportant above  $E/p$  of  $10^3$  v/m/torr. Excitation made a difference of 100% in the mid range of the temperature curve, and considering the outstanding agreement of the trajectory theory above  $E/p$  of  $10^5$ , it is probable that the remaining 25% discrepancy below that point is a result of including only the four excited states for which measurements are available. In fact, if it is assumed that the  $A^3\Sigma$  state has a cross section like that of the  $C^3\Pi$ , 1/3 of the needed correction is achieved. The result of using a Maxwell distribution under the usual assumptions of straight line paths at constant velocity between collisions is also shown as broken curves. The trajectory approach is much more significant for temperature than drift velocity.

In Fig. 9 the result of calculating Townsend's  $\alpha/p$  is given. To obtain it from  $\beta$ , the velocity of the current which would be measured in a Townsend amplification measurement is needed. This can be calculated by the trajectory method also (5). Again the lower values of  $E/p$  are strongly influenced by excitation, but the agreement is excellent in the higher ranges for which it is intended, and agrees with Harrison (1956) over all his range. It is not evident that the result could be improved if the electron distribution function were also altered.

### Conclusion

The ionization cross section varies rapidly along the trajectory of an accelerating electron in a strong field, and cannot be treated as constant over this

flight as is generally done in Boltzmann equation theory. An attempt has been made to incorporate this variability and the additional factor of non-rectilinearity in a closed form expression for the ionization rate. This has seemed to be successful in the two or three cases to which it has been applied.

**TABLE 1**  
Fitting Constants

Gas	W	A <sub>1</sub>	n <sub>1</sub>	Transition X	A <sub>2</sub>	n <sub>2</sub>	Transition X	C	b
He	24.472	1.6852	1.1715	2.189	1.732	1.0126	3.72	6.604	.5509
Ne	21.402	1.8727	1.1835	2.968	2.349	1.1835	6.28	23.75	.3200
Ar	15.686	14.456	1.2855	1.990	14.400	.8922	6.25	61.20	.4561
Kr	13.924	17.895	1.3053	2.293	19.586	.9497	7.06	107.17	.3653
Xe	12.092	21.796	1.1868	2.434	23.734	.9504	7.06	169.09	.3083
CO	13.5	7.292	1.634	1.205	8.188	1.2047	5.79	78.87	.3249
H <sub>2</sub>	15.461	4.741	1.0184	3.180	5.630	.7979	5.96	15.06	.6418
O <sub>2</sub>	11.95	1.0319	1.8738	4.167	6.291	1.2904	7.39	102.80	.2571
N <sub>2</sub>	15.311	6.8475	1.4265	4.306	13.779	.8404	10.39	66.59	.3746
CO <sub>2</sub>	13.029	7.262	1.594	1.269	9.116	1.2692	6.60	121.38	.2819
N <sub>2</sub> O	12.111	8.333	1.530	2.392	8.980	1.3065	6.59	131.12	.2792
NO	8.00	6.40	3.40	1.701	3.31	1.545	6.3	142.53	.2154
CH <sub>4</sub>	12.897	14.453	1.565	2.078	15.036	1.0400	5.66	94.04	.3728
D <sub>2</sub>	15.484	5.282	1.1018	1.780	5.1069	.9652	3.27	15.68	.6120
SF <sub>6</sub>	14.998	13.693	2.271	2.232	16.738	1.3094	6.96	246.96	.2755

**TABLE 2**

**Fitting Comparison, Helium Ionization Efficiencies (ion pairs/cm)**

<b>Energy (Nominal, ev)</b>	<b>Efficiency (Experimental RE-G)</b>	<b>Efficiency (Fitted)</b>	<b>Efficiency (Experimental T-S)</b>
25	.018	.018	.022
25.5	.040	.039	.045
26	.062	.061	.069
26.5	.083	.084	.092
27	.107	.107	.114
60	1.027	1.031	1.025
70	1.136	1.135	1.11
80	1.217	1.215	1.178
200	1.226	1.216	1.149
500	.793	.783	.728
800	.582	.584	.530
1000	.498	.503	.448
2000	---	.306	.26
4000	---	.181	.142

Table 3

Ionization Thresholds

Gas	Ionization Potential (13)	Ionization Threshold (R-EG)	Difference	Ionization Threshold (T-S)
He	24.580	24.473	.107	24.375
Ne	21.559	21.402	.157	21.03
Ar	15.755	15.686	.069	15.2
Kr	13.996	13.924	.072	
Xe	12.137	12.092	.045	
H <sub>2</sub>	15.427	15.461	-.034	
N <sub>2</sub>	15.576	15.311	.265	
O <sub>2</sub>	12.063	11.95	.113	
CO	14.013	13.5	.513	13.67
CH <sub>4</sub>	12.99	12.897	.093	
NO	9.5 (9.25*)	8.00	1.5	9.07
CO <sub>2</sub>	14.4 (13.79*)	13.029	1.371	
D <sub>2</sub>	15.46	15.484	.024	
N <sub>2</sub> O	12.894	12.111	.783	
SF <sub>6</sub>		14.998		

\*Watanabe et al. (15)

Table 4

Wave Constants for Helium

Dimensionless energy ratio ( $e\phi_z/mV^2$ )	Momentum loss rate ratio to electric force, $\kappa$
.0001	1.410
.001	1.310
.01	1.303
.1	1.200
.25	1.000
1.0	.770
2.0	0.673
4.0	0.560

**ACKNOWLEDGEMENT**

This research was supported in part by the National Science Foundation Division of Atmospheric Sciences under Grant No. ATM 7918510. We would like to thank them for their support.

REFERENCES

- (1) Smit, J.A., Physica 3, 543 (1936)
- (2) Kontoleon, N., Lucas, J. and Virr, L.E., J. Phys. D: Appl. Phys. 6, 1237 (1973)
- (3) Baraff, G.A. and Buchsbaum, S.J., Phys. Rev. 130, 1007 (1963)
- (4) Fowler, R.G., Phys. Fluids 21, 1972 (1978)
- (5) Fowler, R.G., J. Phys. D: Appl. Phys., 11, 1843 (1978)
- (6) Shelton, G.A., Dissertation, Univ. Okla. (1967); Shelton, G.A. and Fowler, R.G., Phys. Fluids 11, 740 (1968) ; Fowler, R.G. and Shelton, G.A., Phys. Fluids 17, 334 (1974)
- (7) Smith, P.T., Phys. Rev. 36, 1293 (1930); Smith, P.T., Phys. Rev. 37, 808 (1931); Tate, J.T. and Smith, P.T., Phys. Rev. 270 (1932)
- (8) Rapp, D. and Englander-Golden, P., J. Chem. Phys. 43, 1464 (1965)
- (9) Wannier, G.H., Phys. Rev. 90, 817 (1953)
- (10) Fowler, R.G., Electrically Energized Shock Tubes, Univ. Okla. Res. Inst. (1963); Fowler, R.G., Adv. Electronics Electron Phys. 35, 1 (1974)
- (11) Green, A.E.S., Jackman, C.H. and Garvey, R.H., J. Geophys. Res. 82, 5104 (1977)
- (12) Jackman, C.H., Garvey, R.H. and Green, A.E.S., J. Geophys. Res. 82, 5081 (1977)
- (13) Handbook of Chem. and Phys., Chemical Rubber Co., Cleveland (1981)
- (14) Fowler, R.G., Hemmati, M. and Parsenajadh, S., J. Geophys. Res. (submitted 1982)
- (15) Watanabe, K., Nakayama, T. and Mottl, J. J.Q.S.R.T. 2 369 (1962)
- (16) Schlumbohm H., Z. Phys. 184 492-505 (1965)
- (17) Townsend J.S. and Bailey V.A. Phil. Mag. 42 270-7 (1921)
- (18) Blevins H.A. and Hasan M.Z. Aust. J. Phys. 20 741 (1967)
- (19) von Engel A. Ionized Gases (Oxford) (1965).
- (20) Raether, H., Electron Avalanches and Breakdown in Gases, Butterworths, London (1964)

- (21) Harrison, M.E., Phys. Rev. **105**, 366 (1956)
- (22) BOWLS, W.E., Phys. Rev. **53**, 293 (1938)
- (23) Engelhardt, A.G., Phelps, A.V. and Risk, C.G., Phys. Rev. **135**, A1566 (1964)
- (24) Stanton, P.N. and St. John, R.M., J. Chem. Phys. **59**, 253-60 (1969)

### Captions

- Fig. 1. Geometry of collision process.  $\xi$  is measured backward from  $f$  to  $o$  along the free trajectory.
- Fig. 2. Phase space geometry of the integration and variable changes.
- Fig. 3. Topology of the domain of integration of the final integral. A roughly Gaussian wrinkle of exponentially declining amplitude runs from the origin to infinity between the lines Z and U. Vertical traverses find the maxima on curve U, horizontal on curve Z. The geometrical significance of the constants A, B and C in defining the range of integration is depicted.
- Fig. 4 Ionization frequency  $\beta$  as a function of scaled electron temperature  $\theta = kT/2e\phi_i$ , with scaled field  $\eta = eE/mkV_i$  marked on each curve. Entire figure is for electron drift velocity  $v = V_i = (2e\phi_i/m)^{1/2}$ .
- Fig. 5 Same as Fig. 4 except that  $v = 0$ .
- Fig. 6. Same as Fig. 4 except that  $v = -V_i$ .
- Fig. 7 Result of integrating the electron fluid equations to obtain profiles of field, electron velocity, temperature, and ionization rate in the wave sheath for a relatively fast wave ( $V = 3 \times 10^7$  m/sec) in helium. The wave thickness is scaled with the distance over which an electron acquires ionizing potential energy in the field.
- Fig. 8 Trajectory ionization theory (T) applied to calculation of electron temperatures and drift velocities in swarms, contrasted with use of a simple Maxwellian calculation (M) based conventionally on linear constant speed paths between collisions. Hollow stars are from Schlumbohm (16); solid five-point stars are from Kontoleon et al.; and other stars are from Townsend and Bailey (17). Diamonds are from Blevins and Hasan (18).
- Fig. 9 Townsend's  $\alpha/p$  derived by the trajectory method (T), contrasted with the conventional approach (M). Solid dots are taken from von Engel (19); stars in dots are from Kontoleon et al.; hollow stars are from Raether (20); small asterisks are from Harrison (21); and large asterisks are by Bawls (22).

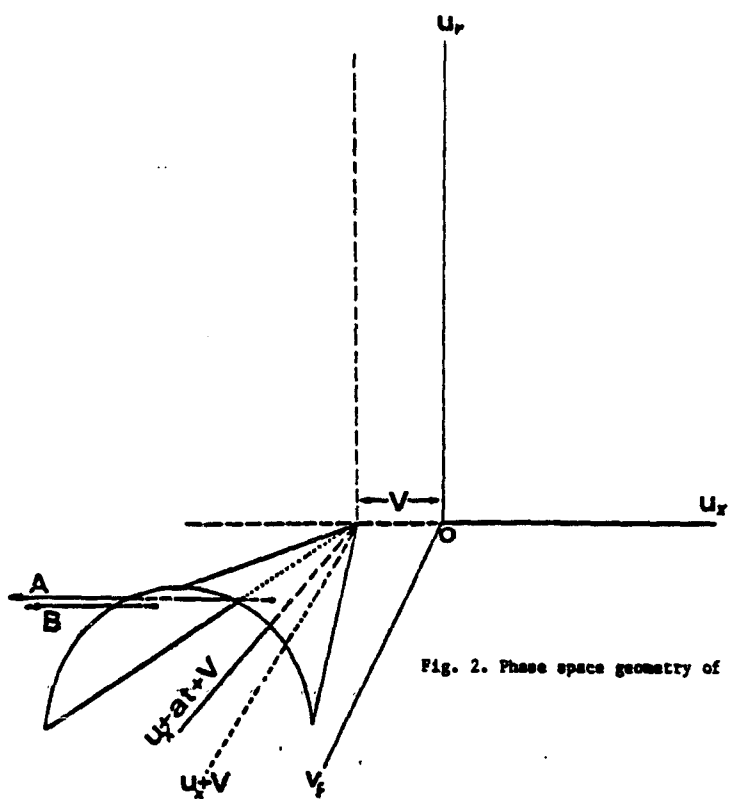


Fig. 2. Phase space geometry of the integration and variable changes.

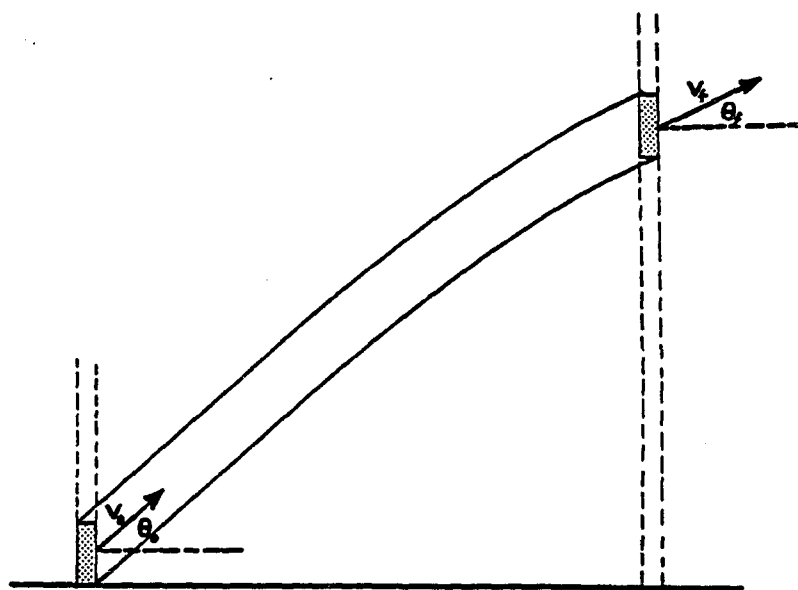


Fig. 1. Geometry of collision process.  $\xi$  is measured backward from  $f$  to  $o$  along the free trajectory.

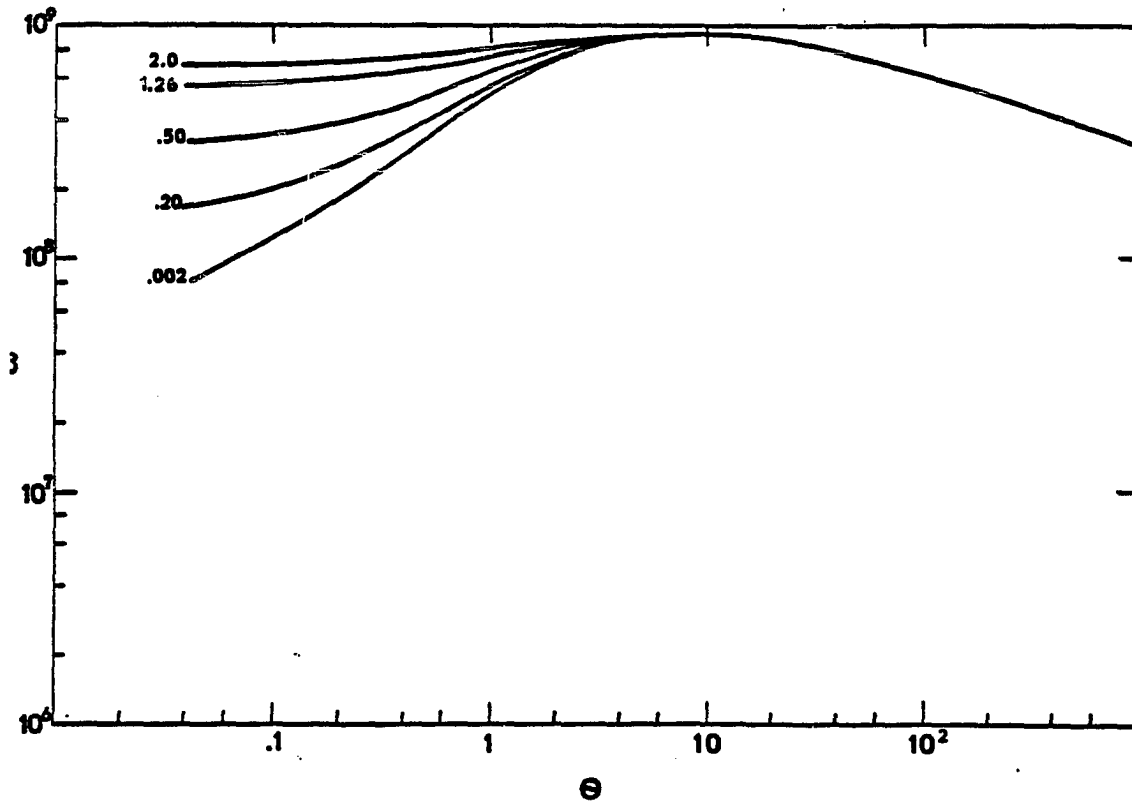


Fig. 4 Ionization frequency  $\beta$  as a function of scaled electron temperature  $\Theta kT/2e \phi_1$ , with scaled field  $\eta = eE/mkV_i^2$  marked on each curve. Entire figure is for electron drift velocity  $v = V_i = (2e \phi_1/m)^{1/2}$

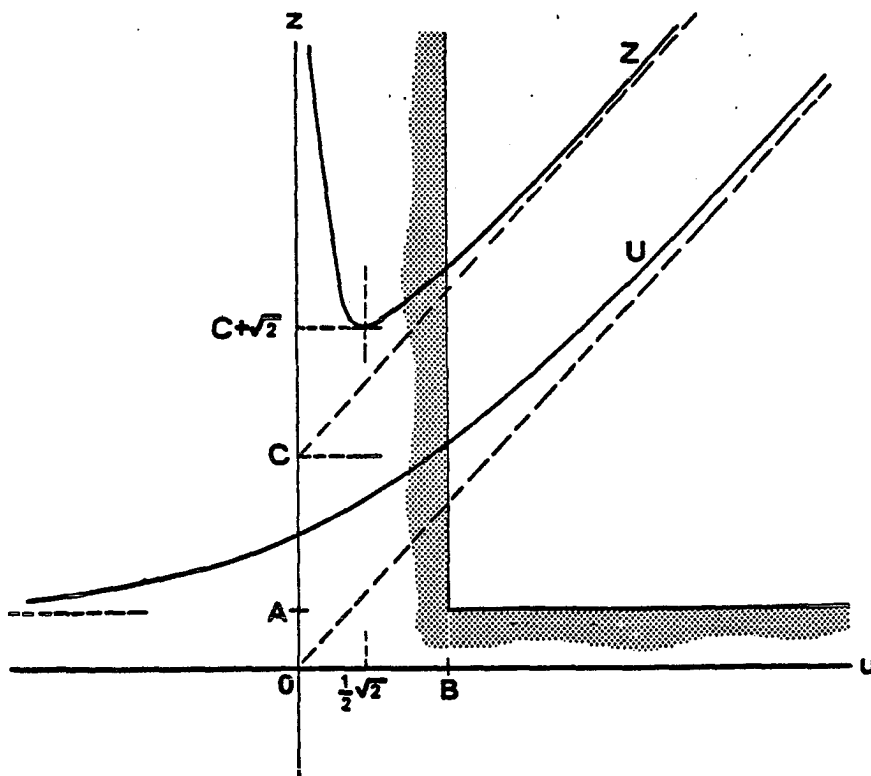


Fig. 3. Topology of the domain of integration of the final integral. A roughly Gaussian wrinkle of exponentially declining amplitude runs from the origin to infinity between the lines Z and U. Vertical traverses find the maxima on curve U, horizontal on curve Z. The geometrical significance of the constants A, B and C in defining the range of integration is depicted.

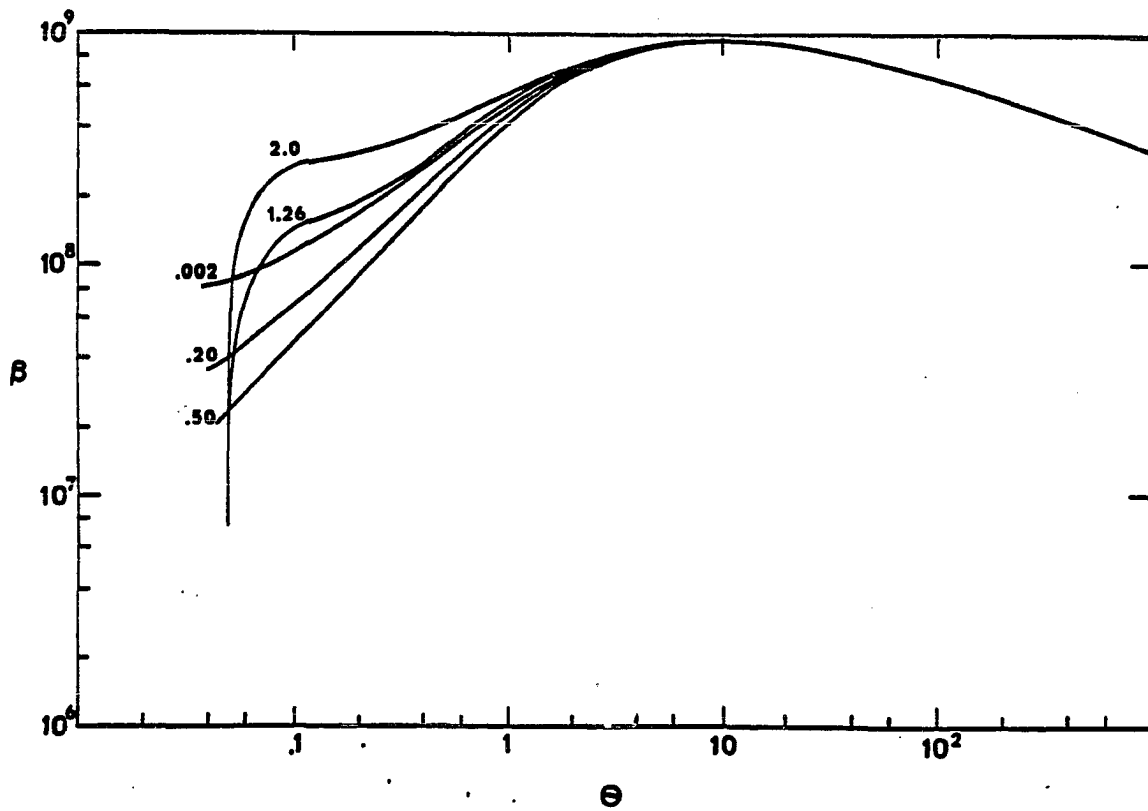


Fig. 6. Same as Fig. 4 except that  $\nu = -V_i$ .

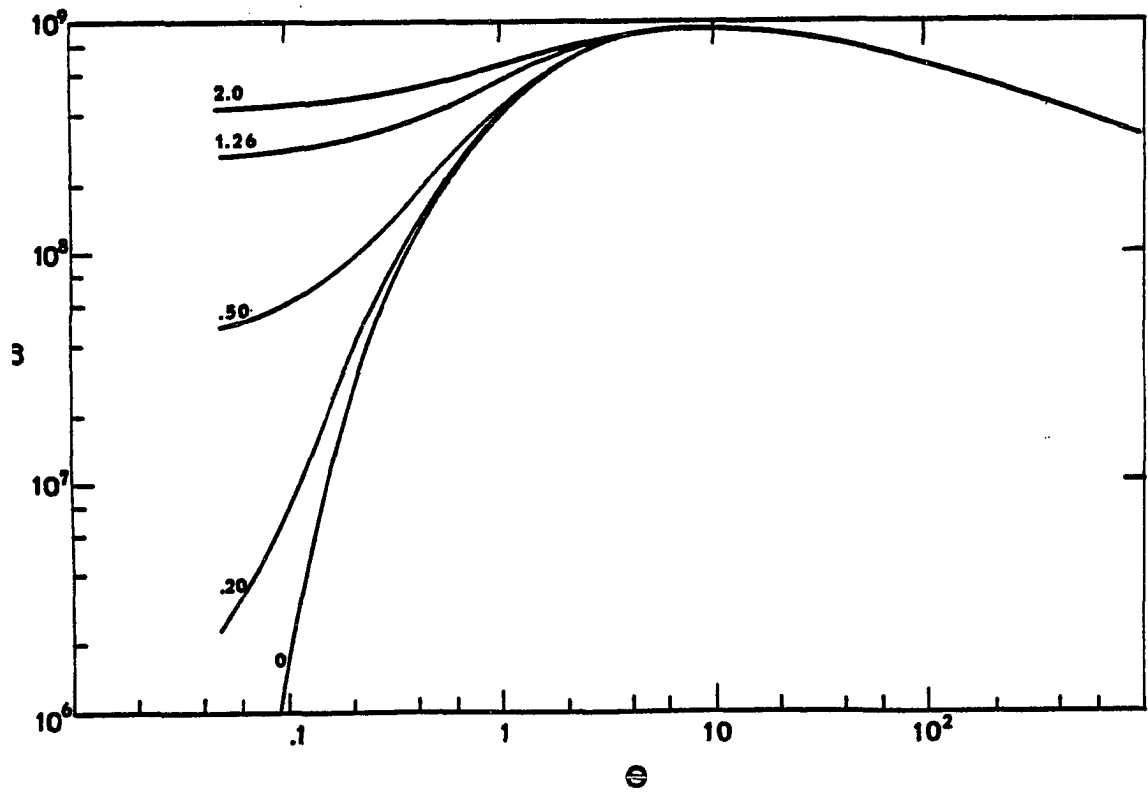


Fig. 5 Same as Fig. 4 except that  $\nu = 0$ .

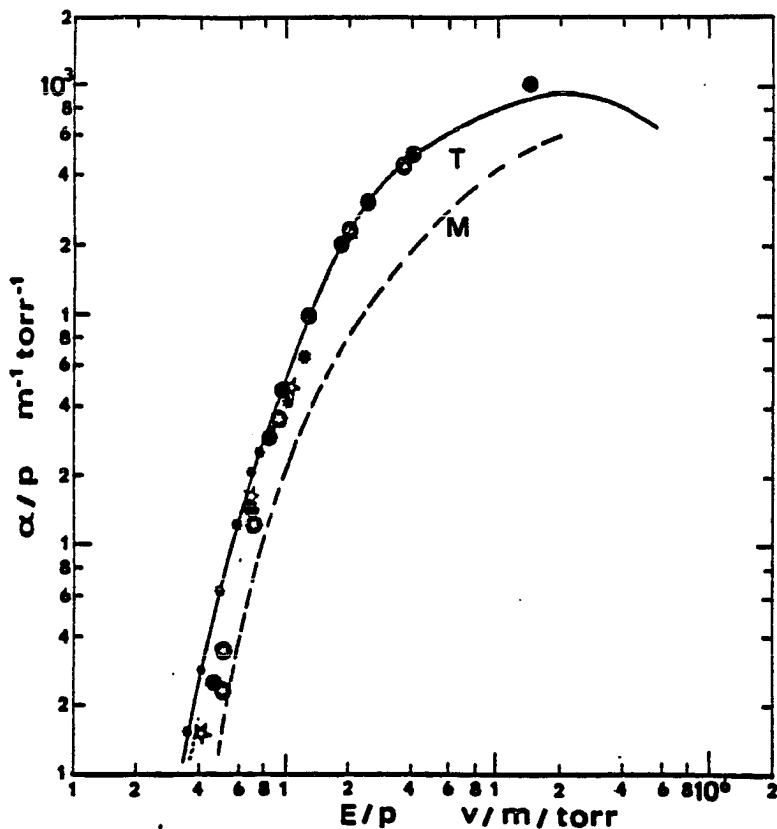


Fig. 8 Trajectory ionization theory (T) applied to calculation of electron temperatures and drift velocities in swarms, contrasted with use of a simple Maxwellian calculation (M) based conventionally on linear constant speed paths between collisions. Hollow stars are from Schlumbohm (16); solid five-point stars are from Kontoleon et al.; and other stars are from Townsend and Bailey (17). Diamonds are from Blavins and Hasan (18).

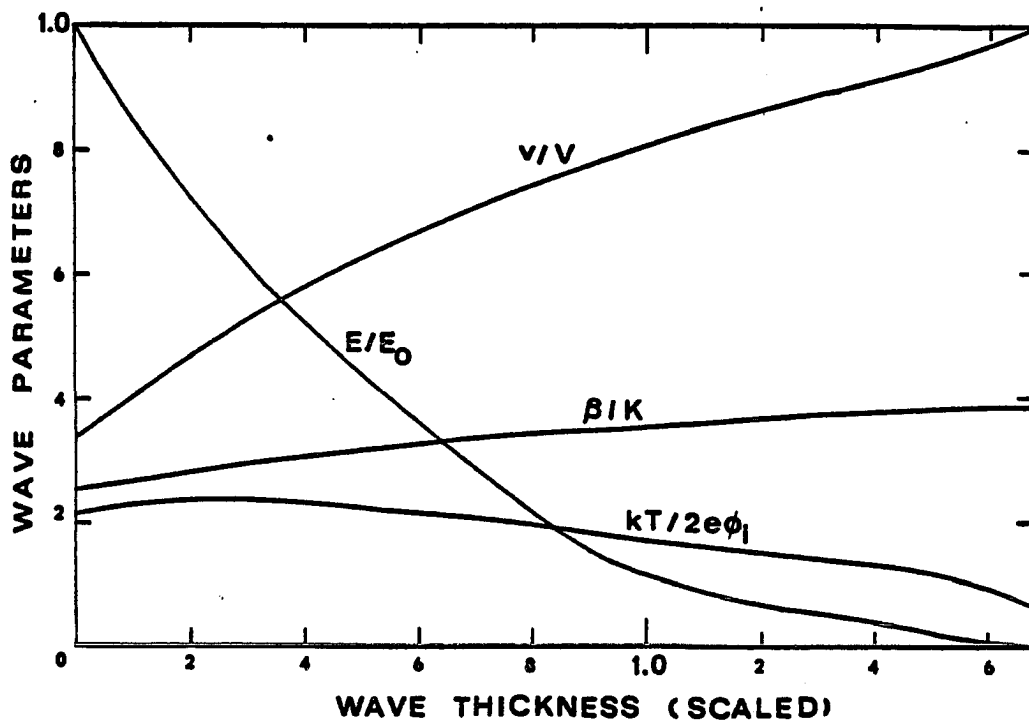


Fig. 7 Result of integrating the electron fluid equations to obtain profiles of field, electron velocity, temperature, and ionization rate in the wave sheath for a relatively fast wave ( $V = 3 \times 10^7$  m/sec) in helium. The wave thickness is scaled with the distance over which an electron acquires ionizing potential energy in the field.

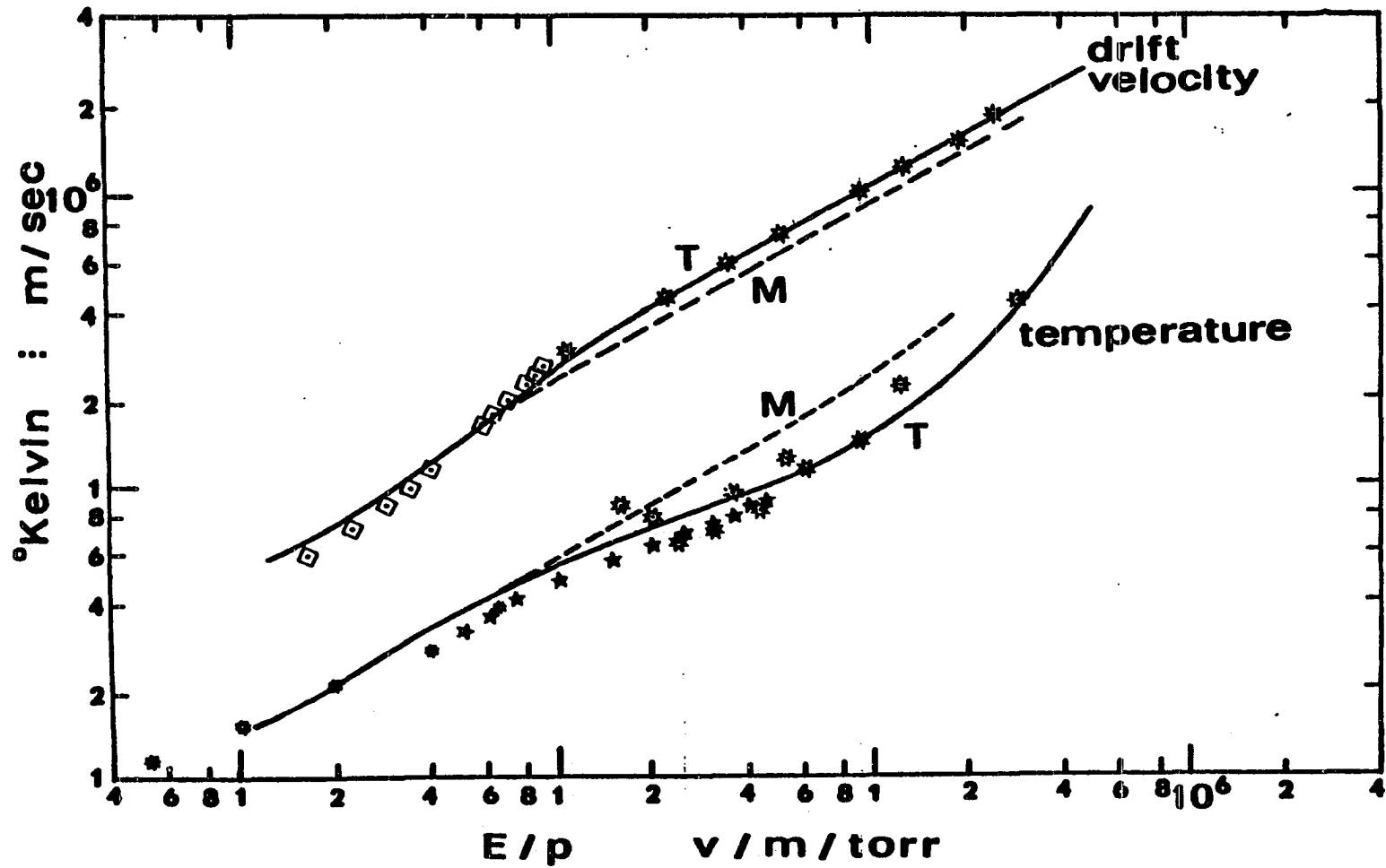


Fig. 9 Townsend's  $\alpha/p$  derived by the trajectory method (T), contrasted with the conventional approach (M). Solid dots are taken from von Engel (19); stars in dots are from Kontoleon et al.; hollow stars are from Raether (20); small asterisks are from Harrison (21); and large asterisks are by Bowls (22).